HYDROTHERMAL   ALTERATION

WITHIN   THE

COALSTOUN

PORPHYRY COPPER PROSPECT,

GAYNDAH,   QUEENSLAND.

by

W.G. BILLINGTON.   B.A.

This thesis is submitted in partial fulfillment of

the requirements for the degree of Bachelor of Arts,

with Honours.

7th November, 1975.

Macquarie University
School of Earth Sciences
Supervisor: Prof. P.F. Howard.

FRONTISPIECE.

Primary magmatic biotite fringed by
green hydrothermal biotite.

(CL268; plane polarized transmitted light).

TO MY FIANCEE,

JUDITH,

WITHOUT WHOSE PATIENCE,

UNDERSTANDING AND ENCOURAGEMENT

THIS THESIS WOULD

NOT BE.

ABSTRACT

The Coalstoun porphyry copper prospect lies adjacent to the north-northwest trending Perry Fault system. The intrusives of the prospect comprise porphyritic biotite $\pm$ hornblende quartz diorite and tonalites, their porphyritic microcrystalline equivalents and associated dykes. The composite intrusion appears to have attained shallow crustal levels which has produced fracturing and brecciation of the overlying, and surrounding sediments.

Pervasive hydrothermal alteration / sulphide mineralization accompanied the final states of crystallization and culminated in the formation of veins and fracture fillings. The zonal pattern of this alteration / mineralization resulted in a deep core low in both copper and total sulphides, a surrounding biotite zone within which all significant copper mineralization occurs, and a fringe of chloritized - pyritized intrusive and surrounding metasediments. These alterations are almost isochemical, with dominant variations in K, Ca, Rb, Sr and Cu.

Petrographic observations and microprobe analyses of hydrothermal biotites showed that they are characteristically different in composition and form to those of primary magmatic biotites, including lower Ti, lower total Fe as FeO, lower Fe/ Mg and Si / Al ratios, and possibly an increase in the Fe^{3+} / Fe^{2+} ratio. They are much finer

grained and possess a greenish colour to their pleochroism.

A model is suggested to explain the high level of the intrusion, its effects upon the surrounding sediments, the association of copper mineralization and biotitization, the characteristics of this biotite, the surrounding chlorite zone and the subsequent veining and later andesitic-dacitic dyke emplacement. The model shows similarities to those proposed by Guilbert and Lowell (1974), and Carson and Jambor (1974).

The work contained within this thesis has not
been submitted in any form for another degree
or diploma at any other university or
institution. Information derived from the
published or unpublished work of others has
been acknowledged within the text and a list
of references is given.

W.G. Billington.

7th November, 1975.

ACKNOWLEDGEMENTS:-

It is with great pleasure that I am able to express my appreciation to Esso Australia Ltd., for firstly allowing me to make a study of the hydrothermal alteration at Coalstoun as my Honours thesis, and secondly for making funds available through the School of Earth Sciences for assistance with the project.   I am especially indebted to Mr. Tom McLaren, Manager of the Minerals Department.

I wish also to thank my supervisor, Prof. P.F. Howard, Macquarie University, for guidance and discussion throughout the year, and Dr. Paul Ashley, Esso Australia Ltd., for his generous time in guiding me around the prospect area and its environs.   Appreciation is also given for his valuable assistance in many aspects of this study.

Thanks must also go to staff of the School of Earth Sciences of Macquarie University, particularly Dr. R.H. Flood, who aided in many aspects of the study.

Most of all I would like to thank my mother and father, whose encouragement, continual support and readiness to assist kept an end in sight.

In regard to the typing of this thesis, thanks must go to Mrs. Bye for her fine effort.

TABLE OF CONTENTS

LIST OF FIGURES

Page.

LIST OF PLATES

LIST OF TABLES

CHAPTER 1.   INTRODUCTION

General background to Porphyry
Copper Deposits.

Purpose of study and method of
investigation.

Location.

Previous investigations.

1. <u>INTRODUCTION</u>

<u>GENERAL BACKGROUND TO PORPHYRY COPPER DEPOSITS</u>:-

Several recent publications (Lowell and Guilbert,
1970; Rose, 1970; James, 1971; De Geoffroy and Wignall,
1972;) have developed the concept that unifying geological
characteristics are displayed to varying degrees by what are
termed 'porphyry copper and molybdenum deposits'. Lacy
(1974) reviewed proposed porphyry copper definitions and
demonstrated that with changes in technology and economics
the characteristics of porphyry copper deposits will
constantly change.

In this thesis porphyry copper deposits are consid-
ered in the context of Titley and Hicks (1966); Lowell and
Guilbert (1970); De Geoffroy and Wignall (1972); Lowell
(1973) and Guilbert and Lowell (1974). They describe them
as disseminated and stockwork veinlet copper/molybdenum
sulphide deposits, with an overall size in the ranges
from 1000-20 million tonnes, and a variable grade dependent
upon current economics and technology. The deposits are
usually associated with high-level calc-alkaline intrusions,
compositionally varying from adamellites through to
diorites and exhibiting a porphyritic texture. Their
concomittant ore bodies are oval in plan with exposed
dimensions of 1km x 2km and pipe-like in three dimensions

(Guilbert and Lowell, 1974). Mineralization is arranged within a zonal alteration pattern of potassic core, outwardly passing through phyllic (quartz-sericite-pyrite), argillic (quartz-kaolin-montmorillonite) and propylitic (epidote-chlorite-carbonate) zones. Over the same interval sulphide species vary from chalcopyrite-molybdenite-pyrite through successive assemblages to an assemblage of galena and sphalerite.

The difficulty in interpreting the geometry of porphyry copper alteration has led to diverse attempts to classify alteration assemblages into meta morphic facies (Creasey 1959, 1966; Burnham, 1962), stages (Kents, 1963), metasomatic changes (Gupta et. al., 1965; Hemley and Jones, 1964) and zones or envelopes (Meyer and Hemley, 1967; Lowell, 1968; Lowell and Guilbert, 1970).

The writer has therefore termed Coalstoun, the area under study, a Porphyry Copper Prospect, although it may be better defined as a low grade disseminated copper prospect with porphyry ore deposit characteristics.

PURPOSE OF STUDY AND METHOD OF INVESTIGATION:-

The main purpose of this study was to investigate the hydrothermally induced alteration within the "Coalstoun Microtonalite" intrusive. The mineralogical and chemical changes within the alteration were examined and mapped in order to determine the three dimensional pattern of sulphide mineralization and associated alteration

assemblages.

Available, and accessable, drill core was logged
and sampled, numerous polished thin sections were
produced, and detailed petrographic examinations were
carried out.   Representative bulk samples and ferromagnesian
minerals were analysed in order to reveal general external
and internal parameter variations.   Variations between
primary magmatic and secondary hydrothermal ferromagnesian
minerals, to date, have not been extensively examined
within porphyry copper deposits.   It is hoped that any such
variations will be expanded and published.

LOCATION:-

The Coalstoun Porphyry Copper Prospect is located
east of the township of Gayndah, approximately 85 kms west
of Maryborough and 250kms north-northwest of Brisbane
(figure 1).

The prospect area is located within the Seven
Sisters area of the Walla Range and has been investigated
by several companies over the past decade, including
Kennecott Explorations (Aust.) Pty. Ltd., Mines Adminis-
tration and presently Esso Australia Ltd. who have secured
a mining lease within the prospect area.

PREVIOUS INVESTIGATIONS:-

An extended outline of the work involved within the
area was given by Graham (1975) and is briefly reviewed
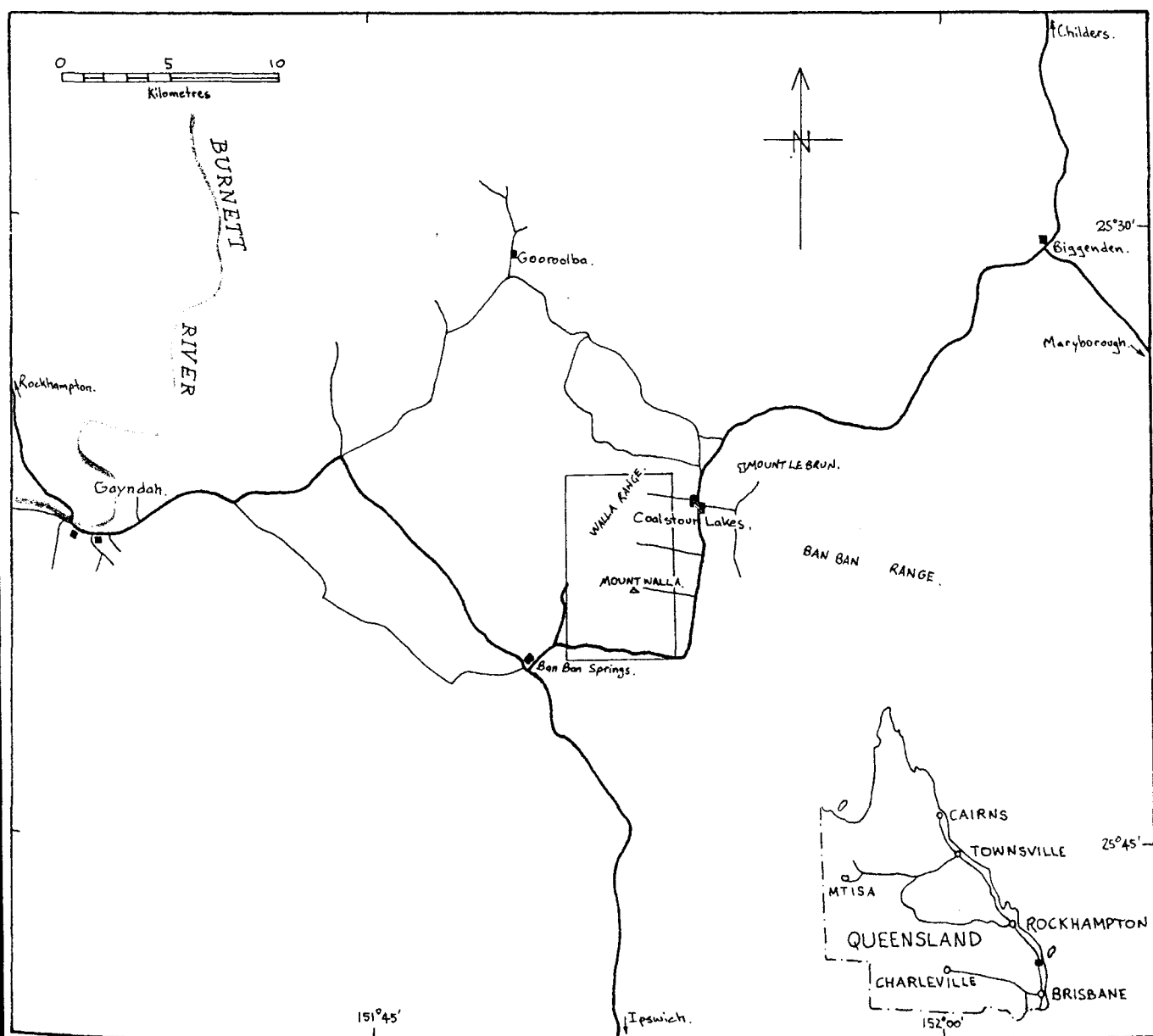
Figure 1.   Locality Map.

here accompanied with additional information from more
recent Esso Australia Ltd. explorations.

In the early 1900's gold was searched for within the
Walla Range, with leases being visited by Government
Geologists in 1921 and 1935.   In 1964 a mineralized
gossanous vein rich in gold and silver was examined by
J.H.Brooks of the Queensland Mines Department who recom-
mended that the Department carry out drilling on behalf of
Golden Plateau N.L. under the subsidy Act;   this was done
in 1967.

W.S. Yeaman of Kennecott was invited to examine the
area in 1967 and recognized porphyry copper type mineraliz-
ation associated with porphyritic intrusive rocks near to
the gold leases examined.   Mapping, rock chip geochemistry,
induced polarization, ground magnetics and diamond drilling
were conducted by Kennecott between 1967 and 1970 and
intersected weak hypogene copper mineralization with patchy
supergene enrichment.

Mines Administration Pty. Ltd. carried out per-
cussion drilling in 1971 but abandoned the area after not
finding a high grade supergene copper zone.

Esso Australia Ltd. acquired the area in May 1972
and followed the previous work by extending and refining
the existing mapping of Kennecott.   Accompanied with this,
Esso conducted valley soil geochemistry, an extension of
Kennecott's I.P. work, ground and airborne geophysics, all
in the aim of delineating individual intrusives and
locating possible drill hole targets.

The authority to prospect was relinquished in 1974, with the mineralized area secured by mining lease; application Gympie -731.   In all, a total sum of 42 holes were drilled by Esso to a total length of over 12,000 metres.

CHAPTER 2.   REGIONAL GEOLOGY and

STRUCTURAL SETTING.

2.   REGIONAL GEOLOGY AND STRUCTURAL SETTING

The Coalstoun prospect lies immediately adjacent to the
trace of the north-northwest trending Perry Fault within the
Coastal Block of the structural classification proposed by
Day et. al. (1974).   The rocks are composed of siltstone,
greywacke, chert, shale and minor limestone, basalt, dolerite
and jasper (Neale, 1974) which have been regionally metamor-
phosed to lower - intermediate greenschist facies.   They are
tentatively correlated with the ?Devonian-Carboniferous
Neranleigh-Fernvale Beds in the Brisbane area to the south-
east, and to the Curtis Island Group east of Monto to the
north.   The region surrounding the Coastal Block comprises
the Permo-Triassic Gympie Basin, the Lower ? - Middle
Triassic Esk Trough and the Yarraman Block (figure 2) of
Day et. al. (1974).

The Coalstoun prospect occurs near the eastern margin of
the Coastal Block, where the metasediments are faulted
against or unconformably overlain by the ? Carboniferous -
Lower Permian Biggenden Beds which form the lower unit of the
Gympie Basin (named by Hill, 1955, p 92).   To the northeast
of Coalstoun Lakes the Biggenden Beds are comprised of low
grade regionally metamorphosed basalt, dolerite, greywacke,
mudstone, tuff and minor limestone and acid volcanics
(Ashley, 1974).

To the east and south of the Coalstoun prospect, both the
Biggenden Beds and the Coastal Block metasediments are
unconformably overlain by the Middle Triassic Neara Volcanics,
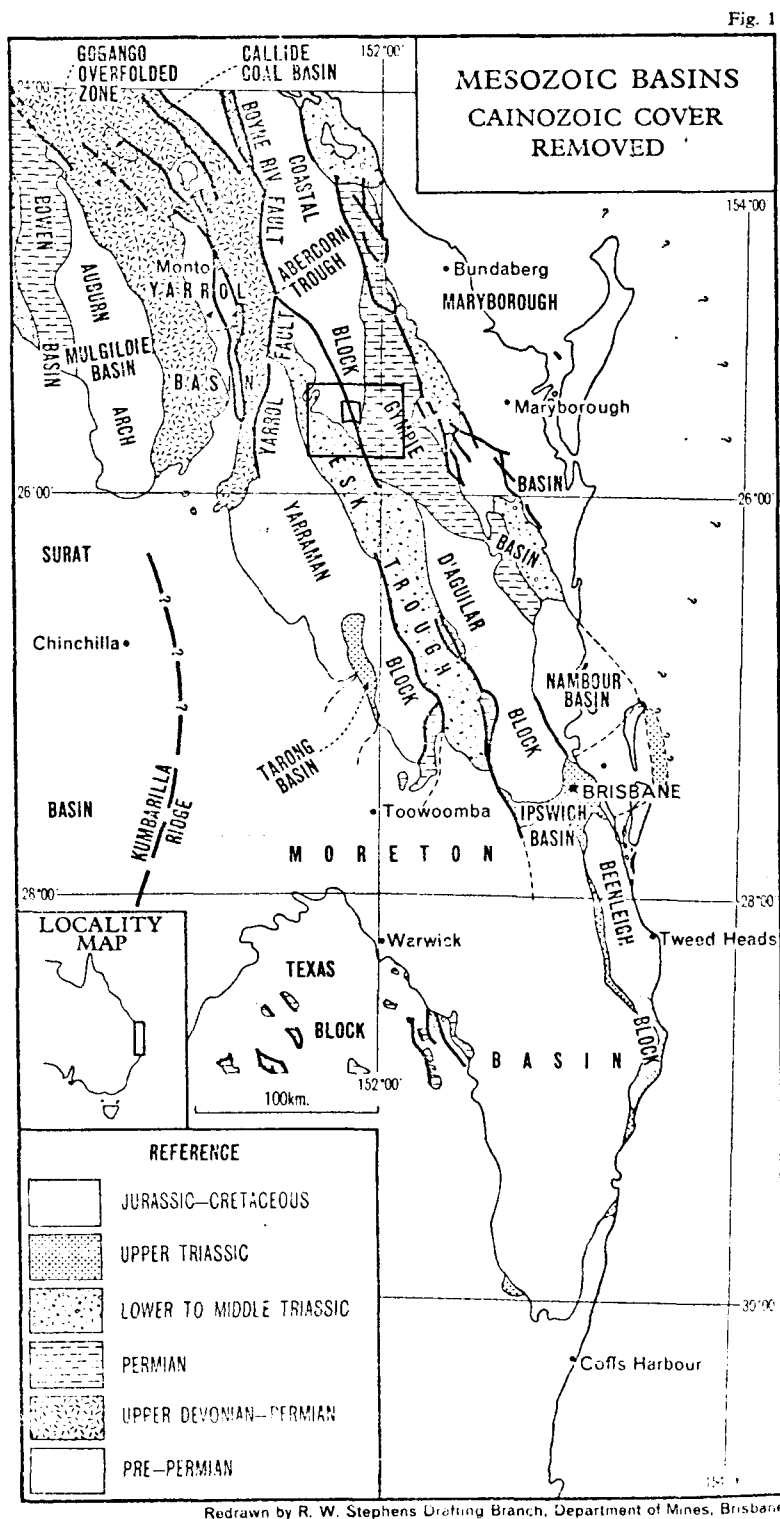
Figure 2.   Structural setting of Mesozoic Basins in southeasten Queensland (after Day et. al.; 1974).   Location of figure 1 indicated by ▢ .

which in the Coalstoun area are composed of andesitic to
rhyolitic volcanics, tuffaceous equivalents and minor
mudstone and sandstone, which represents a northerly extension
of the Esk Trough of Day et. al. (1974).

A protracted period of intrusive activity affected this
area in Upper Permian to Middle Triassic times. To the
northwest of Coalstoun Lakes, the Coastal Block has been
intruded by the Upper Permian Perry Complex (249 m.y.;
Ellis, 1968) composed largely of dioritic to granodiorite
rocks (see figure 4), and a series of intrusives ranging from
monzonite to adamellite to microgranite outcrop to the north-
west, northeast, and east of Coalstoun Lakes. These high
level intrusives include the "Oaky Creek Monzonite", and the
Chowey, Degilbo and Mungore Adamellites (figure 4). The
latter two plutons are of Lower to Middle Triassic age which
gave potassium/argon age dates on biotite concentrates of
215^{+}_{-} 5 m.y. and 207^{+}_{-} 5 m.y. respectively (Ellis, 1968;
Webb and McDougall, 1967). The intrusive "Coalstoun
Microntonalite" (figure 3) is of Permo-Triassic age, 235 m.y.
(Graham, 1975).

Following these phases of intrusive activity and the
deposition of the Neara Volcanics, the region appears to have
been relatively stable. However, a large porphyritic
arfvedsonite-aegirine-quartz microsyenite dyke outcrops
approximately 3 km east of Coalstoun Lakes (figure 4) which
Ashley (1974) suggested to be of Miocene age based on
comparison with rocks of similar petrography in the Glasshouse
Mountains north of Brisbane (24-25 m.y.; Webb et. al; 1968).

LEGEND

RECENT	Qa	Stream deposits, soil, talus
PLEISTOCENE	Qpb	Barambah Basalt Vesicular & massive Olivine Basalt, minor Basaltic Agglomerate, interflow stream deposits & soil
? MIDDLE TRIASSIC	Ra	Aranbanga Beds Porphyritic Andesite, Andesitic Basalt
? LATE PERMIAN To EARLY TRIASSIC	R-Pv	? Ooramera Volcanics Porphyritic Rhyodacite, Dacite, Andesite Rhyolite breccia, tuffaceous & agglomeratic equivalents, minor tuffaceous mudstone, siltstone, sandstone
? LATE PERMIAN	Pmo	"Oaky Creek Monzonite" Biotite – Hornblend Monzonite, minor Tourmaline – bearing aplite & pegmatite
LATE PERMIAN	Pdc	"Coalstoun Microtonalite" Porphyritic Biotite (Hornblende) Microtonalite, Microdiorite Breccia
CARBONIFEROUS To EARLY PERMIAN	Pzub	? Biggenden Beds in Part Porphyritic & Amygdaloidal Metabasalt, Meta-andesite minor Agglomerate, Greywacke
? DEVONIAN	Pzus	Biggenden Beds in Part Neranleigh – Fernvale Group in part, Siltstone, Chert, Jasper, Greywacke, Conglomerate, Slate, Schistose Marble

———— Outcrop boundary definite, inferred

===== Highway

===== Road

Creek

▬▬ Boundary of A. to P. 1050 M.

COALSTOUN - PROJECT 317
A to P 1050M - QUEENSLAND

RECONNAISSANCE
OUTCROP MAP
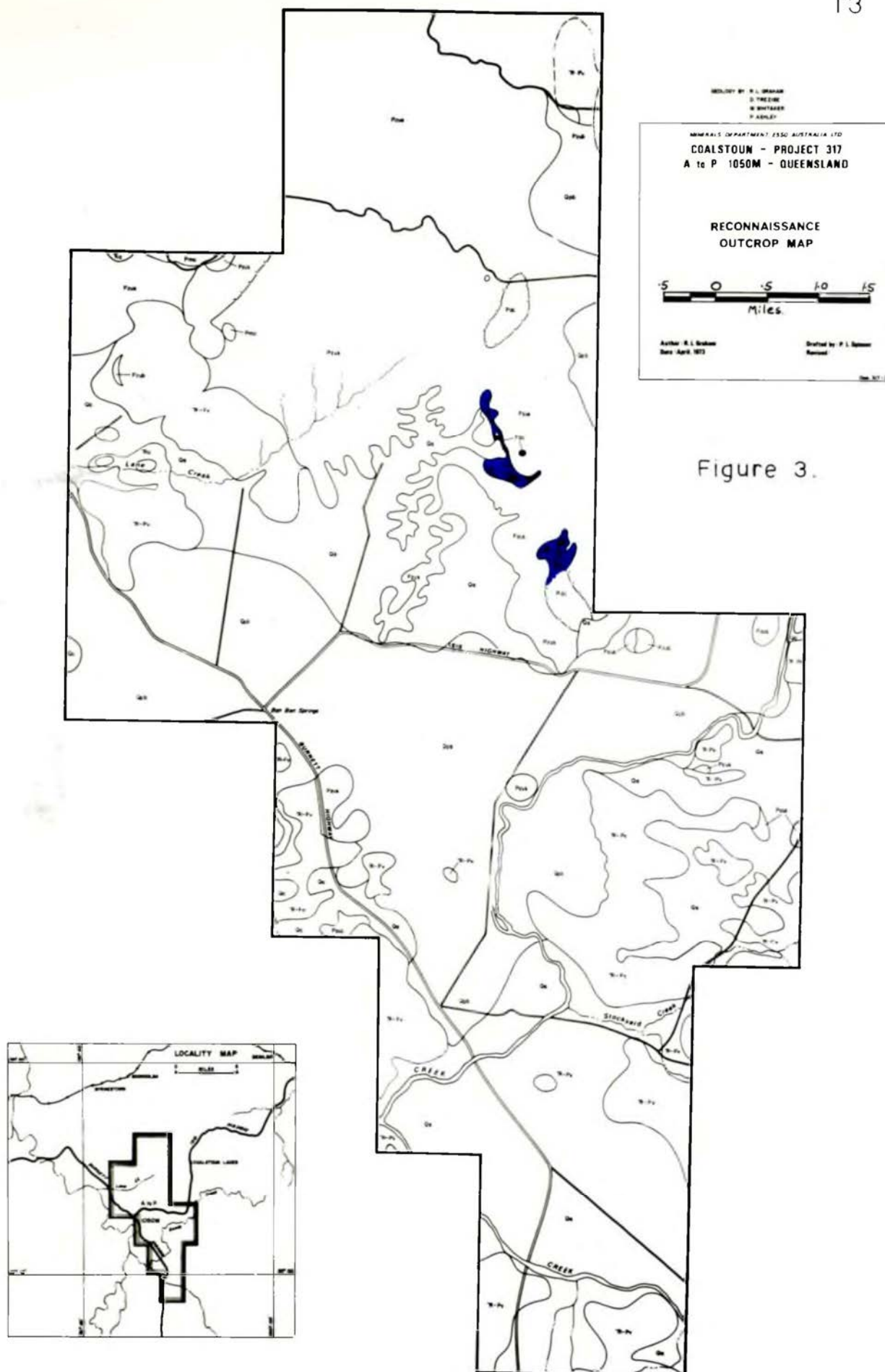
Figure 3.

LEGEND

RECENT	Qa	Soil, talus, stream deposits
? PLEISTOCENE	Qpa	Arkose, conglomerate (developed over granitic rocks)
PLEISTOCENE	Qpb	Barambah Basalt. Vesicular and massive olivine basalt, basaltic agglomerate (near vents), minor interflow stream deposits and soil
? TERTIARY	Ts	Porphyritic arfvedsonite-aegirine-quartz microsyenite dyke
? MID-TRIASSIC	Ra	? Aranbanga Beds Porphyritic andesite, andesitic basalt

EARLY TRIASSIC

	Rgd	Degilbo Adamellite Biotite adamellite, minor biotite-hornblende micromonzonite
	Rgc	Chowey Adamellite Biotite adamellite, aplite
	Rgm	Mungore Adamellite Biotite adamellite, aplite

? LATE PERMIAN TO EARLY TRIASSIC	R - Pv	? ≡ Ooramera Volcanics Porphyritic rhyodacite, dacite, andesite, rhyolite, breccia, tuffaceous and agglomeratic equivalents, minor tuffaceous sandstone, mudstone, siltstone
LATE PERMIAN	PgP	Perry Complex Biotite-hornblende adamellite
? LATE PERMIAN	Pmo	"Oaky Creek Monzonite" Biotite-hornblende monzonite, minor tourmaline-bearing aplite and pegmatite
? CARBONIFEROUS TO EARLY PERMIAN	Pzub	≡ Biggenden Beds in part Porphyritic and amygdaloidal metabasalt, minor metadolerite, diorite, metagabbro, meta-andesite, conglomerate, greywacke, siltstone, hornfels
? DEVONIAN TO EARLY PERMIAN	Pzus	≡ Biggenden Beds in part, Neranleigh-Fernvale Group in part Siltstone, chert, jasper, greywacke, conglomerate, slate, minor meta-andesite
? DEVONIAN TO CARBONIFEROUS	Pzum	? Neranleigh-Fernvale Group Quartz-mica schist, mica-andalusite schist, phyllite, quartz-feldspar-mica gneiss, minor amphibolite, haematite quartzite

✕   Mine working

Figure 4.

The next and last major period of activity is recorded during the Pleistocene, when highly vesicular olivine basalt poured from vents immediately to the northeast of the prospect. These extremely fluid lavas flowed down the drainage systems of Sandy Ck - Barambah Ck - Burnett River from cones now called Mount Le Brun, Harvey Knob and Hunters Volcano (figure 4). This, the Barambah Basalt (Stevens, 1961) has been dated at 0.6 m.y. by Wellman (1971). Recent alluvium now occurs deposited along many of the present and former creeks and valleys in the district.

The Perry Fault, a major structural feature of southeast Queensland, is not well defined in the Coalstoun prospect area, although it is expressed topographically and geologically within 30 km to the north-northwest and south-southeast. The fault zone occurs both within the Coastal Block and separating the Coastal Block from the Gympie Basin. The fault appears to have been active intermittently from Lower Permian times, having had a controlling influence on the location of the Permo-Triassic intrusives (e.g. the "Coalstoun Microtonalite"), Pleistocene volcanicity (the Barambah Basalt) and seismic activity, as the epicentre of the 1935 Gayndah earthquake was located on the fault (Byron and Whitehouse, 1937).

It has been suggested (Ashley (1974) and Graham (1975)) that the Perry Fault occurs as a 10 — 15 Km wide imbricate zone of subparallel and arcuate deep-seated regional fractures, probably with a large strike - slip component.

CHAPTER 3.   GEOLOGY WITHIN THE COALSTOUN PROSPECT.

Introduction.

Regional metamorphism.

Upper ? Palaeozoic metasediments.

Biggenden Beds.

Intrusive rocks

- Petrographic description.

Barambah Basalt.

Recent alluvium.

3. GEOLOGY WITHIN THE COALSTOUN PROSPECT

INTRODUCTION:-

The Coalstoun prospect is depicted on Plate 1, and can be divided topographically into three separate but related valley areas isolated by the ridges of the Seven Sisters which form part of the Walla Range, and are here termed the northern, central and southern areas.

Graham (1975) recorded that the intrusive rocks in the prospect "are a comagmatic suite of dioritic and tonalitic rocks" which are mostly porphyritic in texture and vary in their principal constituents and degree of alteration.

The ridges and the peaks of the Seven Sisters are comprised of metasediments and colluvium. These Palaeozoic (? Devonian - Carboniferous) metasediments are within the Coastal Block and are possible equivalents of the Neranleigh-Fernvale Beds.

REGIONAL METAMORPHISM:-

Investigations by Ashley (1974) on the volcanics of the Biggenden Beds (metabasalt, metadolerite and volcanoclastic greywacke) to the immediate east of the prospect showed mineral assemblages of albite, epidote, actinolite, chlorite, calcite, haematite, and minor clinopyroxene, ilmenite, sphene and pumpellyite. These assemblages are consistent with lower greenschist facies of Winkler (1967).

UPPER ? PALAEOZOIC METASEDIMENTS:-

Recrystallized siltstone and quartzite form the two
main types of pre-intrusive sediment within the prospect
area. The siltstones are fine grained grey to buff coloured
rocks and are severely weathered in outcrop. Angular
fragments of quartz are irregularly scattered in a
microcrystalline quartz matrix. Narrow veins of chlorite,
limonite and quartz pervade hand specimens.

The quartzites are white to light grey in colour. As
well as these, several black cherty rocks, possibly hornfelsed
black shales, have been intersected in drill core.

Nearer the Coalstoun intrusives the metasediments show
extensive recrystallization and brecciation and therefore
resist erosion and form the ridges of the Seven Sisters
(plate 2). The peaks of these ridges are the most intensely
affected areas due to their cores being composed of pipe-
like breccias (Graham, 1975). The dominant components of
these breccia pipes are fragments of variable size of
metasediments and minor porphyritic intrusive rocks.

BIGGENDEN BEDS:-

Three small hills in the southeastern part of the
prospect area were investigated by Ashley (1974) and Graham
(1973). The first and largest of the three is reported to
be composed of flowbanded and brecciated pyritic rhyolite and
the other two of amygdaloidal metabasalt.

Plate 2.

View of the Seven Sisters area within the Walla Range.
Taken from 2km outside Coalstoun Lakes
on the Biggenden road.

(please note: photo print reversed).

INTRUSIVE ROCKS:-

The intrusive rocks largely form the three valleys of
the northern, central and southern areas.   In the southern
area, (plate 1) three main intrusive bodies are exposed, with
extensions of intrusive rock under the basalt and alluvial
cover to the southeast.   The oldest of these exposed
intrusive rocks is labelled (Graham, 1975; plate 1) as a
"complex zone of mixed porphyries", ranging from diorite
porphyry, quartz diorite porphyry, andesite porphyry to
granodiorite porphyry.   It is basically a porphyritic
diorite intrusion with some microdiorite phases possibly
due to chilled margin effects with minor felsic and andesitic
dykes.   Neale(1974) recorded sulphides ranging from
1-3 wt % and a pyrite to chalcophyrite ratio of 3:1 to
10:1.

A T-shaped "quartz eye" diorite porphyry, possibly
intruded along a fault intersection (Graham, 1975), is
weakly porphyritic with euhedral quartz phenocrysts up to
4 mm across.   The intrusive contains minor biotite and is
strongly fractured.   Sulphides consist mostly of pyrite
and vary from 2-20 wt %, increasing with the degree of
brecciation.

The third intrusive is a leucocratic quartz diorite or
trondhjemite, low in mafic minerals and sulphides.   Small
pipes of quartz diorite porphyry and hornblende diorite
porphyry also outcrop in the southern valley.   Diamond drill
holes which have penetrated post intrusive cover have also
intersected porphyritic biotite $\pm$ hornblende quartz diorites

in the southern valley.

In the northern valley weathered feldspar porphyry
crops out sparsely, although from ground magnetic geophysical
evidence, it was inferred that a dioritic intrusive occured
at shallow depth (Neale,1974). Subsequent drilling
intersected weakly to moderately altered porphyritic biotite
$\pm$ hornblende quartz diorite with sulphide content ranging
up to 1.5 wt % and with pyrite to chalcopyrite ratio of
>10:1 to <1:1.

Within the central area an elongate stock possessing
maximum dimensions of 3 km x 2 km, roughly orientated in a
north-south direction is exposed and is termed (Graham, 1975)
a biotite diorite porphyry, as shown on plate 1. The
contacts with the wall rocks, where observable or, as
determined by drilling, are undulant and steeply dipping
outward from the centre of the stock. In detail they are
rendered irregular by possible magmatic stoping of
metasedimentary blocks and by the presence of andesitic -
dactic and aplitic dykes or sills protruding through the
intrusive host into the adjoining wall rocks. The location
and orientation of these protrusions is possibly controlled
by pre-existing fractures. In fact, the complex shape of
the stock and its location within the district appears to be
controlled by the intersection of pre-intrusion north-
northwest faults (the "dominant fault direction" of Graham;
1975, p. 16) and southwest fractures and faults.

Discontinuous pods of intrusion breccia, angular

fragments of siltstone and quartzite with an intrusive rock

matrix, are commonly developed in the northern part of this

stock, as are large inclusions or rafts of sedimentary wall

rocks, several of which are exposed in the central part

of the intrusion (plate 1).

Extensive hydrothermal alteration of the stock makes

recognition of the original rock type somewhat difficult.

Nevertheless, microscopic examination of numerous samples,

especially from deep in the core and in the southern valley,

shows that the original rocks were porphyritic biotite

quartz microdiorite or microtonalite. Textural and

compositional variations within the stock are believed to

reflect, for the most part, position within the stock,

marginal effects regarding cooling history, fracture

intensity and the degree of subsequent alteration.

Accurate modal comparison (table 1) of certain igneous

rocks at Coalstoun is complicated by the fine-grained nature

of the matrix and textural variability.   Chemical analysis

and normative compositions (table 2) have been useful in

establishing compositional characteristics and trends

(figures 5-8) not fully detectable by petrographic methods.

The stock is composite, with the bulk consisting of

porphyritic biotite microtonalite transitional in

composition to porphyritic biotite quartz microdiorite.

Typical examples of the "Coalstoun Microtonalite" rock

textures can be seen in plates 3 to 8.   Variations in these

Porphyritic micro tonalite -

Porphyritic quartz micro diorite -

Biotite ± Hornblende quartz diorite -

Aplite -   X

Porphyritic andesite-

Sample No.	ESSO						CL				
	4	9	17	21	23	26	268	452	580	626	627
Quartz	14	28	tr	29	11	22	26	40	21	21	22
Plagioclase	59	52	17	56	60	77	51		54	50	47
K-feldspar	3	2			4	1	3	60	2	2	3
Biotite	6	6	tr	10	16		19		6	23	25
Hornblende	18		29	4	6				11		
Chlorite		3					tr				
Opaques	1	8	3	2	tr	tr	2		2	2	1

Porphyritic micro tonalite - ■

Porphyritic quartz micro diorite - ◗

Biotite ± Hornblende quartz diorite - ●

Aplite - X

Porphyritic andesite- ▲

Sample No.	4	9	17	21	23	580	626	627	628	Sample No.
SiO_2	60.8	62.0	58.3	63.5	60.1	62.63	61.09	61.83	62.35	SiO_2
TiO_2	.78	.65	.07	.6	.97	.66	.70	.68	.69	TiO_2
Al_2O_3	16.4	15.7	15.1	15.4	16.8	16.09	15.98	15.37	15.98	Al_2O_3
Fe_2O_3*	5.44	5.9	5.8	4.8	5.71	5.43	4.73	5.03	5.54	Fe_2O_3
MnO	.09	.03	.06	.03	.05	.04	.02	.02	.02	MnO
MgO	3.15	2.2	5.4	2.1	4.2	2.53	2.52	2.61	2.43	MgO
CaO	4.5	2.9	5.2	3.3	3.6	3.15	3.69	3.82	2.82	CaO
Na_2O	4.5	5.4	3.6	3.9	3.45	4.54	4.30	3.84	4.51	Na_2O
K_2O	2.05	.9	1.5	1.4	2.4	1.32	2.27	2.19	1.70	K_2O
P_2O_5	.23	.15	.20	.20	.25	.21	.22	.18	.20	P_2O_5
LOI.	2.09	3.2	2.85	1.5	2.17	2.23	2.24	1.70	2.06	LOI.
Total	100.03	99.03	98.08	96.73	100.09	98.83	97.76	97.27	98.30	Total
CIPW Norm										
Q	13.57	18.08	13.82	18.66	17.54	21.26	16.37	19.57	20.53	Q
or	12.12	5.34	8.84	8.28	14.18	7.80	13.41	12.94	10.04	or
ab	38.04	45.64	30.44	32.96	29.19	38.40	36.37	32.48	38.14	ab
an	18.49	13.37	20.60	15.07	16.21	14.25	16.86	17.77	12.68	an
C		.94			1.95	2.59	1.97	.27	.17	2.08	C
di	1.81		3.02							di
hy	6.97	5.46	11.99	5.21	10.42	6.30	6.27	6.50	6.05	hy
hm	5.46	5.90	5.81	4.82	5.73	5.43	4.73	5.03	5.54	hm
il	.20	.06	.12	.06	.11	.08	.04	.04	.04	il
ru	.68	.62	.64	.57	.91	.62	.68	.66	.67	ru
ap	.54	.37	.47	.47	.60	.49	.51	.42	.46	ap
Plag An	32.71	22.66	40.36	31.38	35.70	27.07	31.68	35.37	24.95	Plag An
Q	17	22	19	25	23	26	20	24	25	Q
or	15	7	12	11	18	10	16	16	12	or
ab + an	69	72	69	64	59	64	64	61	62	ab + an
symbol	●	■	▲	■	●	●	◖	■	■	symbol

Table 2. Composition and CIPW Norm of relatively unaltered rock samples. *Total Fe as Fe_2O_3.

Porphyritic micro tonalite - ■

Porphyritic quartz micro diorite - ◖

Biotite ± Hornblende quartz diorite - ●

Aplite - X

Porphyritic andesite- ▲
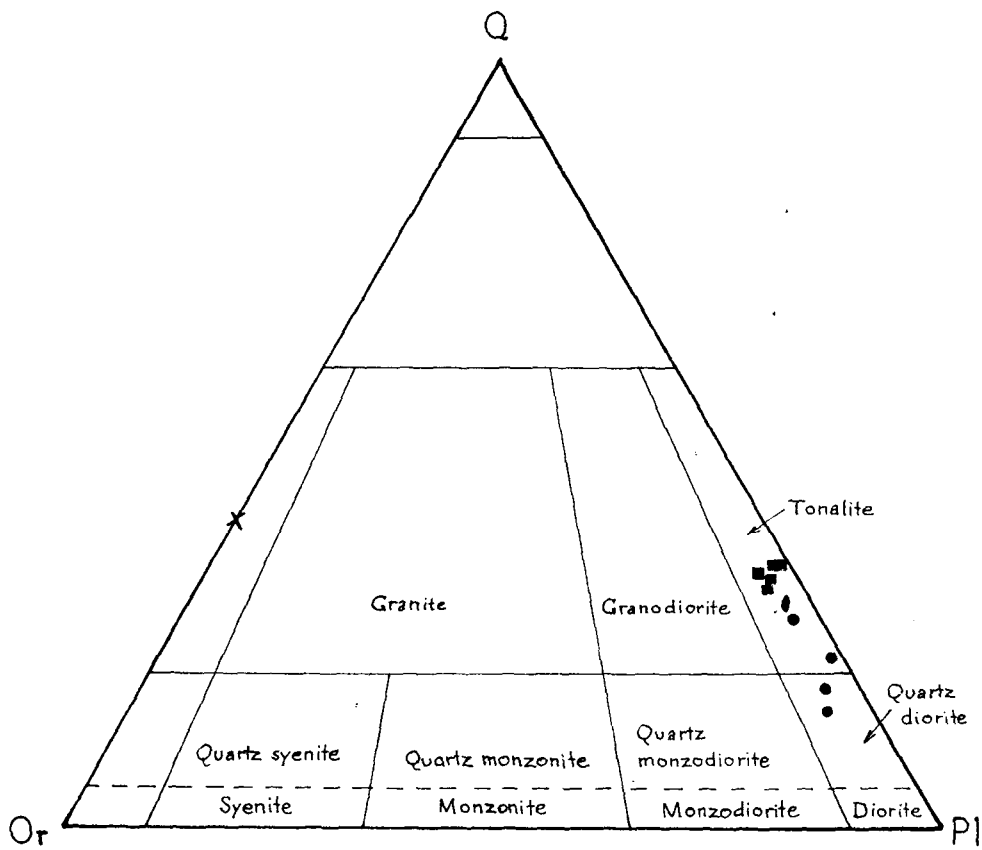
Figure 5.   Modal comparison of unaltered rocks

(after Steckeisen, 1974).
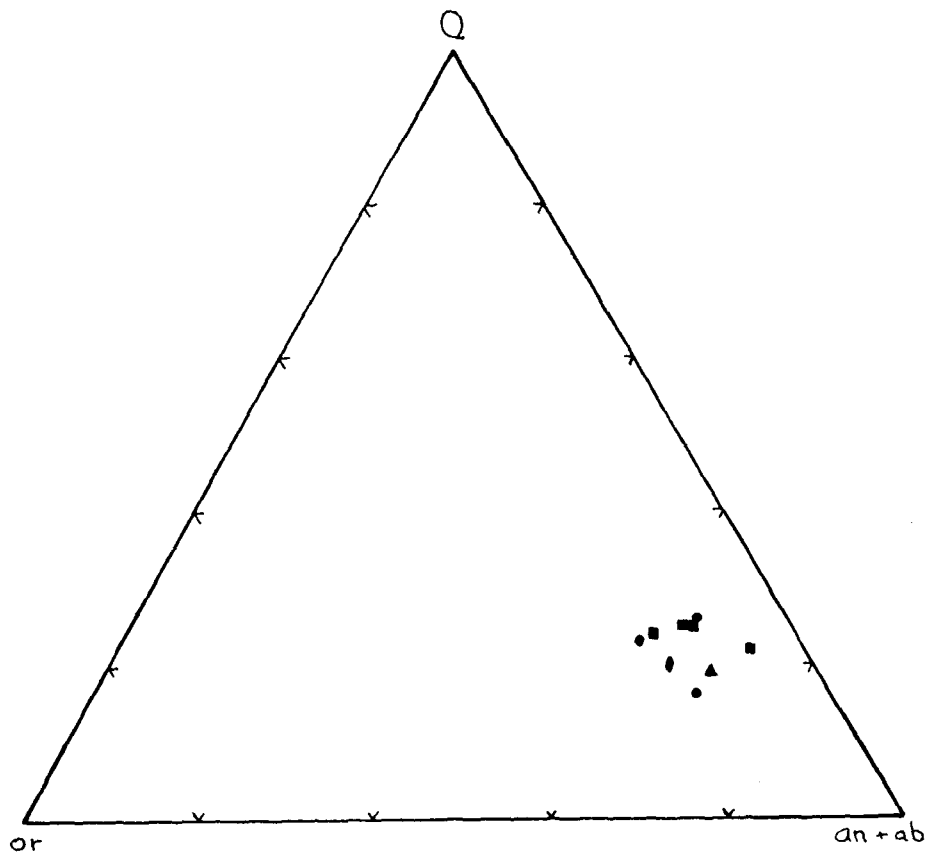
Figure 6.   Normative quartz-feldspar triangle for

unaltered rocks.

Porphyritic micro tonalite - ■

Porphyritic quartz micro diorite - ▮

Biotite ± Hornblende quartz diorite - ●

Aplite - X

Porphyritic andesite- ▲
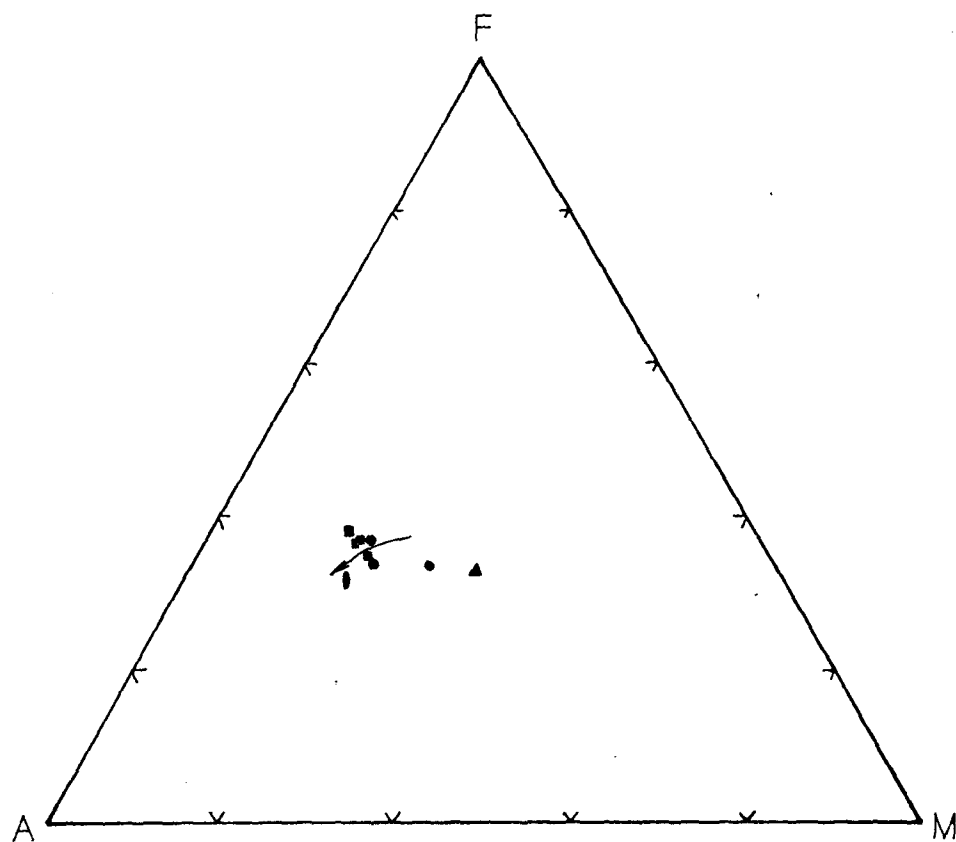
Figure 7.   FMA triangle for unaltered rocks
Possible trend is indicated.
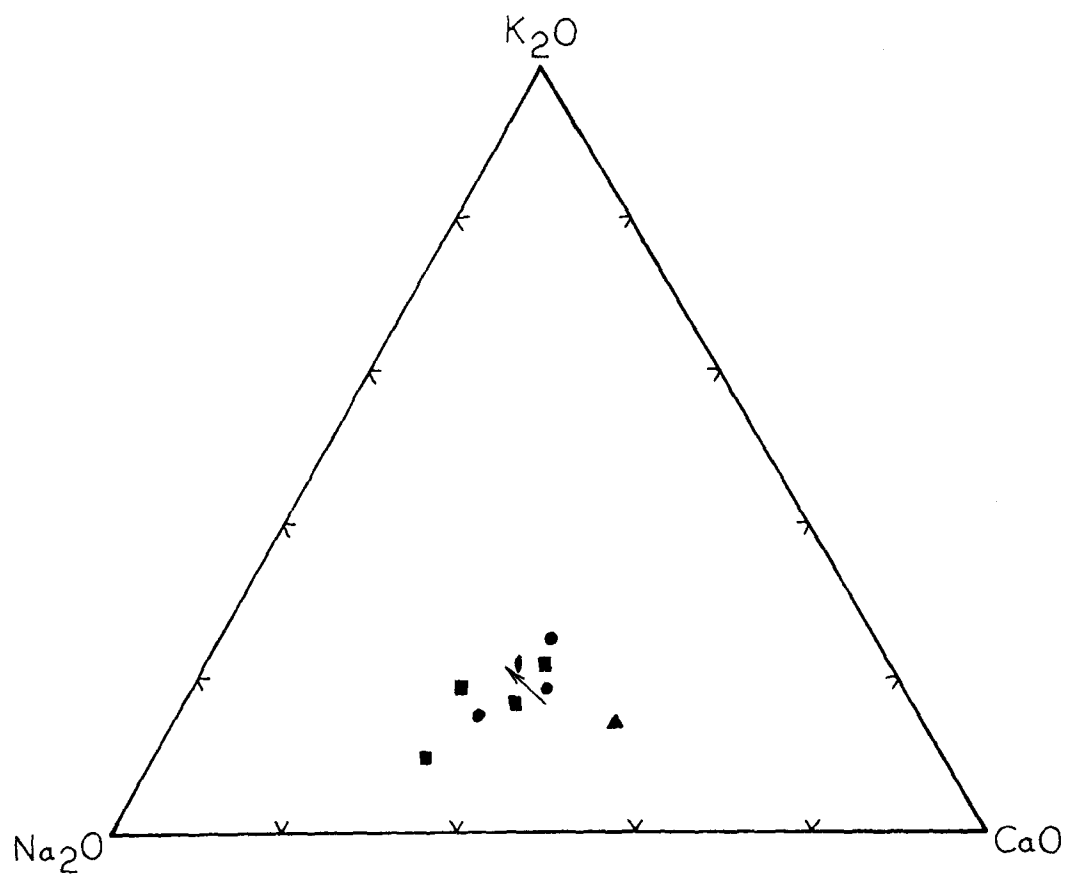
Figure 8.   KCN triangle for unaltered rocks

original igneous textures are identifiable, but the main
textural type recognized and most common could be termed a
porphyritic-aplitic texture.   Phenocrysts of andesine
(An 34 to An 38), biotite and quartz, 0.5 to 5mm in size,
in a sugary textured aplitic groundmass (0.05 - 1mm) which
consists of an interlocking mosaic of quartz and
plagioclase with disseminated minute specks of biotite.

Flow banding, foliation, and lineation of phenocrysts
are essentially absent from the rocks of the pluton,
indicating very little flowage or movement of magma after
the pluton was partially crystallized.   However, minor
lineation of plagioclase laths within dacitic dykes is
observed (plate 9).

Petrographic Description;

The micro tonalite is medium grained with an
allotriomorphic or hypidiomorphic granular texture.
Phenocrysts are abundant and the groundmass to phenocryst
ratio varies from 30 : 70 to 70 : 30.
Phenocrysts :- Plagioclase; anhedral to euhedral grains of
zoned and twinned plagioclase comprise 45 - 60 volume %
ranging from 0.5 to 5mm in dimension. Compositions
determined optically by normal to a method give Andesine;
An34 - An38 for rims and more calcic cores of composition
An44 - An48.   Several electron microprobe results for
plagioclase phenocrysts are shown in Appendix 3.   Minor.
alteration to sericite and/or calcite has occured along some
of the zones or fractures.
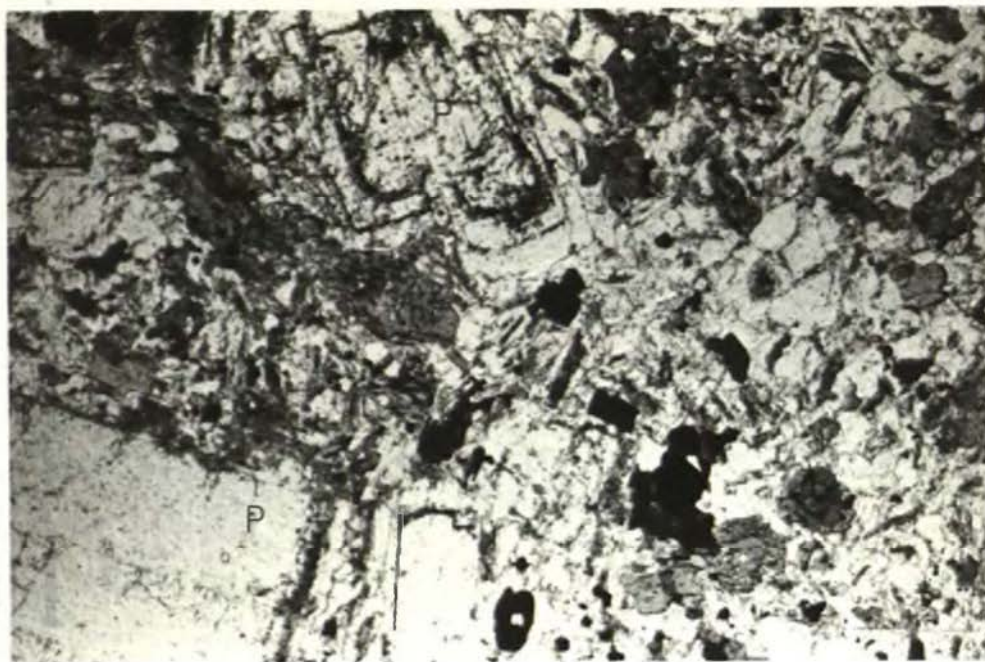
Plate 3:   Porphyritic biotite hornblende quartz diorite
            (E28/311.5').   Plagioclase (P) phenocrysts
            within a matrix of feldspar, quartz,
            hornblende (h), biotite (b) and opaques.
            (Plane polarized transmitted light).
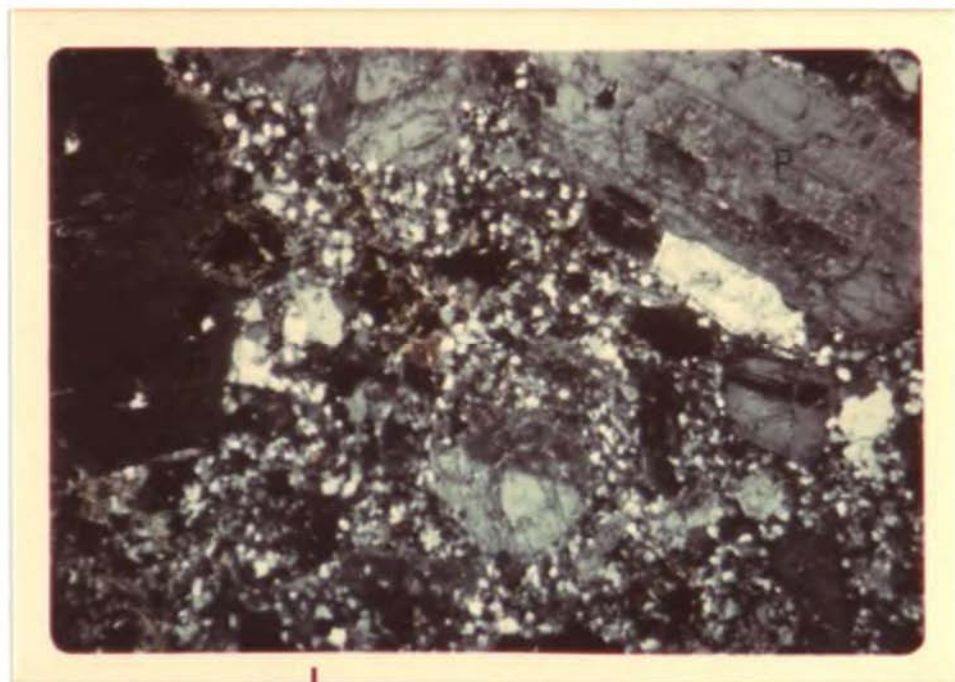
Plate 4:   Porphyritic biotite quartz diorite (CL 269).
            Phenocrysts of plagioclase (P) and
            biotite (B) in a feldspar, quartz, biotite,
            opaque matrix.
            (Transmitted light, crossed nicols).
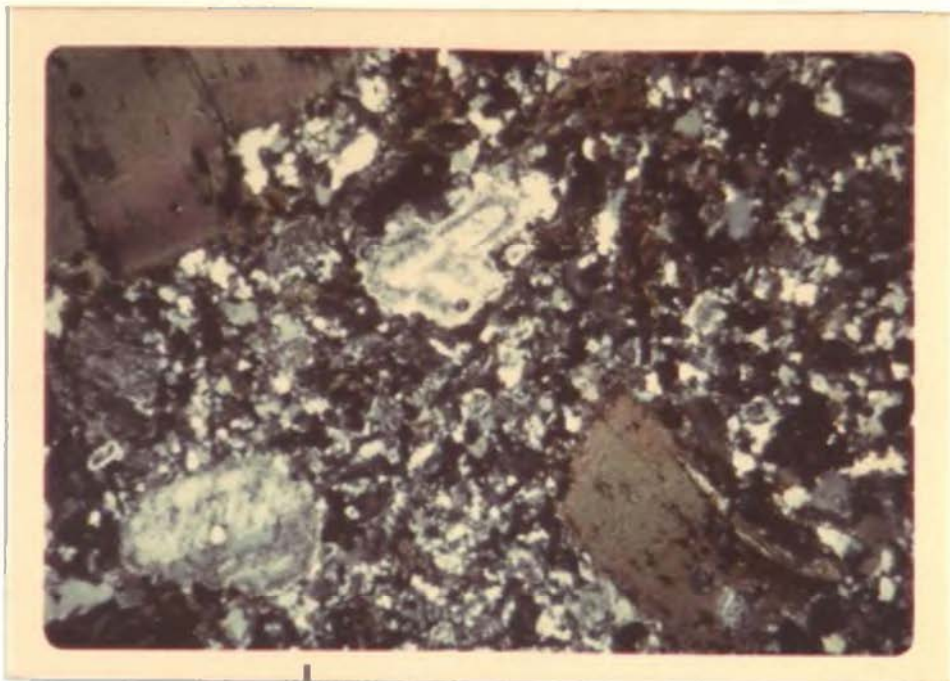
Plate 5:   Porphyritic biotite quartz diorite (CL 265).
            Phenocrysts of plagioclase and biotite
            within a matrix of feldspar, quartz,
            biotite and opaques.
            (Transmitted light, crossed nicols).

Plate 6:   Porphyritic biotite tonalite (CL 626).
            Plagioclase (P) phenocrysts in biotite,
            quartz, feldspar and opaque matrix.
            (Plane polarized transmitted light).
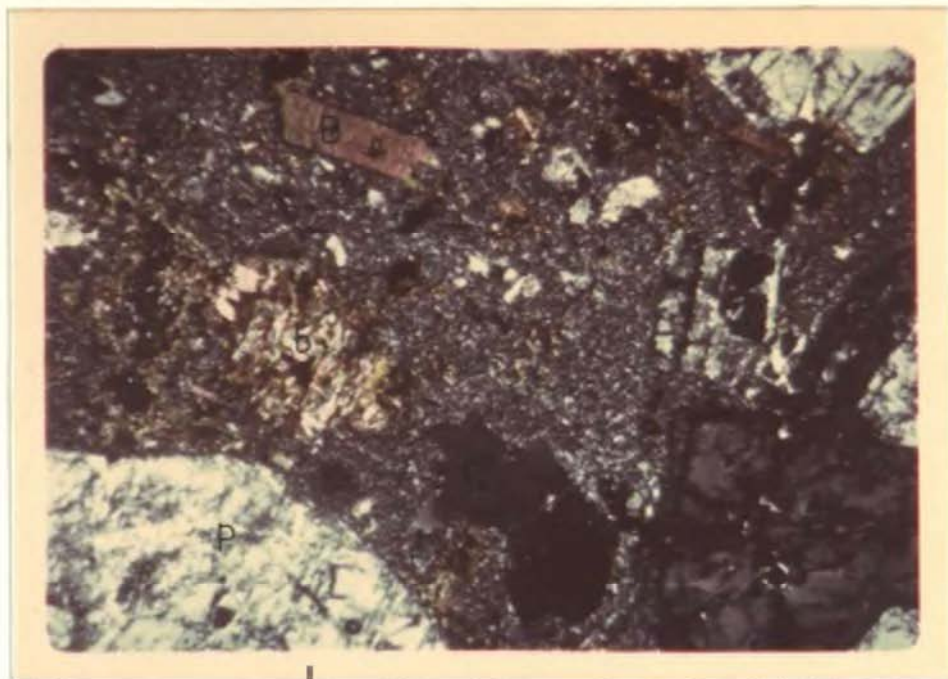
Plate 7: Porphyritic microtonalite (CL 611).
          Phenocrysts of plagioclase (P), resorbed
          quartz (Q), and biotite (B) in a very
          fine grained matrix of feldspar, quartz,
          biotite and opaques. Hydrothermal
          biotite (b) pseudomorphs magmatic
          hornblende.
          (Transmitted light, crossed nicols).
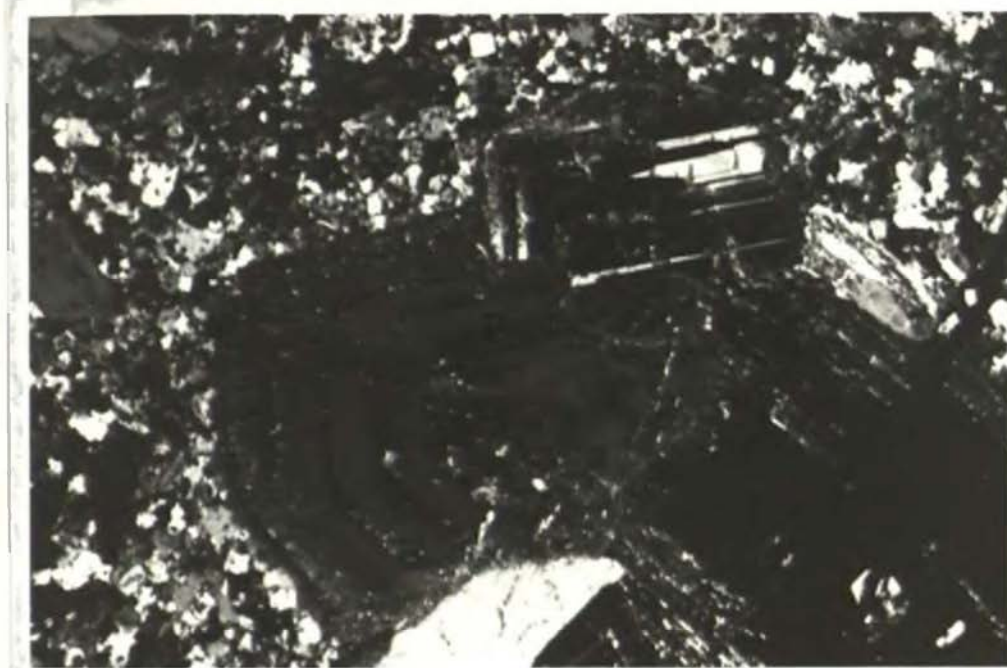
Plate 8: Porphyritic quartz diorite (CL 537).
          Zoned plagioclase phenocryst (P), showing
          minor fracture, cleavage and zonal
          alteration to sericite and calcite,
          within a quartz, feldspar, biotite matrix.
          (Transmitted light, crossed nicols).
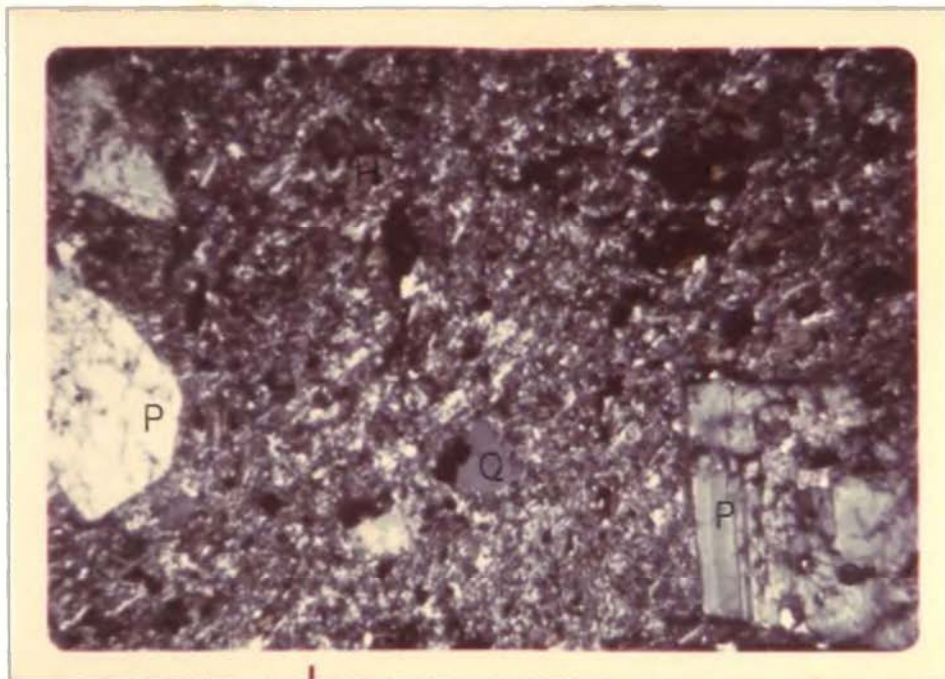
Plate 9:   Porphyritic dacite dyke (CL 156).
            Phenocrysts of plagioclase (P), quartz (Q)
            and hornblende (H), altered to chlorite,
            within a fine grained feldspar, opaque
            matrix.
            (Transmitted light, crossed nicols).

Quartz; anhedral grains usually 1 - 5% by volume but up to 10% in "quartz eye" diorite. Minor resorbed outlines with grains ranging in size from 1mm to 2mm in size.

Biotite; subhedral to euhedral books, flakes or aggregates of biotite showing strong pleochroism from red - brown to fawn. Pleochroic scheme;

α straw yellow, browny yellow or fawn.

$\beta=\gamma$ dark brown or reddish brown.

Biotites comprise 5 - 25% by volume depending on degree of hydrothermal alteration, but has suffered minor retrograde chloritization. Sizes range from 0.5 - 5mm.

Groundmass:- Composed of an equigranular mosaic of anhedral grains of plagioclase, quartz, biotite, hornblende with traces of K - feldspar, apatite, zircon, sphene, rutile, magnetite and haematite. Commonly fine grained and < 1mm.

Veins:- Quartz commonly occurs in veins with or without K-feldspar or sulphides.

The porphyritic microdiorite variety is essentially very similar to that above, but lacking in quartz phenocrysts and may have more amphibole and/or biotite.

The andesitic - dacitic dykes are porphyritic to glomeroporphyritic with phenocrysts of plagioclase, hornblende and infrequent biotite and resorbed quartz, in a

microcrystalline pilotaxitic groundmass of plagioclase,
altered mafic minerals and opaques.   The phenocrysts of
plagioclase (mainly andesine) are subhedral and up to 2mm in
diameter and commonly altered to calcite and epidote.
Hornblende occurs also as subhedral crystals up to 2mm in
size altering to chlorite and epidote.   In all, the
phenocrysts comprise between 20 - 40% by volume of the rock.
The dacitic dykes contain embayed or corroded phenocrysts of
quartz which is lacking in the andesitic dykes.

Large parts of the stock probably crystallized
from a quartz diorite magma with suspended crystals of
plagioclase, hornblende, biotite and quartz that was
injected into the intersection of regional faults.   Initial
crystallization at the margin of the intrusion produced a
shell of medium to fine grained porphyritic quartz diorite or
tonalite around a central mass of partially crystallized
magma.   Subsequent tectonic adjustments may then have
reactivated old fault structures that fractured the solid
shell and led to emplacement of dykes.

The remainder of the magma apparently crystallized
rapidly, possibly at the time of dyke emplacement, producing
a porphyritic - aplitic texture in the centre of the stock
as well as in the dykes.

Volatile constituents released from the magma during
quenching and rapid crystallization of the quartz diorite or
tonalite were probably instrumental in producing mineraliz-
ation and alteration of the stock and adjacent wall rocks.

This is consistent with Neale's (1974) observations of fracture intensity increasing outwards toward the intrusive contacts and decreasing with depth.

BARAMBAH BASALT:-

Post-intrusive Pleistocene flows of olivine basalt encroached into an extension of the southern valley where drill core enabled relatively fresh samples to be found. The flows alternate from highly vesicular to dense fine grained olivine basalt with common fossil soil horizons developed at the top of each flow.   At least six separate basalt flows have been recorded in the southern area (Ashley, 1975, pers. comm.).

Thin section examination shows subidiomorphic to idiomorphic corroded microphenocrysts of olivine, and minor diopsidic augite and/or titanaugite in an inter-granular or subidiomorphic groundmass of labradorite laths and clino pyroxene, with fine acicular crystals of probably titanomagnetite and a brown - green interstitial glass.

RECENT ALLUVIUM:-

Valley fill, gravel and sands now cover most of the valley floors while the hillsides are mantled by scree, in places inhibiting detailed mapping.

CHAPTER 4.   HYDROTHERMAL ALTERATION and
              SULPHIDE MINERALIZATION.

Introduction.

Sulphide mineralization.

-    Oxidized zone.

-    Supergene zone.

-    Hypogene mineralization.

Hydrothermal alteration.

-    Terminology.

-    Previous alteration studies.

-    Alteration types - 1 Biotite Zone.
                         2. Feldspar destructive
                            or quartz-sericite-
                            pyrite   alteration.
                         3. Sericite-clay
                            alteration.
                         4. Chlorite-epidote-
                            carbonate zone.
                         5. Late retrogressive
                            alteration.

Zonation of alteration and mineralization.

4. HYDROTHERMAL ALTERATION

AND SULPHIDE MINERALIZATION

Within the Coalstoun prospect we have a
central elongated stock which has suffered hydrothermal
alteration and sulphide mineralization, possibly in the late
stages of crystallization. Primary hypogene sulphides
within the "Coalstoun Microtonalite" are pyrite, chalcopyrite
and molybdenite with traces of bornite which occur in a
zonal distribution with gangue minerals, the distribution of
which are crudely controlled by the shape and geometry of
the stock. Superimposed upon this zonal pattern has been
the effects of surface weathering and late retrogressive
effects.

The net resultant of all these effects is described
in the following chapter but briefly consists of an oxide
capping and an underlying supergene blanket in the surface
zones. Below this there exists a core of biotitization and
copper mineralization with outward progression to chloritized
intrusive and metasediment.

SULPHIDE MINERALIZATION:-

Mineralization is predominantly confined to the
intrusive rocks, but extension into the immediately surround-
ing metasediments also occurs.

The mineralization occurs in three distinct zones
within the prospect, viz. an oxidized zone, a supergene zone,

and hypogene mineralization; the last type being a major

concern of this thesis.

Oxidized zone:

Oxidation, represented by partial leaching of

sulphides, normally extends downward from the surface to a

maximum depth of approximately 25 metres. Complete leach-

ing may locally extend downward from the surface for a few

metres, though pyrite is normally visible in outcrop. Only

minor amounts of oxidized copper minerals are present in

this zone of partial oxidation, with rare turquoise and

malachite forming fracture and vein coatings or fillings.

Limonite is also common at the surface and comprises

haematite, goethite and jarosite; the former is more common

over chalcopyrite rich zones, whilst jarosite occurs over

pyrite rich zones (Ashley, 1975, pers. comm.)

The oxysalts of copper are readily soluble and

thus migrate downward or away, out of the system in ground-

water. Leaching has not usually been sufficiently intense

to remove all molybdenite from outcrop, and partial oxidation

has resulted in the formation of coatings of possible

ferrimolybdite.

In the downward movement of meteoric waters to

the water table, the waters become depleted in oxygen and

the pH progressively rises by reaction with gangue, and

their effectiveness or reactivity weakens.

Supergene   zone:

The capacity for a given metal to become involved

in the supergene enrichment process depends upon two major factors. Firstly, its affinity for sulphur in relation to other metals in the environment, and secondly, the degree of solubility of the secondary sulphides which may form. These factors determine the capacity of downward migrating metal oxysalts to react with the unaltered hypogene sulphides at, or below, the water table level, or more specifically, the prevailing conditions of Eh and pH of the environment. The maximum capacity for enrichment exists for those metals having highest sulphur affinity and lowest secondary sulphide solubility, well exemplified by copper.

The downward moving copper sulphate ($CuSO_4$), from the oxidized zone, reacts with chalcopyrite and pyrite to produce covellite (CuS). Further reaction between copper sulphate and covellite produced chalcocite (Cu_2S). Several possible reactions, including those of Stokes (1906) are given below;

$$5FeS_2 + 14CuSO_4 + 12H_2O \longrightarrow 7Cu_2S + 5FeSO_4 + 12H_2SO_4$$

$$4FeS_2 + 7CuSO_4 + 4H_2O \longrightarrow 7CuS + 4FeSO_4 + 4H_2SO_4$$

$$CuFeS_2 + CuSO_4 \longrightarrow 2CuS + FeSO_4$$

$$5CuFeS_2 + 11CuSO_4 + 8H_2O \longrightarrow 8Cu_2S + 5FeSO_4 + 8H_2SO_4$$

$$5CuS + 3CuSO_4 + 4H_2O \longrightarrow 4Cu_2S + 4H_2SO_4$$
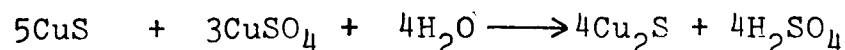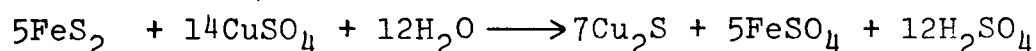
The above processes have been recognized in drill core by replacement textural relationships between the primary sulphides and covellite and chalcocite (plate 10). Characteristic sooty chalcocite is also noticed coating pyrite and fracture partings.

Plate 10:   Supergene sulphide replacement texture
            (E12/111').
            Chalcopyrite (cpy) replaced by
            covellite (cv) replaced by
            chalcocite (cc).
            (Plane polarized reflected light).
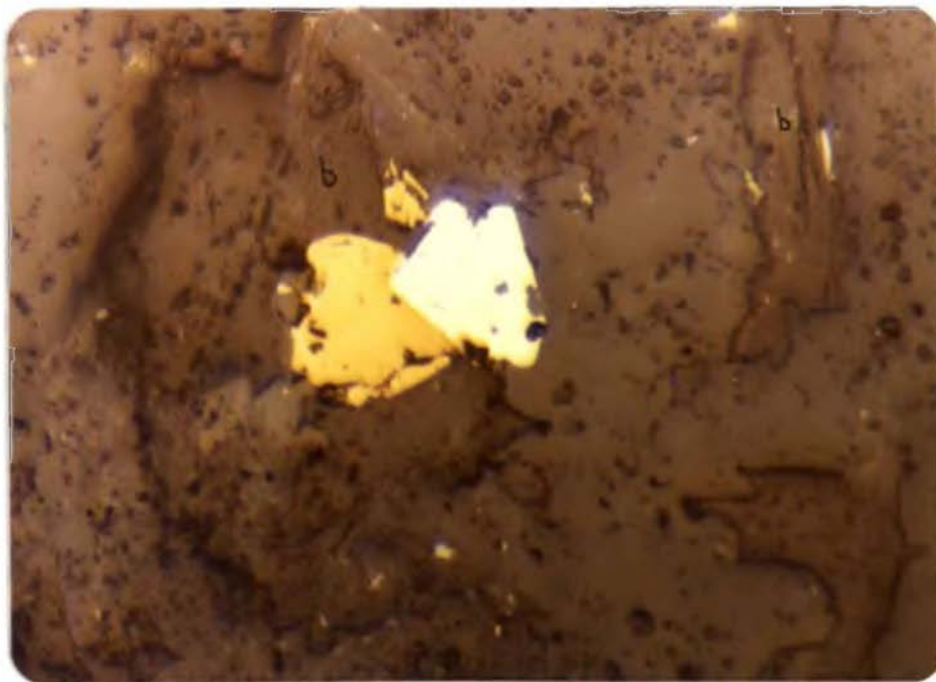
Plate 11:   Pyrite (white), chalcopyrite (yellow)
            associated with hydrothermal
            biotite (b) (E12/682.5').
            (Plane polarized reflected light).

The enrichment pattern of copper varies with depth, and is illustrated in continuous core assays over 10' intervals in figure 9.   Transitions above to oxidized-leached ore, and below to hypogene ore with contrasting mineral assemblages delineates this zone.

Hypogene Mineralization:

Below zones of active surface water interference within the intrusive the primary sulphides are chiefly pyrite, chalcopyrite and molybdenite.

The distribution of copper mineralization is shown in figures 10 and 11.   Mineralization is separable into three zones.   The first of these zones is a low grade deep core with low total sulphides and less than 0.2% Cu. The central zone in the stock is also low in total sulphides (averaging 1-2% by volume) but contains much of the chalcopyrite and molybdenite.   This zone is characterized by abundant quartz-K-feldspar veinlets, hydrothermal biotite, and unaltered to slightly altered igneous plagioclase. Copper within this zone is > 0.17% with pyrite-to-chalcopyrite ratios of approximately 1:1.

High grade 'pockets' within this zone contain > 0.34% Cu, and occasionally > 0.51% Cu (see figure 11). Pyrite-to-chalcopyrite ratios within these areas range between 1:1 and 1:2, or less.   Diffuse zones of increasing pyrite mineralization and successively more destructive alteration of plagioclase feldspar occurs outward from the centre of the stock.   This outer pyrite zone, the third zone,
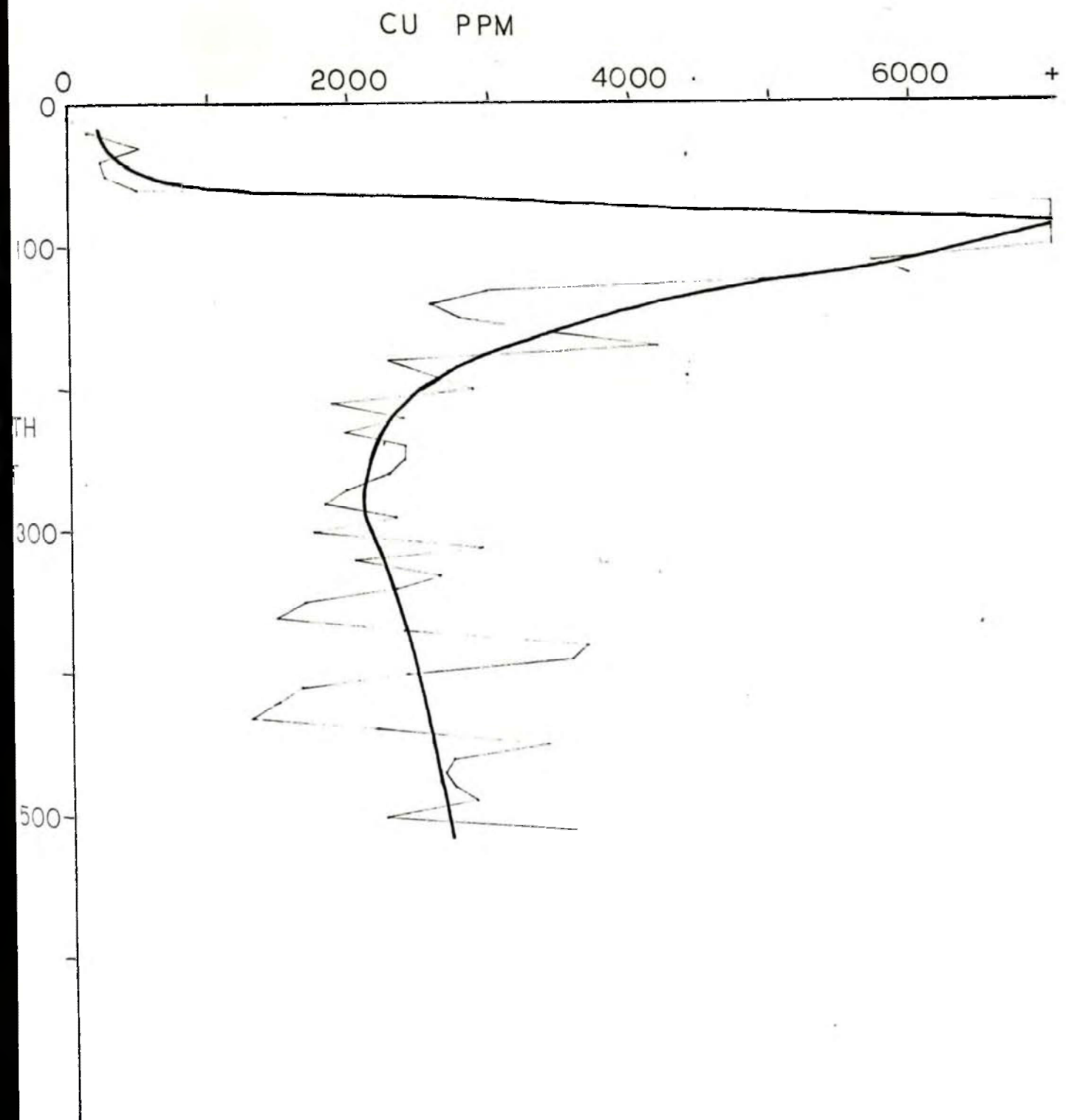
Figure 9.   Continuous drill core assays over 10'
            invervals; DDH 19.

Figure 10.   Plan for hydrothermal alteration and
                sulphide mineralization, with cross-section
                (C-D) mineralization variations.

LEGEND.
Cu mineralization.
> 5100 ppm (~1.5 wt% cpy).
> 3400 ppm (~1.0 wt% cpy).
> 1700 ppm (~0.5 wt% cpy).
(average for 50' intervals).
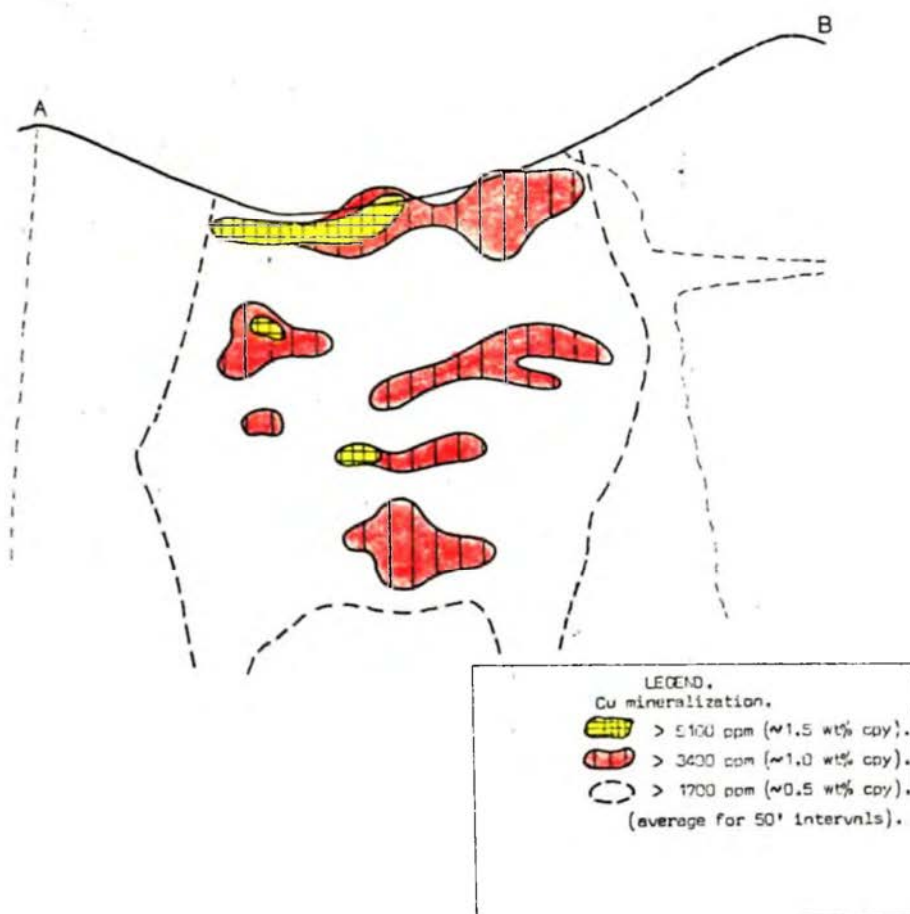
Figure 11.   Copper mineralization within cross-sectional
              projection.

forms a wide band into the surrounding wall rocks and a thin halo in the contact zones. Pyrite in this zone averages 4-10% by volume with pyrite-to-chalcopyrite ratios of > 10:1.   Pyrite, is the most common sulphide in the "Coalstoun Microtonalite" stock and is concentrated in veins with quartz-sericite alteration halos, in pockets of intense quartz-sericite alteration, and in the chlorite-carbonate-epidote alteration zones.

Chalcopyrite comprises 0.5 - 2.0 wt% in the core where the ratio is pyrite to chalcopyrite is < 2:1.   It occurs, together with pyrite, as fine disseminations associated with other ferromagnesian minerals, particularly biotite (see plate 11), and also within quartz-K-feldspar vein fillings and as fracture coatings.

Molybdenite is present chiefly within the core zone where it occurs as scattered flakes (plate 12) or rosettes, with chalcopyrite along thin fractures and more commonly as a constituent of narrow vitreous quartz^{+}-K-feldspar $^{+}_{-}$ pink albite veinlets.

Traces of bornite, sphalerite, galena and tetrahedrite have been observed in some polished sections. Bornite occurs in areas of intense copper mineralization and biotitization.   The other sulphides mentioned occur in infrequent veins.

Magnetite occurs as primary magmatic dissemin-ations averaging 1% by volume within the intrusive, where it has been partly replaced by haematite (plate 13).
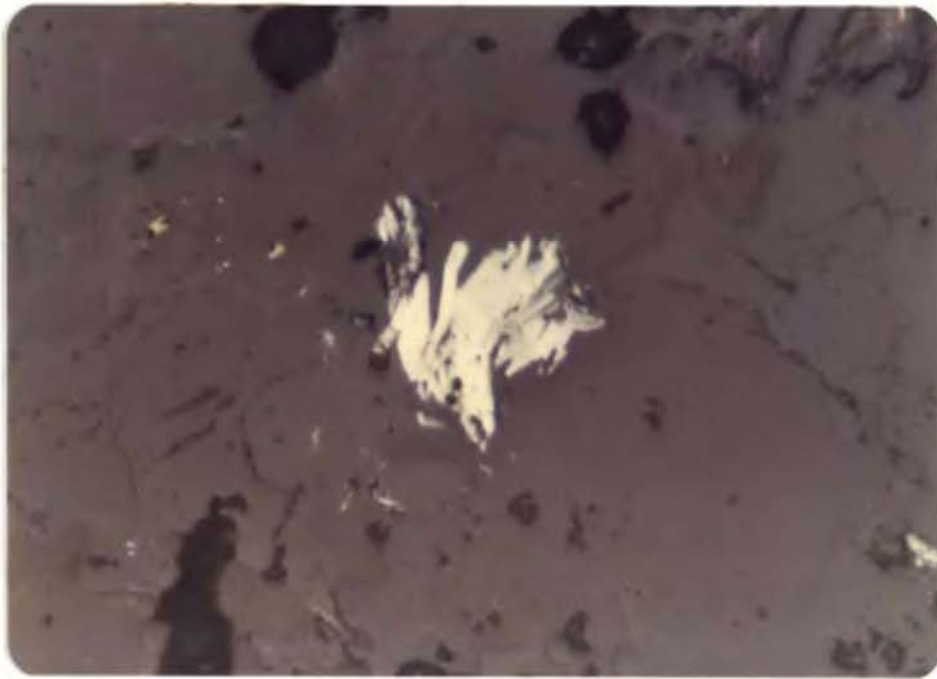
Plate 12: Molybdenite flakes (blue white)(E12/387').
           (Plane polarized reflected light). $\underset{mm}{\overset{0 \qquad\qquad .2}{\rule{2cm}{0.4pt}}}$
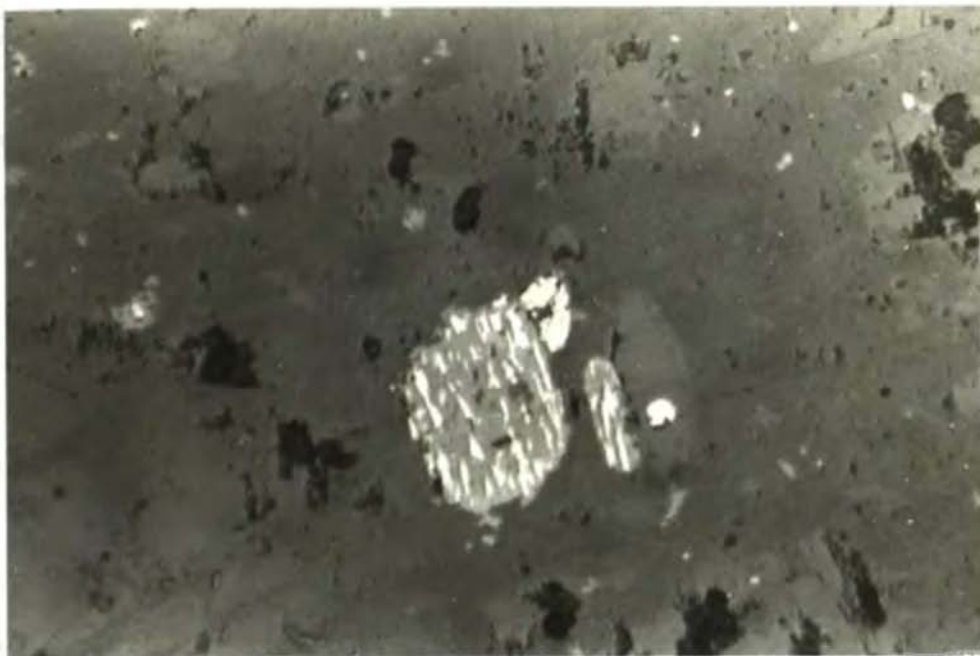
Plate 13: Martitization of magnetite (CL 707).
           Magnetite (light grey) altering to
           haematite (white grey) in
           silicates (dark grey).
           (Plane polarized reflected light). $\underset{mm}{\overset{0 \qquad\qquad .1}{\rule{2cm}{0.4pt}}}$

Magnetite also occurs in fine veins associated with chalcopyrite. Gold assays were reported by Neale (1974) to show strong positive correlation with copper, with averages of 30 - 55 ppb. One 10' interval assayed 2700 ppb (figure 16c).

HYDROTHERMAL ALTERATION:-

Terminology:

Lowell and Guilbert (1970) used the terms propylitic, argillic, phyllic, and potassic to describe the effects of hydrothermal alteration within porphyry copper deposits. They (Lowell and Guilbert, ibid, p.376) defined these types of alterations by the following assemblages:-

propylitic	chlorite - calcite - epidote - adularia - albite.
argillic	quartz - kaolin - montmorillonite - chlorite - biotite.
phyllic	quartz - sericite - pyrite with less than 5% kaolin, biotite, or K-feldspar
potassic	introduced or recrystallized K-feldspar and biotite, with minor sericite, and highly variable but persistant and generally minor amounts of anhydrite.

These terms have been widely used in the literature in current years, and though they **vary** in precise definition and

detail (Burnham, 1962; Creasey, 1959, 1966; Meyer and Hemley, 1967; Lowell and Guilbert, 1970; and many more), they accurately describe zonal sequences consisting of a peripheral propylitic zone with inward progression to a potassic core. Mineralization is regarded as conformable to these alteration zones, with the ore zone overlapping the potassic and phyllic zones (Lowell and Guilbert, 1970).

As with some British Columbian porphyry copper deposits (Carson and Jambor, 1974), the phyllic zone is not well developed at the Coalstoun prospect, and the ore is closely associated with secondary biotitization, so a new approach must be found.

Following similar methods of Bray (1969), Carson and Jambor (1974), Fountain (1972) and Rose (1970), the type of hydrothermal alteration at the Coaltoun prospect is named according to the principal alteration minerals present. Two main alteration types occur, these being the biotite zone and the chlorite-epidote-carbonate zone, with minor quartz-sericite-pyrite and clay-sericite types. These types roughly correspond to potassic, propylitic, phyllic and argillic respectively, but this terminology is not used as it is less descriptive and liable to some ambiguity.

In regard to the distinction between wallrock and pervasive alteration, the definitions proposed by Fountain (1972) are adhered to in this thesis. He regards alteration as all changes which are interpreted as resulting from reactions between solid rock and circulating fluids, and he

distinguishes between wall rock and pervasive alteration
where the former has an obvious relationship to veins and
fractures, and the latter has no relation to such veins or
fractures but is evenly disseminated through the rock.
The intensity of a particular alteration type is used in
reference to pervasive alteration where hydrothermal mineral
assemblages dominate, having destroyed most of the original
rock textures, eg. strong biotitization.

Previous Alteration Studies:

Neale (1974, p.3) reported the presence of varying
degrees of hydrothermal alteration with recognition of
"propylitic, phyllitic, and potassic alteration facies" but
these were discussed only to the extent of outlining the
major mineralogical changes.

Graham (1975) attempted to assess drill core logs in
terms of an alteration pattern using the logs of several
company geologists. However, with the complete lack of
petrological study and consequent inaccuracies his work was
severely hindered. He did however recognize what he termed
to be a potassic core, a sodic halo and a feldspar destruc-
tive zone, as well as propylitically altered intrusive and
country rock and late retrogressive effects. No zones were
delineated sufficiently to be portrayed on maps or sections,
though he believed the type fitted the model proposed by
Lowell and Guilbert (1970).

It is therefore the major aim of this thesis to
describe the alteration pattern more accurately by

petrological and analytical investigations.   To this end

the available (and accessable) drill core was examined,

sampled, relogged and the results of the overall investi-

gations described in the following chapters.

Alteration Types:

     1.   Biotite Zone:

Five significant types of biotite occur in rocks of

the "Coalstoun Microtonalite" and these are listed below:

     i.   Large euhedral, bright black, shiny books or

flakes representing primary magmatic biotite;

     ii. Aggregates of small flakes pseudomorphous after

preexisting mafic minerals, eg. hornblende and biotite;

     iii. Pervasive fine replacements of groundmass

feldspars giving a smoky-grey pigmentation to the altered

rock;

     iv. Hairline veinlet fillings with chalcopyrite and

other alteration silicates;

     v. Microscopic fringe replacement of magmatic

biotite.

     All, with the exception of euhedral magmatic biotites,

are products of hydrothermal alteration and referred to as

hydrothermal biotite.   Rocks which show presence of hydro-

thermal biotite, either megascopically or microscopically,

were placed within the biotite zone.

     Microscopically, the primary magmatic biotite is

coarse grained (up to 5mm in size), euhedral, and shows a

distinct red-brown to fawn pleochroism.   Contrary to this

Plate 14: Felted mat of hydrothermal biotite
           pseudomorphically replacing hornblende.
           Magmatic biotite adjacent is preserved
           in a porphyritic microtonalite (CL 601).
           (Plane polarized transmitted light).
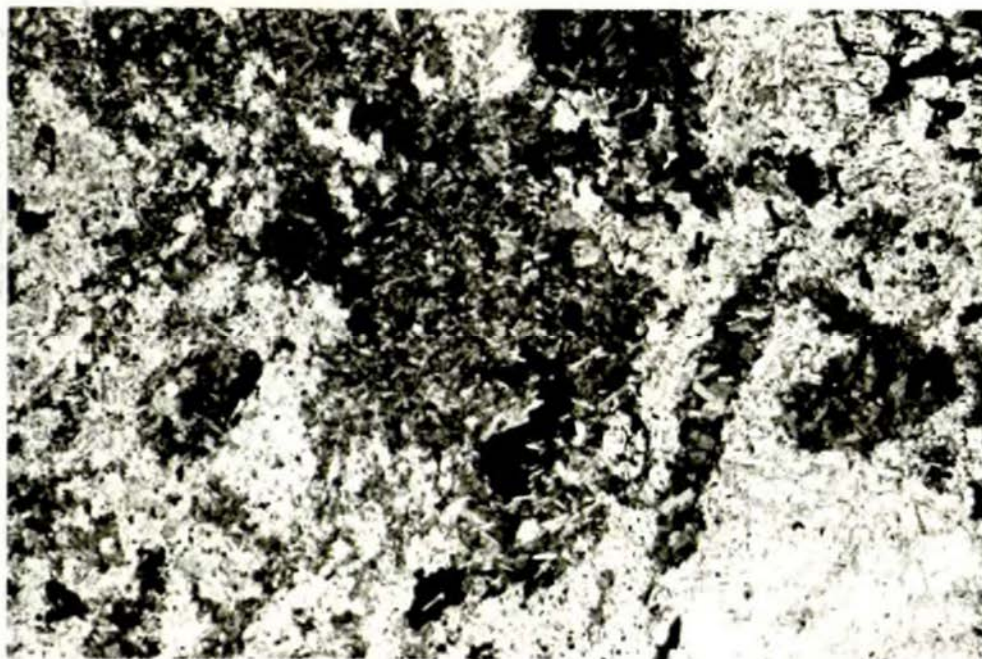

Plate 15: Hydrothermal biotites replacing both
           magmatic hornblendes and biotites,
           associated with sulphides (E12/401.5').
           (Plane polarized transmitted light).

however, are the pleochroic colours and the form of hydro-
thermal biotites, which lack the red tint and are much
finer grained.

Those hydrothermal biotites replacing amphibole
phenocrysts are pale brown with weak pleochroism, and occur
as a felted mat preserving the euhedral habit of the
replaced hornblende (plates 14 and 15). A similar type,
but coarser grained is also observed replacing magmatic
biotite, either partially, with relict cores of primary
biotite (plate 16), or totally so that no magmatic biotite
is preserved (plate 17). These typically have a greeny –
brown tint. Pleochroic scheme;

α - greeny yellow or greeny brown.

$\beta=\gamma$ - dark greeny brown.

Hydrothermal biotites pervasively replacing ground-
mass feldspars are generally fine grained, sugary-textured,
pale brown to greenish in colour, and are commonly associated
with anhydrite and sulphides (plate 18). Fringe replacements
of biotite phenocrysts occasionally occurs by a very fine
grained greenish biotite (frontispiece, and plate 19) which
has a higher birefringence than the coexisting replaced
biotite. These primary magmatic and hydrothermal biotites
differ markedly in several chemical components and will be
discussed in chapter 6.

The abundance of pseudomorphic and sugary-textured
matrix hydrothermal biotites varies within the biotite zone.
Areas of intense matrix biotitization (plate 20), with an

Plate 16: Magmatic biotite (core) partially replaced
by hydrothermal biotites and sulphides
(E12/401.5').
(Plane polarized transmitted light).

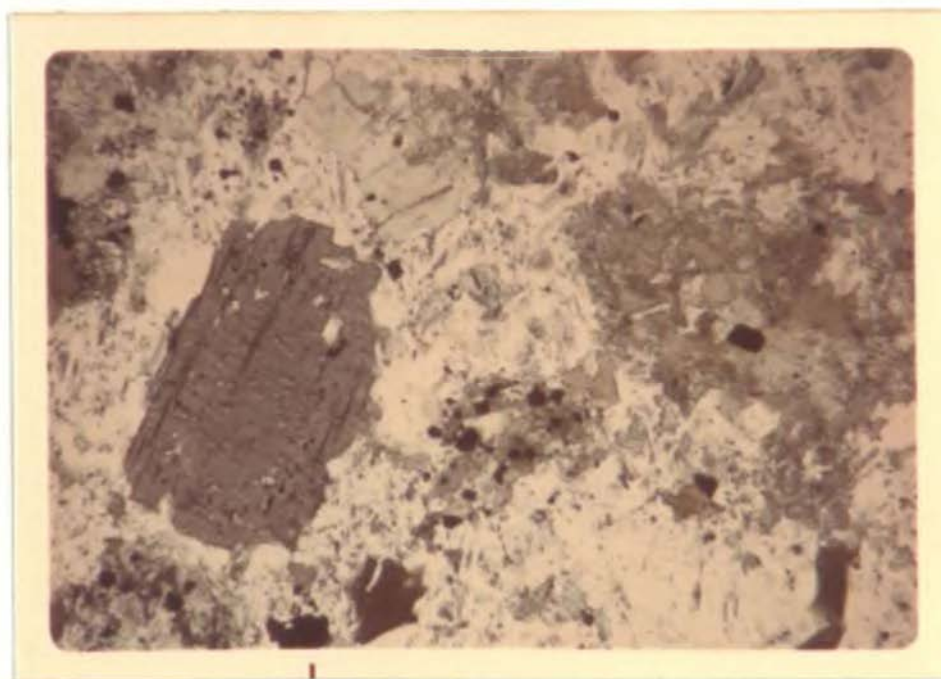Plate 17: Magmatic biotite phenocrysts both fresh
and replaced by hydrothermal greenish
brown biotites, and sulphides (CL 614).
(Plane polarized transmitted light).
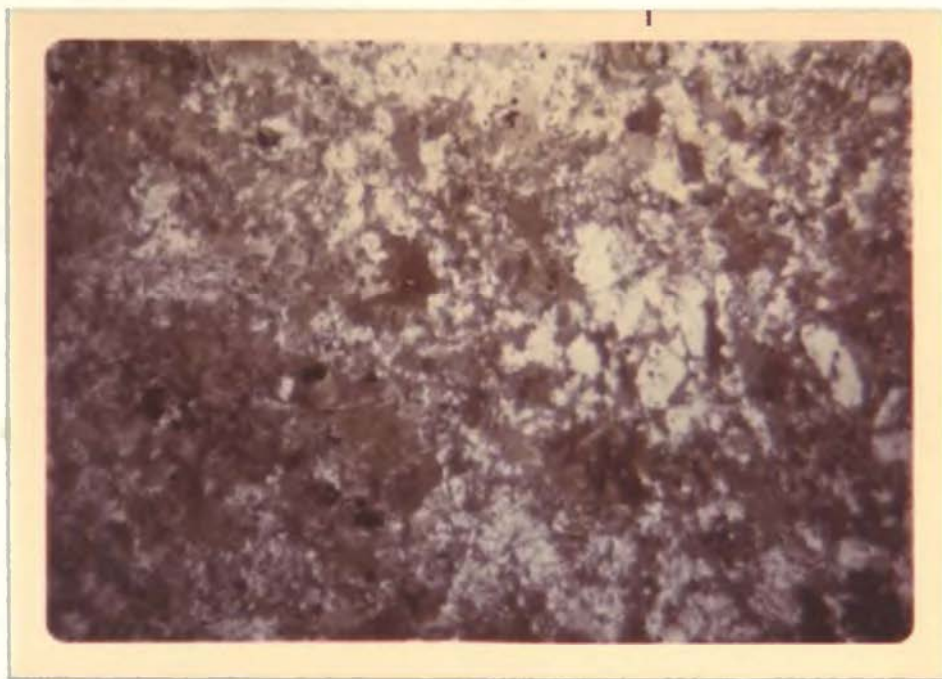
Plate 18: Sugary textured pervasive greenish brown
hydrothermal biotites (E12/401.5).
(Plane polarized transmitted light).

Plane 19: Magmatic biotite phenocryst fringed by
greenish hydrothermal biotite (CL 269).
(Plane polarized transmitted light).

absence of magmatic biotite, are also areas of high copper

mineralization.   For example sample CL179 averages 45% by

volume biotite (predominantly all hydrothermal), and

contains 0.3 wt % Cu with a pyrite to chalcopyrite ratio

of ≪ 1:1.

    Within the biotite zone, areas of decreasing

intensity biotitization also show decrease in copper

contents and increasing pyrite to chalcopyrite ratios.

Movement away from intense biotitization is therefore marked

by five factors;

  i.   decrease in abundance of matrix biotite,

  ii. increase in content of magmatic biotite,

  iii. a higher proportion of hydrothermal biotite as

    amphibole pseudomorphs,

  iv. a decrease in copper grade, and

  v.   an increase in the pyrite to chalcopyrite ratio.

    In addition to the above, several other aspects of

hydrothermal alteration were observed within this zone.

Plagioclase retains a fresh appearance, although minor

replacement by phyllosilicates (dominantly sericite) along

cleavage, fractures and compositional zones occurs

microscopically.   The presence of anhydrite, of character-

istic lavender to place brown colour in hand specimen,

occurs associated with hydrothermal biotite.   Rutile is

present and originated from the titanium that was present in

magmatic biotite and amphiboles during alteration.   These

rutile grains occur as small prismatic crystals, often in

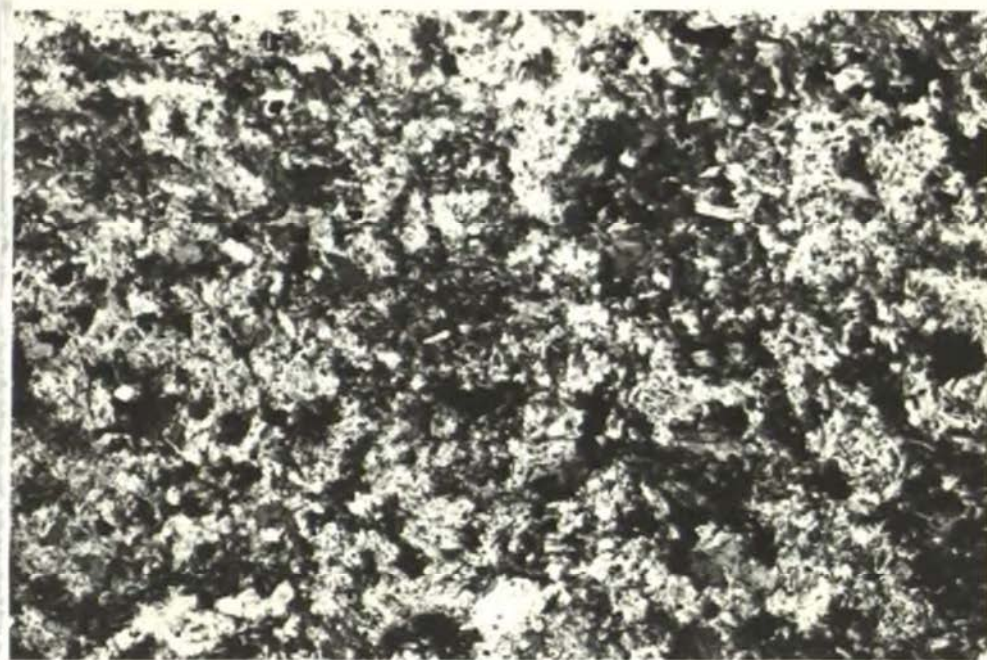small concentrations, and adjacent to hydrothermal biotites.

Plate 20:   Intense matrix biotitization (E12/401.5').
             (Plane polarized transmitted light).

One occurence of fluorite was noted in drill hole E28, where it replaced magmatic biotite within a brecciated fragment of intrustive rock, and was accompanied by abundant anhydrite.

Stockwork of short irregular veinlets containing one or more of quartz, biotite, anhydrite, K-feldspar, chalcopyrite, pyrite, molybdenite and magnetite pervade the biotite zone. Quartz veinlets with or without K-feldspar, biotite, anhydrite or magnetite commonly carry sulphides and are generally earlier than veinlets carrying quartz alone. Marginal replacement of plagioclase by pink or white K-feldspar is common on these veinlets. Sulphides within the biotite zone are dominantly chalcopyrite with equal or lesser amounts of pyrite and subordinate molybdenite and bornite. Pyrite is uncommon in the most intensely biotitized areas of the intrusion but increase in amount toward the feldspar destructive alteration and chlorite-epidote-calcite alteration zones. These sulphides occur in veinlets, short hairline partings and as disseminations.

2. Feldspar destructive or quartz-sericite-pyrite alterations;

This type of alteration is not well developed at the Coaltoun prospect, but where observed it is typified by the pseudomorphic replacement of plagioclase phenocrysts by sericite; the latter commonly being a characteristic pale green colour.
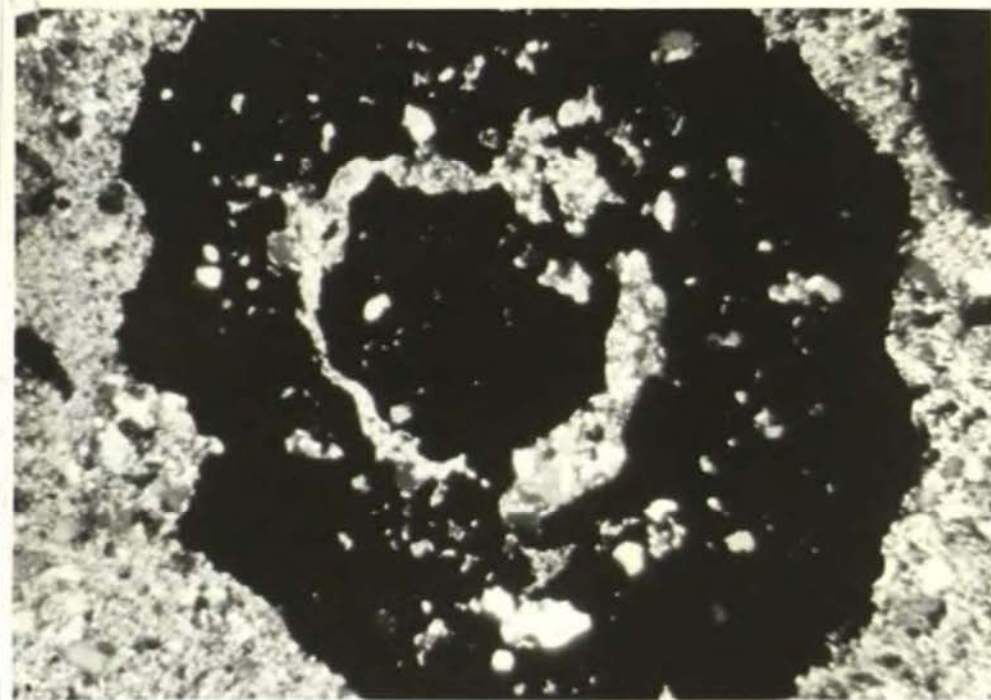
Plate 21:   Spherical pyrite with inclusions of quartz
            and sericite (CL 152).
            (Transmitted light, crossed nicols).

In some cases the green colour is absent and all trace
of a porphyritic texture has been lost, with the resultant
assemblage being of quartz-sericite-pyrite.   Commonly
pyrite forms spherical balls as in plate 21;   these balls
show numerous rings of inclusions of silicates and may
represent episodes of alteration or fluid activity.   The
pyrite present in these rocks is absent in the greenish
sericite-bearing rocks.

3.   Sericite - clay alteration;

Destructive alteration of feldspars is also present
within the leached, oxidized and supergene capping of the
prospect as well as in shear zones where sericite - clay -
chlorite assemblages prevail.   In the supergene zone
pyrite is still present along with chalcocite and covellite.
The clays present vary in abundance and type with the
dominant mineral species being kaolinite, with illites
and montmorillonites.

4.   Chlorite - epidote - carbonate zone;

The key identification minerals within this zone are
chlorite, epidote - clinozoisite and carbonate (predominantly
calcite) with trace abundances of albite, montmorillonite,
sericite, rutile, sphene, and Fe - carbonate.

Amphibole phenocrysts are pseudomorphically replaced
by chlorite with exsolution of titanium which forms a criss -

crossing network of rutile crystals (plate 22). Magmatic biotite phenocrysts, and occasionally relict hydrothermal biotites, were susceptable to replacement also by chlorite (plate 23), as well as carbonate and minor sericite. This replacement begins along cleavage planes in areas of weak to moderate alteration, and totally replaces the biotite phenocryst in zones of strong pervasive alteration (plate 24).

Plagioclase is replaced by sericite and carbonate (calcite) which penetrate along cleavage planes, fractures and compositional zones. In areas of more intense alteration the feldspars are replaced by fine granules of apple green epidote and calcite similar to plate 25. Feldspar phenocrysts within porphyritic andesite - dacite dykes are clouded due to the presence of montmorillonite and alteration to a bronze or flesh coloured albite.

The fine grained groundmass of the intrusive rocks within this alteration zone appears to be less altered than the phenocrysts, but closer to the biotite zone the matrix contains substantial amounts of chlorite, carbonate, sericite, pyrite and clay as compared to the contact zones.

Chlorite-epidote-carbonate alteration coexists with low grade copper mineralization in which pyrite is the dominant sulphide varying from 2-6 volume % and locally up to 10%, and chalcopyrite is rare. Pyrite to chalcopyrite ratios are always > 3: 1 and averages approximately 10:1. This alteration assemblage is seen in both the porphyritic intrusions as well as in the surrounding
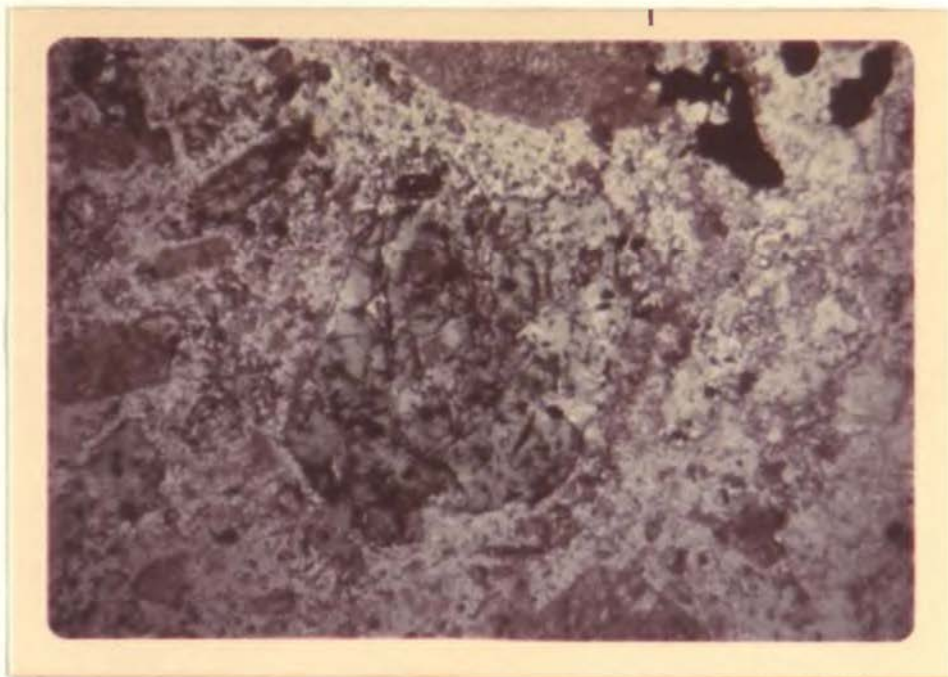
Plate 22: Amphibole pseudomorphed by chlorite (green)
with criss-crossing network of rutile
crystals. Feldspar phenocrysts altering
to clays (CL 253).
(Plane polarized transmitted light).

Plate 23: Biotite (dark grey) phenocryst being
replaced by chlorite (light grey) along
cleavage (CL 625).
(Plane polarized transmitted light).
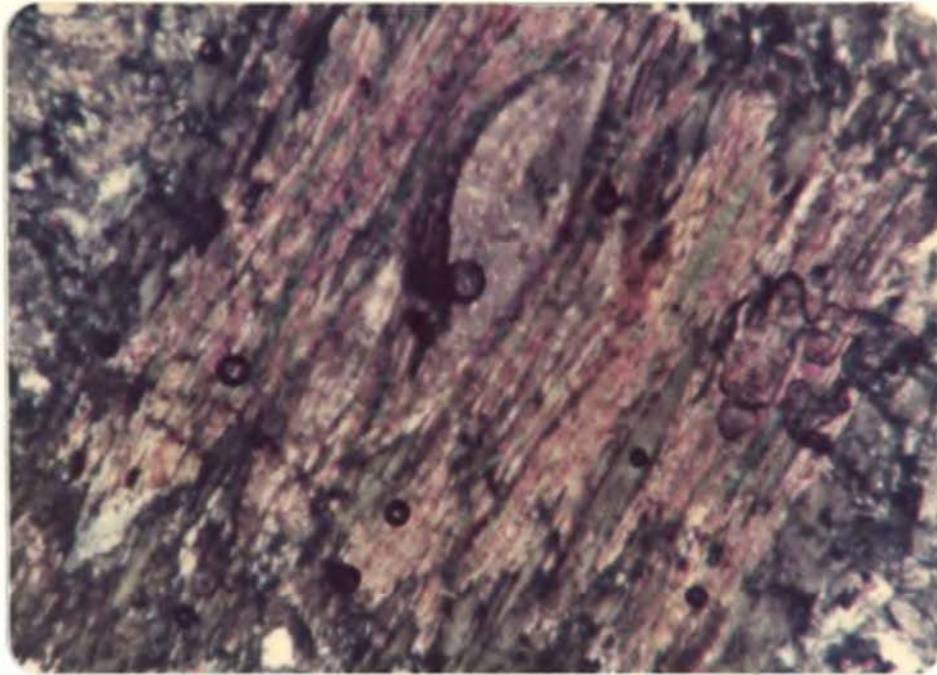
Plate 24: Biotite replaced by chlorite (green) and
calcite along cleavage planes (CL 538).
(Transmitted light, crossed nicols). $\underset{mm.}{0 \quad\quad 2}$
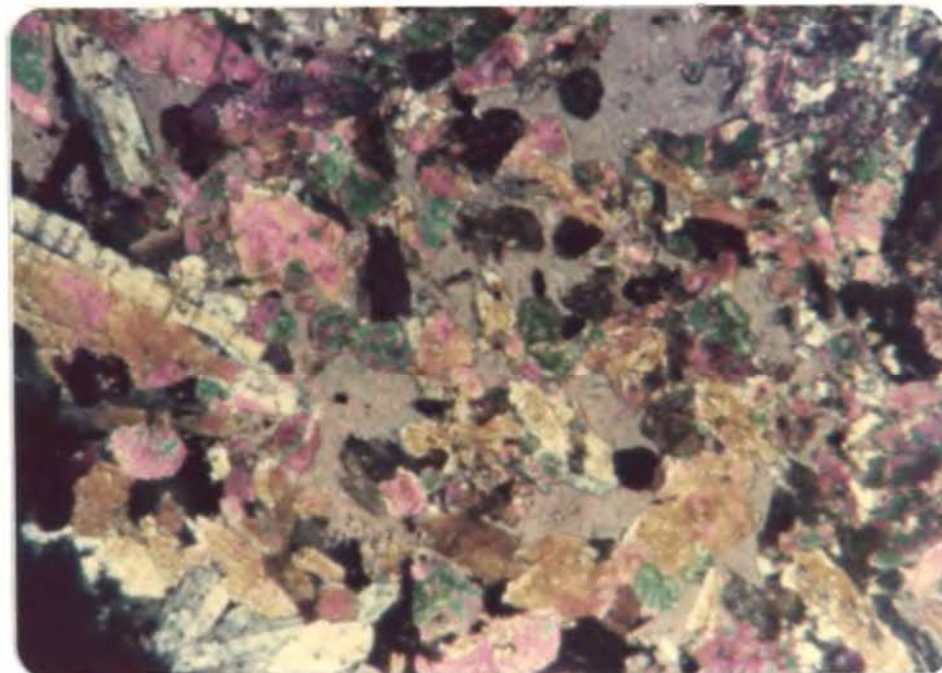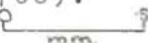
Plate 25: Epidote and calcite replacing both
phenocryst and matrix feldspars (CL 708).
(Transmitted light, crossed nicols). $\underset{mm.}{0 \quad\quad 5}$

metasediments.   Carbonate veining is ubiqiutous to this type
of alteration.

5.   Late Retrogressive Alteration;

Intense chloritization occurs accompanied by clay-
pyrite alteration halos, along slickensided shear zones.
Minor chlorite and carbonate also occur, replacing biotites
within the biotite zone, but they are less abundant than in
the chlorite-carbonate zone.

Gypsum is relatively common as veins, and is
typically colourless to orange-pink and semi fibrous and is
possibly a hydration product of anhydrite.

ZONATION OF ALTERATION AND MINERALIZATION:-

One of the major problems in mapping the alteration
pattern within the Coalstoun prospect is caused by the
separation of the intrusives by the metasedimentary ridges.
Compounded with this are the presence of inhomogeneities
within the intrusives themselves caused by the presence of
metasedimentry rafts, dykes (mainly andesitic to dactic),
faulting and brecciation, and minor bulk rock chemical
differentitation.

Graham (1975, p 18) recognized that the sulphide
content became "coarser and more abundant in the south -
central part" of the central valley around drill holes E12,
E14, E15 and E25 (plate 1), compared with finer grained
sparse sulphides in other outcrop areas.   Limonite

development also showed stronger development and was associated with a "higher grade of alteration due to deeper erosion" (Graham, ibid, p 18-19).

With these considerations in mind, it was decided to concentrate on the alteration pattern displayed in this area (figure 12) using a series of illustrative figures. Two diagramatic methods are used to locate the distribution of the alteration and mineralization; the first of which is a plan, elevation =150 m ASL, results of which are shown in figure 14; and the second is a cross-sectional projection approximately striking NE-SW through drill holes E15 and E18 (figure 12). Drill holes up to 150 metres on either side of this section are projected onto the plane keeping the same topographic collar height (figure 13).

A well developed zonal distribution of the alteration types is present and comprises a central zone of hydro-thermal biotite alteration, which is surrounded by pockets or pods of feldspar destructive alteration (possibly related to faulting) which passes outward into chlorite - epidote - carbonate alteration.

This concentric alteration pattern is clearly centred on the porphyritic microtonalite intrusive stock and the economically most important type of alteration is that of hydrothermal biotite, within which all the signifi-cant Cu-Mo mineralization encountered is associated.

The distribution of these alteration types is shown on figures 14, 15 and 16; which are reductions of overlays
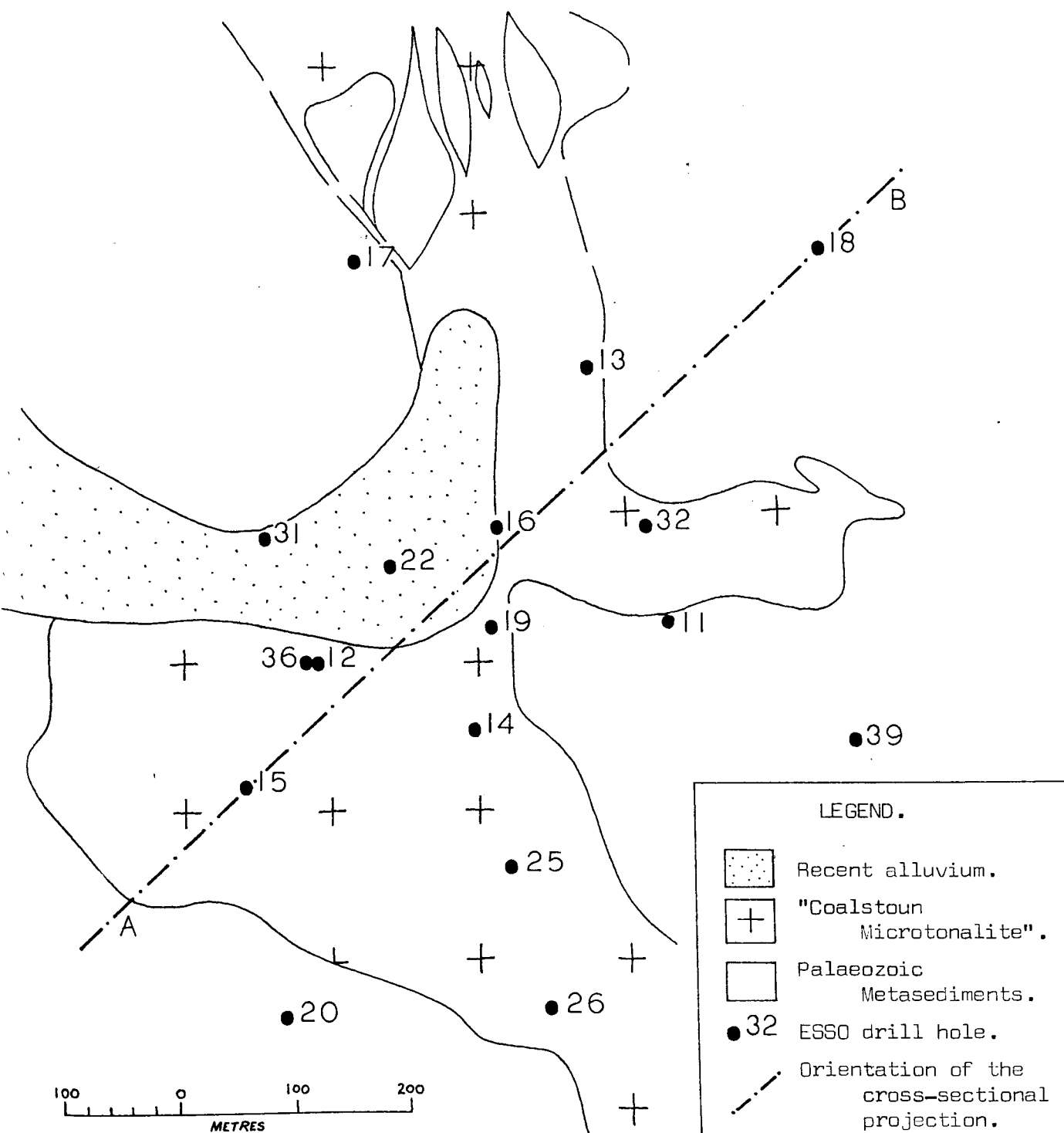
Figure 12.   Coalstoun prospect, surface geology plan.
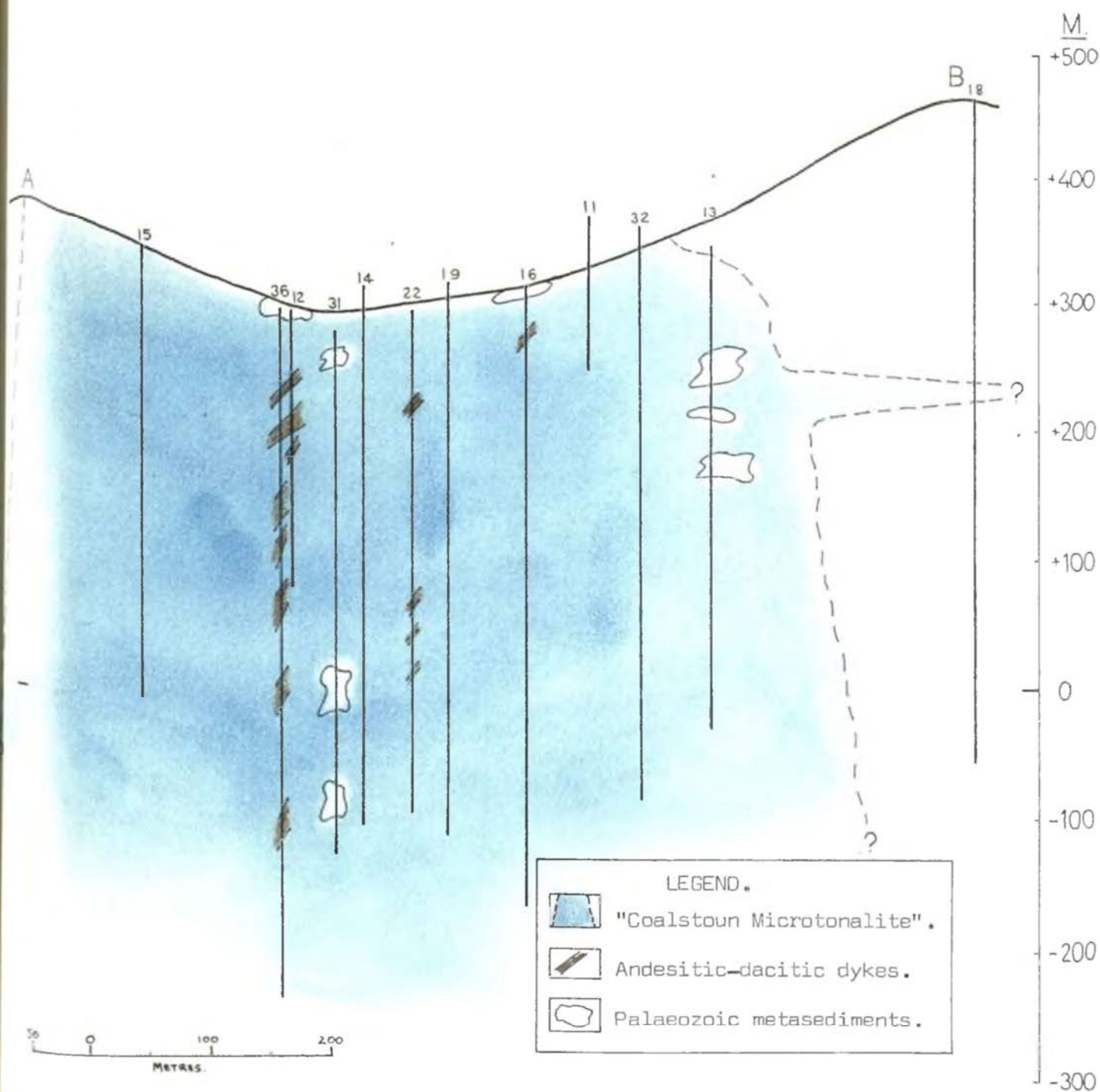
Figure 13.   Cross-sectional projection showing number,
position and depth of projected drill holes.

LEGEND (for figure 14)

- drill hole.

Pervasive alteration:-
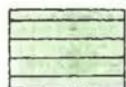
Strong hydrothermal biotitization.
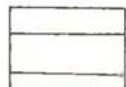
Weak hydrothermal biotitization.

Chloritization.

Pyrite: Chalcopyrite ratios:-

$< 1:1$.
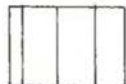
$2:1 - 1:1$.
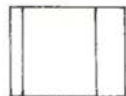
$5:1 - 2:1$.

Average sulphide content (volume %):-

limit of 2% sulphides.
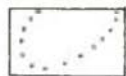
limit of 4% sulphids.

Copper content (from drill core assays):-
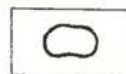
> 3400 ppm (≈ 1.0 wt % chalcopyrite).
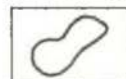
> 1700 ppm (≈ 0.5 wt % chalcopyrite).
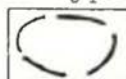
Rock types:-

inferred boundary of intrusion.
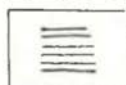
metasediment.
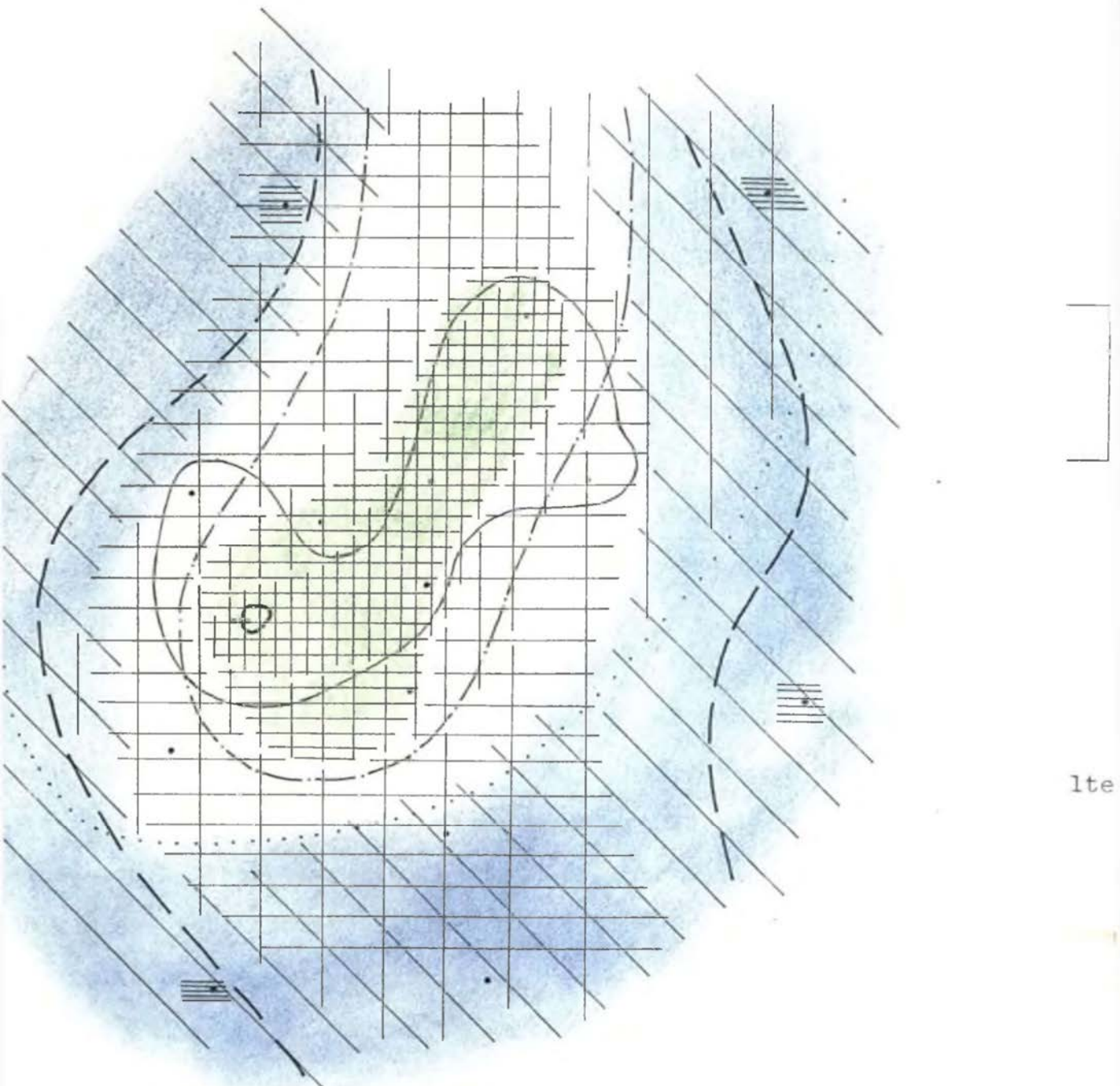
lte

Figure 14.   Plan of alteration and sulphide
              mineralization at +150 asl.

1-7 respectively and appended inside the ·rear cover.   The
use of the overlays facilitates the comparison between
intensity and type of alteration, abundances and ratios of
dominant sulphides, and copper and molybdenum
mineralization.

From examination of these diagrams it can be seen
that the chlorite-epidote-carbonate zone is confined to the
surrounding metasedimentary formations and the outermost
limits of the intrusive stock adjacent to the wall rocks.
The zone is defined by the abundance of chlorite in hand
specimen, along with other diagnostic minerals previously
mentioned in this chapter.   Sulphides within this zone are
always > 2% with pyrite to chalcopyrite ratios > 5:1 and
usually further away from the intrusive > 5% sulphides
exist with ratios >> 10:1.

Inward progression from the chlorite - epidote -
carbonate zone passes into the centrally located biotite
zone and is marked by the appearance of hydrothermal
biotite, characteristics of which have previously been
discussed.   The outer limits of this central zone possesses
only weak biotitization, sulphides ranging from 2-3% with a
pyrite to chalcopyrite ratio of 2 : 1 - 1 : 1.   The
core of this zone is marked by strong pervasive
biotitization with sulphides generally < 2% and a ratio of
pyrite to chalcopyrite at < 1:1.

The "orebody" is located entirely within this
biotite zone, as demarked by the 0.17% Cu limit (figure 16 b,
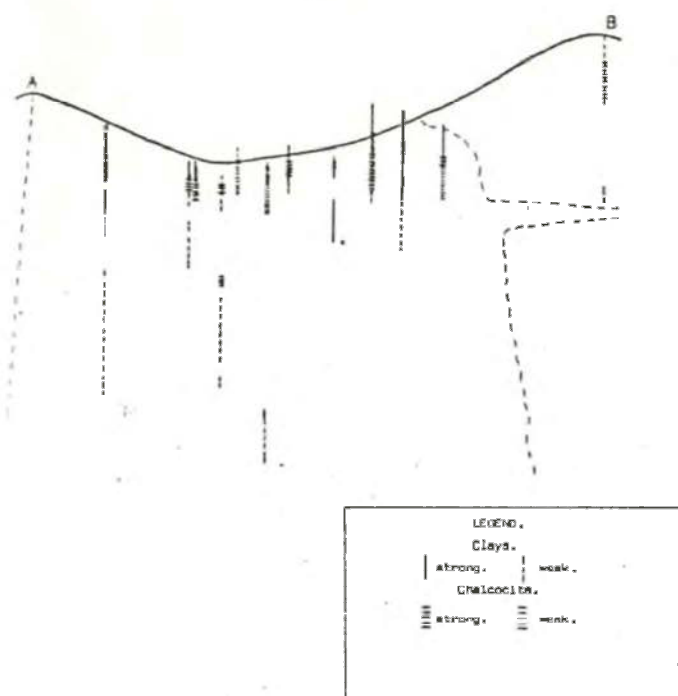
a.   Clay and chalcocite.

b.   Chloritization.

LEGEND.
Clays.
strong.   weak.
Chalcocite.
strong.   weak.

LEGEND.
Chloritization.
strong.   weak.
F   Fault or shear zone.
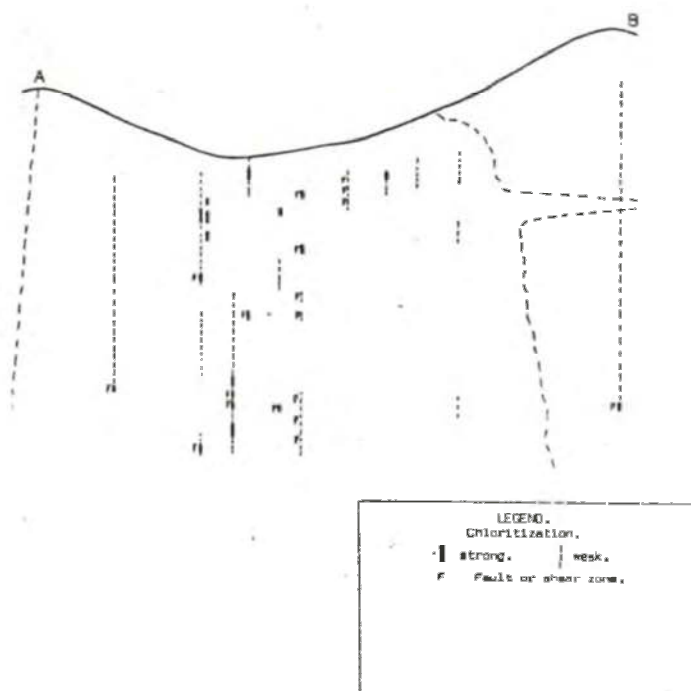
Figure 15.   Cross-sectional projections of alteratic

mineral intensities.
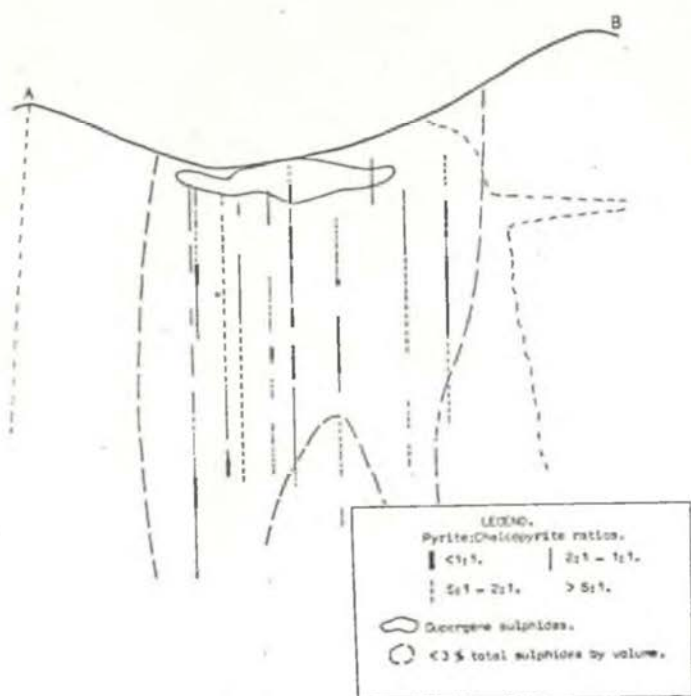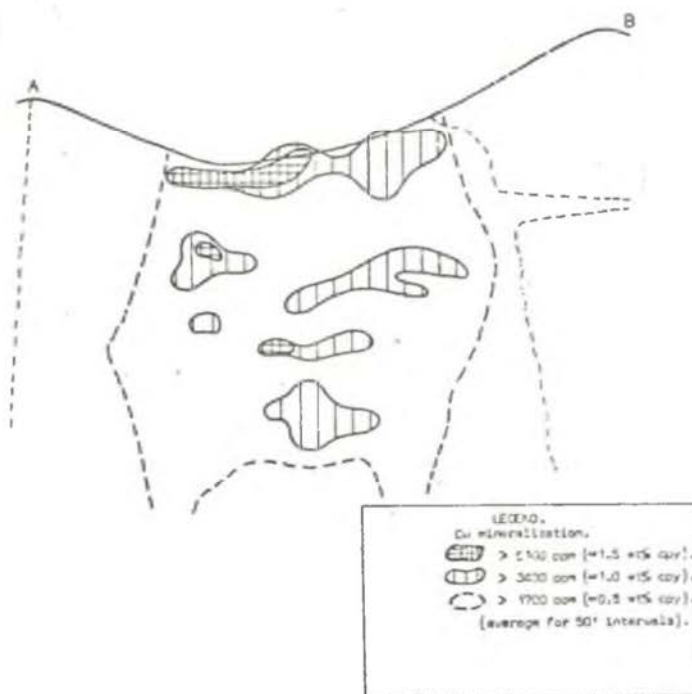
a.   Pyrite: Chalcopyrite ratios.   b.   Cu mineralization.   c

Figure 16.   Cross-sectional projections of mineralizati

or overlay 6), and pockets within this zone are seen to have up to 0.51% Cu (or the equivalent of 1.5 wt % chalcopyrite). These pockets of high grade mineralization possess the most intense areas of hydrothermal biotitization. Deep within this central biotite zone, a relatively unaltered and unmineralized core can be delineated by the low content of sulphides, generally all on veins and fractures, with copper values < 0.17 wt%.

Abundant clay - sericite alteration is confined to the surface zones (figure 15a, overlay 2) where it is strongly associated with pyrite and supergene sulphides. Clays are also represented within parts of the chlorite - epidote - carbonate zone as well as along shear zones. Chlorite is abundant along shear zones (figure 15b, overlay 3) and in the lower reaches of surface weathering. Minor irregularities in the presence of chlorite within the biotite zone is brought about by the presence of andesitic - dacitic dykes, which only alter to chlorite - epidote - carbonate - albite - clay assemblages.

CHAPTER 5.   HYDROTHERMAL ALTERATION:

CHEMICAL ASPECTS.

Introduction.

Major elements.

Trace elements.

5. HYDROTHERMAL ALTERATION:
CHEMICAL ASPECTS

Interpretation of chemical variations is, to some degree, complicated owing to the fact that many rock samples have suffered late retrogressive alteration. This is evidenced by minor chloritization of ferromagnesian minerals, alteration of plagioclase feldspars by sericite and calcite, and martitization of magnetite within hydro-thermally unaltered and altered intrusive rocks.

Compounded with this is the effect of inhomogeneities within the composition of the stock produced by differen-tiation, and the superposition of early biotite alteration by later chlorite-epidote-carbonate alteration.

Two relatively fresh samples and eighteen hydro-thermally altered rocks were analysed for both major and trace elements, and the results are listed in tables 3 and 4. The two relatively fresh samples were used as reference points to compare and contrast the differences in the chemistry of the alteration types. As the alteration described in Chapter 4 clearly divides the hydrothermally altered intrusive rocks into two zones; namely the biotite zone and the chlorite-epidote-carbonate zone, with minor quartz-sericite-pyrite and sericite-clay assemblages, rocks were therefore selected to be representative of each of these alteration types.

So as to enable easy separation of the alteration

Biotite zone assemblages - ⊡

Quartz-sericite - pyrite assemblages - ▽

Sericite-clay assemblages - ◊

Chlorite zone - after porphyritic tonalites, etc. - ⤬

Chlorite zone - after andesitic - dacitic dykes - ✕

Porphyritic microtonalite - unaltered - ▨

Porphyritic andesite - unaltered - ▲

Sample No.	CL 151	CL 152	CL 156	CL 179	CL 180	CL 263	CL 427	CL 437	CL 537	CL 580	CL 585	CL 609	CL 610	CL 619	CL 622	CL 626	CL 627	CL 628
SiO_2	65.35	51.36	58.75	61.10	55.40	61.97	62.05	63.44	60.85	62.63	67.33	56.12	61.05	57.03	60.11	61.09	61.83	62.35
TiO_2	.53	.37	.86	.96	1.08	.71	.66	.70	.72	.66	.71	.83	.70	.84	.67	.70	.68	.69
Al_2O_3	14.30	10.10	16.47	16.75	15.70	15.50	16.81	16.62	15.79	16.09	17.26	15.17	15.62	15.29	14.79	15.98	15.37	15.98
Fe_2O_3*	8.21	21.31	7.20	6.74	9.32	4.58	3.97	1.31	5.50	5.43	3.56	8.89	5.89	6.41	6.44	4.73	5.03	5.54
MnO	.01	.01	.02	.03	.04	.02	.02	.02	.02	.04	.00	.11	.05	.07	.03	.02	.02	.02
MgO	.79	.58	3.03	4.82	5.96	2.69	2.92	1.07	2.50	2.53	.57	4.60	2.78	4.17	3.35	2.52	2.61	2.43
CaO	.01	.01	2.83	1.94	1.82	3.69	1.24	4.28	3.63	3.15	.95	1.20	5.50	3.98	2.88	3.69	3.82	2.82
Na_2O	.50	.41	4.12	4.21	3.60	4.00	3.00	3.56	3.50	4.54	.25	4.27	4.20	4.86	4.33	4.30	3.84	4.51
K_2O	4.24	3.12	2.31	3.67	3.77	1.99	3.98	2.91	2.37	1.32	4.66	1.26	2.70	1.95	2.71	2.27	2.19	1.70
P_2O_5	.04	.03	.22	.20	.22	.17	.21	.05	.21	.21	.12	.20	.17	.22	.20	.22	.18	.20
LOI.	6.98	12.78	3.27	.97	1.58	3.41	6.85	6.13	3.60	2.23	4.36	5.37	3.10	3.34	1.11	2.24	1.70	2.06
Total	100.96	100.08	99.08	101.39	98.49	98.73	101.71	100.09	98.69	98.83	99.77	98.52	98.76	98.16	96.62	97.76	97.27	98.30
CIPW Norm.																		
Q	45.14	36.24	16.01	11.81	7.89	19.67	22.97	21.04	20.53	21.26	45.50	14.71	17.29	8.10	14.00	16.37	19.57	20.53

Sample	151	152	156	179	180	263	427	437	537	580	585	609	610	619	622	626	627	628
Y	15	24	32	24	21	15	nd	8	17	17	4	22	18	22	18	19	19	13
Sr	32	11	451	385	338	347	nd	165	380	555	25	254	412	347	435	636	456	501
Zr	155	115	149	153	124	159	nd	115	115	150	148	152	144	158	146	150	145	151
U	8	7	5	5	4	6	nd	3	7	3	4	5	6	3	5	7	6	4
Rb	108	83	128	132	133	103	nd	122	128	56	141	75	129	94	136	86	79	52
Th	11	17	3	6	6	3	nd	4	6	3	6	16	22	9	4	3	7	5
Pb	74	54	17	23	25	17	nd	15	24	20	18	29	27	20	15	16	14	13
Ga	16	16	23	23	22	20	nd	18	20	21	14	25	22	23	24	23	21	22
Zn	13	9	45	71	105	49	29	48	39	51	7	143	69	63	61	45	43	44
Cu	1881	3644	52	3156	1465	433	40	89	444	84	48	1394	234	350	454	918	126	135
Ni	23	56	33	78	97	26	36	33	32	32	18	71	34	66	52	27	35	29
Mn	6	6	254	369	455	197	200	270	266	276	57	935	541	638	250	272	219	231
Cr	32	19	32	226	228	48	55	31	54	39	29	168	91	178	120	62	81	49
V	91	64	124	168	222	117	96	84	116	86	70	152	114	156	114	118	113	107
Ti	2895	1766	5209	5477	6433	4238	4161	4159	4304	3936	3743	4667	3695	4815	3848	4218	3966	4145
Ba	200	388	2883	267	274	473	3	91	418	975	210	115	351	92	197	405	301	266
Rb/Sr	3.38	7.55	.28	.34	.39	.30	—	.74	.34	.10	5.64	.30	.31	.27	.31	.14	.17	.10

Table 4. Trace elements within alteration assemblages and unaltered rocks. (nd = not determined). Values as ppm.

types within the following diagrams, each alteration type is assigned a symbol which will be adhered to throughout this chapter.

MAJOR ELEMENTS:-

Variations within major oxide contents are shown in figures 17 and 18, but can be more conveniently shown in FMA and CKN diagrams (figures 19 and 20 respectively). The most distinctive of the alteration types is seen in the quartz-sericite-pyrite assemblage which has suffered a major loss of magnesium, calcium and sodium. The only components remaining are potassium, alumina and iron, which therefore results in the observed mineral assemblage, sericite and pyrite. Silica and potassium may have been introduced assisting in the formation of sericite and quartz. These rocks are also characterized by large losses on ignition due to their high content of sulphur and water (as sulphides and sericite). Calculation of CIPW Norms for these rocks shows that they are high in normative corundum and low in normative feldspars, the negative value for normative anorthite is due to insufficient CaO for alloc-ation with P_2O_5 in normative apatite. It could therefore be inferred that hydrothermal fluids rich in sulphur, potassium, and possibly aluminium and iron, caused destruction of plagioclase feldspar with concommittant crystallization of sericite, quartz and pyrite and strong leaching of bases; sodium, magnesium and calcium.

Biotite zone assemblages - ▣

Quartz-sericite - pyrite assemblages - ▽

Sericite-clay assemblages - ◊

Chlorite zone - after porphyritic tonalites, etc. - ✕

Chlorite zone - after andesitic - dacitic dykes - ✗

Porphyritic microtonalite - unaltered - ▪

Porphyritic andesite - unaltered - ▲

Figure 17.   Chemical variation diagram.

Biotite zone assemblages -   ⊡

Quartz-sericite - pyrite assemblages - ▽

Sericite-clay assemblages -   ⬯

Chlorite zone - after porphyritic tonalites, etc. - ✕

Chlorite zone - after andesitic - dacitic dykes - ✗
 Porphyritic microtonalite - unaltered - ▩

Porphyritic andesite - unaltered -   ▲

Figure 18.   Chemical variation diagram.

Biotite zone assemblages - ⊡

Quartz-sericite - pyrite assemblages - ▽

Sericite-clay assemblages - ◊

Chlorite zone - after porphyritic tonalites, etc. - ✕

Chlorite zone - after andesitic - dacitic dykes - ✗

Porphyritic microtonalite - unaltered - ▦

Porphyritic andesite - unaltered - ▲
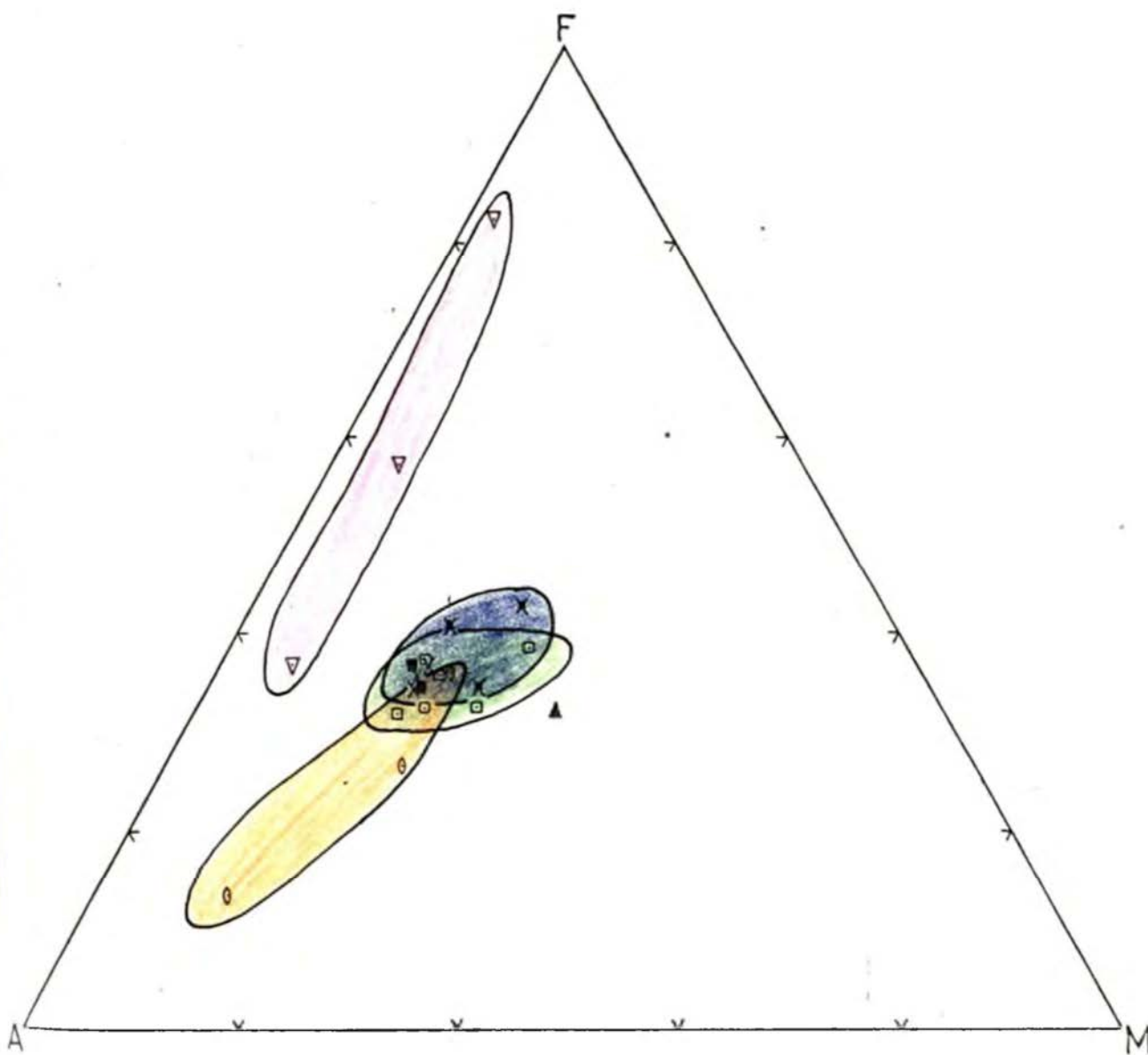
Figure 19.   FMA diagram for alteration assemblages.

Biotite zone assemblages -   ⊡

Quartz-sericite - pyrite assemblages - ▽

Sericite-clay assemblages -   ◊

Chlorite zone - after porphyritic tonalites, etc. - ✕

Chlorite zone - after andesitic - dacitic dykes - ✻

Porphyritic microtonalite - unaltered - ▨

Porphyritic andesite - unaltered -   △
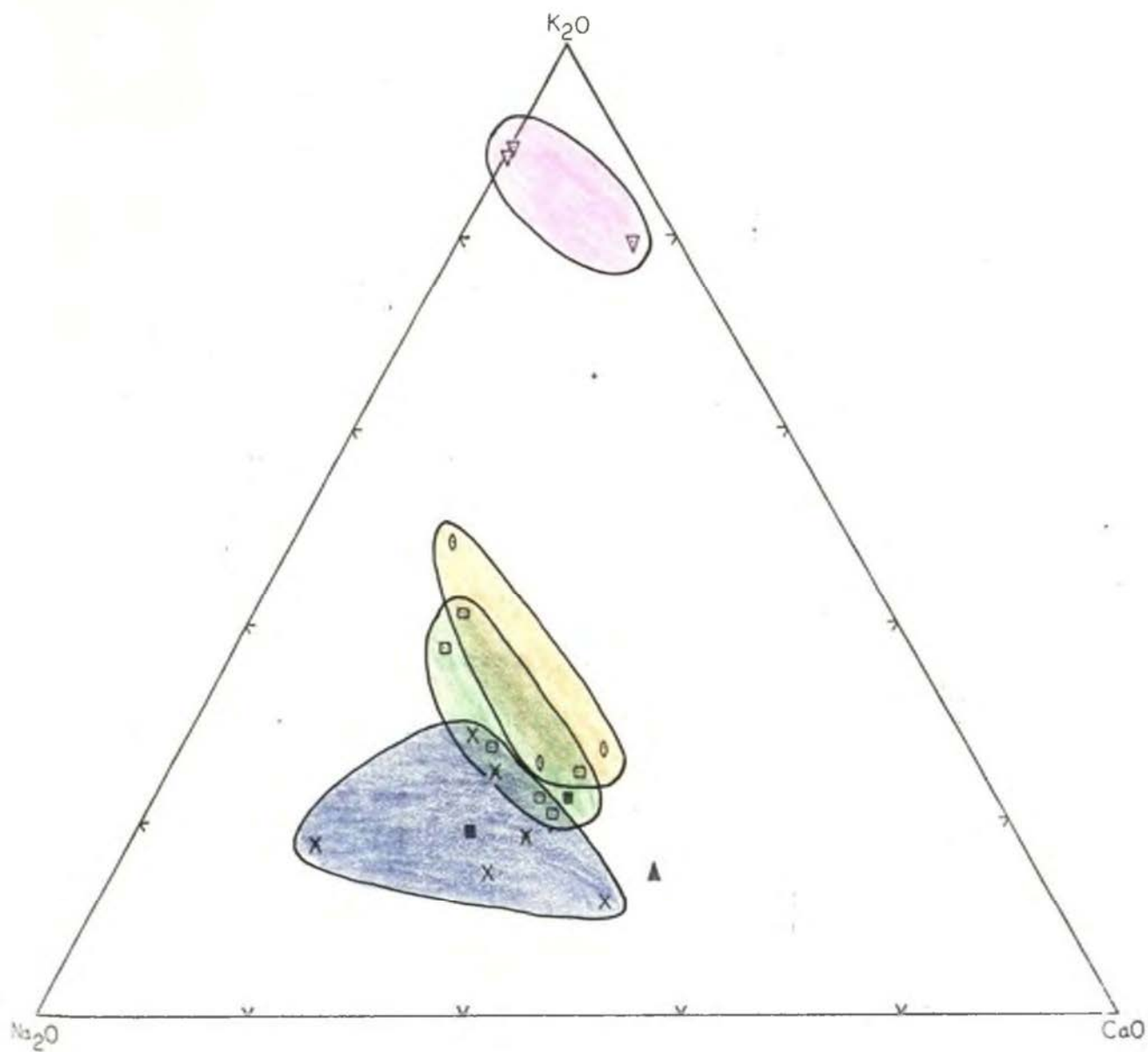
Figure 20.   CKN diagram for alteration assemblages.

The sericite-clay assemblage shows a decrease in the abundance of iron and magnesium due to the breakdown of ferromagnesium minerals and lack of sulphides. The resulting assemblages are relatively enriched in alumina and alkali (figures 19 and 22); the potassium, sodium, aluminium and calcium contents vary depending upon the abundance of illite, sericite, kaolinite, calcite or montmorillonite. The abundance of these hydrous minerals causes the observed high values for loss on ignition. These samples, like those of quartz-sericite-pyrite assemblage, are high in normative corundum, but differ by having higher normative feldspars.

The biotite zone and chlorite-epidote-carbonate zone alterations show only slight diversions from being isochemical. Chlorite-epidote-carbonate alteration, both within the intrusive microtonalite and in the andesitic-dacitic dykes, shows a slight decrease in the potassium content along with slight increases in iron, magnesium, calcium and ignition loss. These changes can be accounted for by the chloritization of ferromagnesian minerals, biotite and amphibole, albitization of plagioclase and crystallization of epidote, calcite and pyrite. Overall only the removal of small amounts of potassium is necessary to explain the mineralogical changes.

Biotitization, by comparison, shows a gain in potassium as well as increases in iron, magnesium and ignition loss due to the increase in hydrothermal biotite

Biotite zone assemblages -   ⊡

Quartz-sericite - pyrite assemblages - ▽

Sericite-clay assemblages -   ◊

Chlorite zone - after porphyritic tonalites, etc. - ✕

Chlorite zone - after andesitic - dacitic dykes - ✕

Porphyritic microtonalite - unaltered - ▨
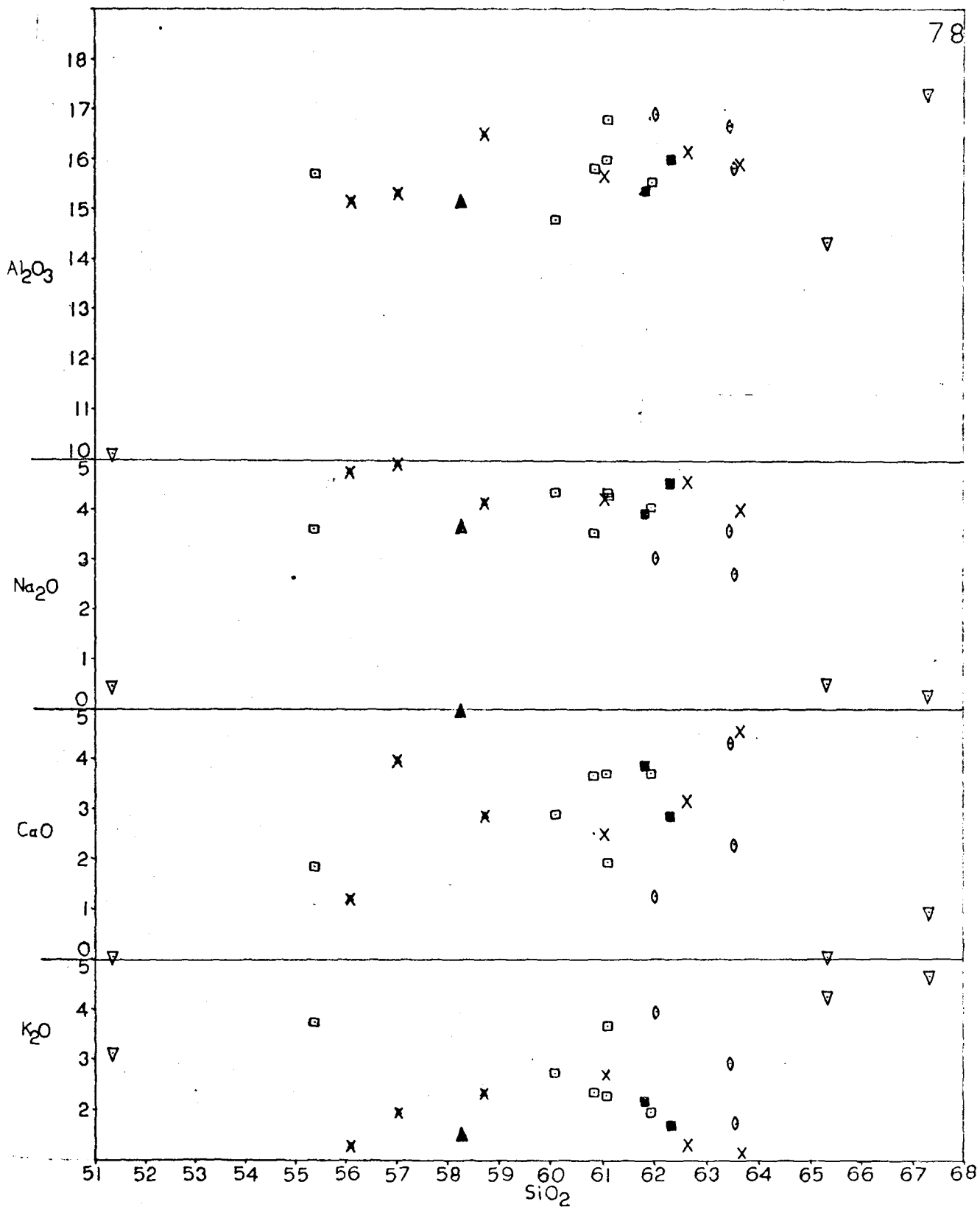
Porphyritic andesite - unaltered -   ▲
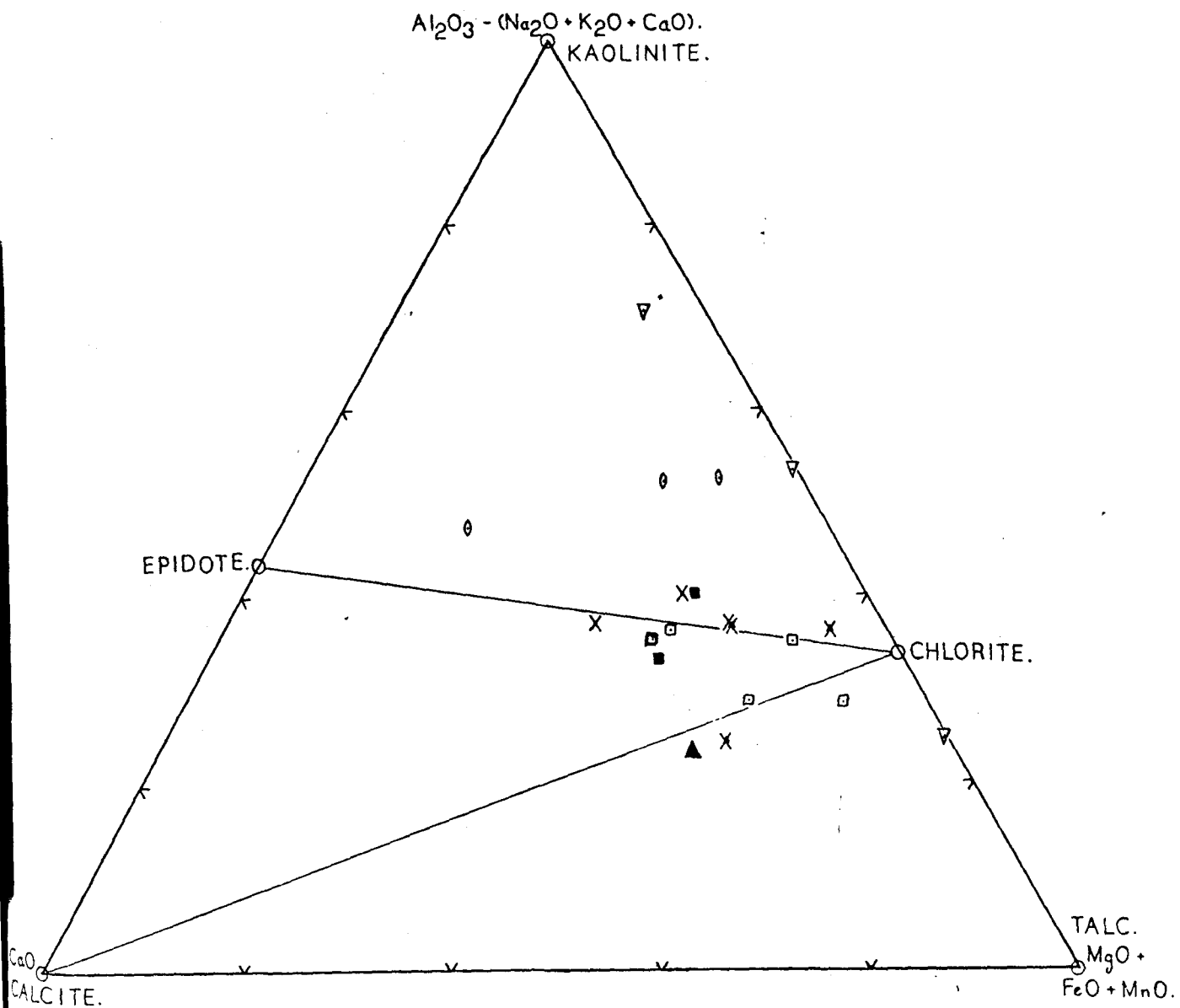
Figure 21.   ACF diagram for alteration assemblages, with
some equilibrium assemblages indicated
(after Creasey, 1966).

Biotite zone assemblages -   ☐

Quartz-sericite - pyrite assemblages - ▽

Sericite-clay assemblages -   ◊

Chlorite zone - after porphyritic tonalites, etc. - ✕

Chlorite zone - after andesitic - dacitic dykes - ✕

Porphyritic microtonalite - unaltered - ▨

Porphyritic andesite - unaltered -   ▲
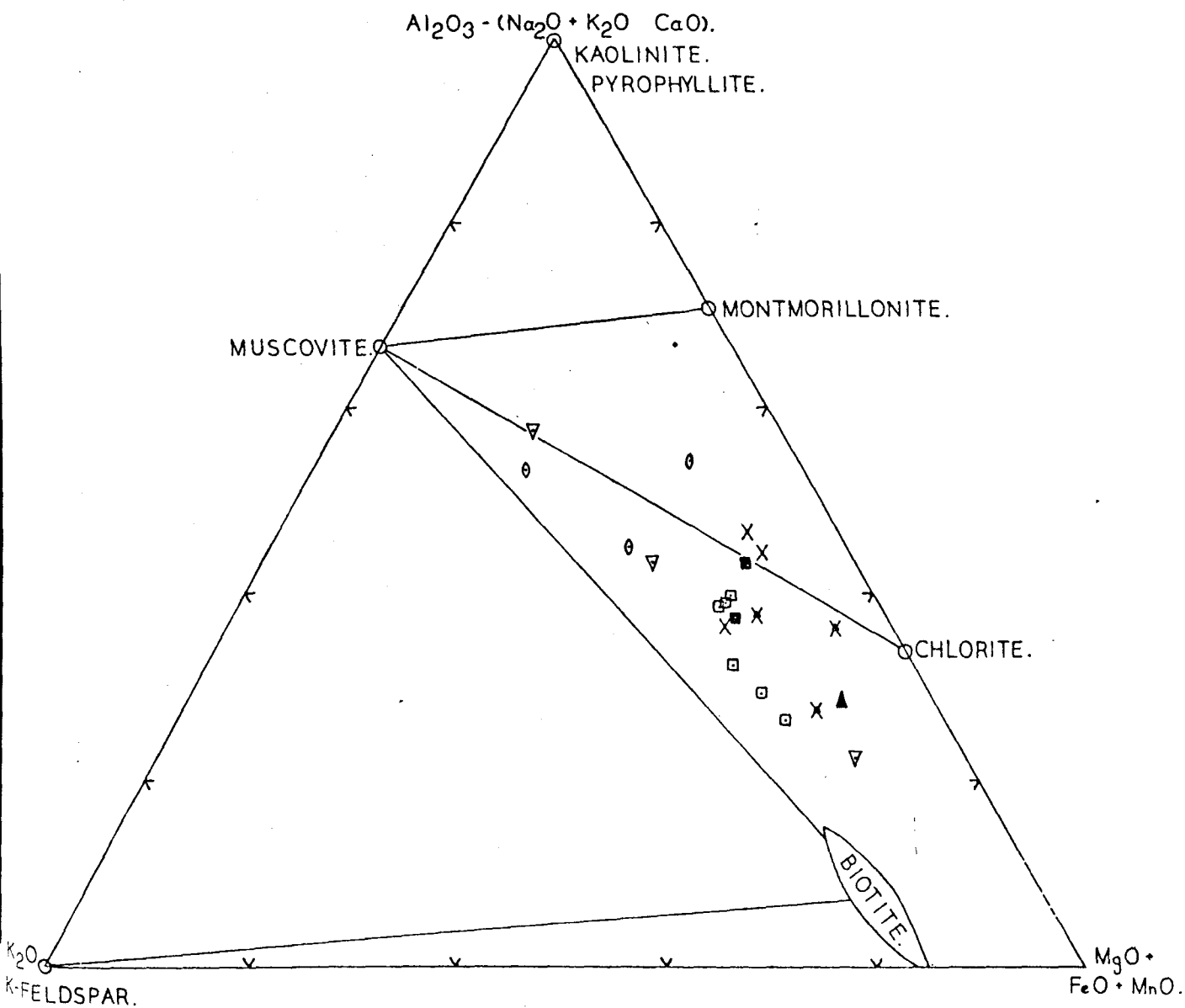
Figure 22.   AKF diagram for alteration assemblages, with
some equilibrium assemblages indicated
(after Creasey, 1966).

Biotite zone assemblages - ⊡

Quartz-sericite - pyrite assemblages - ▽

Sericite-clay assemblages - ⬠

Chlorite zone - after porphyritic tonalites, etc. - ✕

Chlorite zone - after andesitic - dacitic dykes - ⨯

Porphyritic microtonalite - unaltered - ▣

Porphyritic andesite - unaltered - ▲
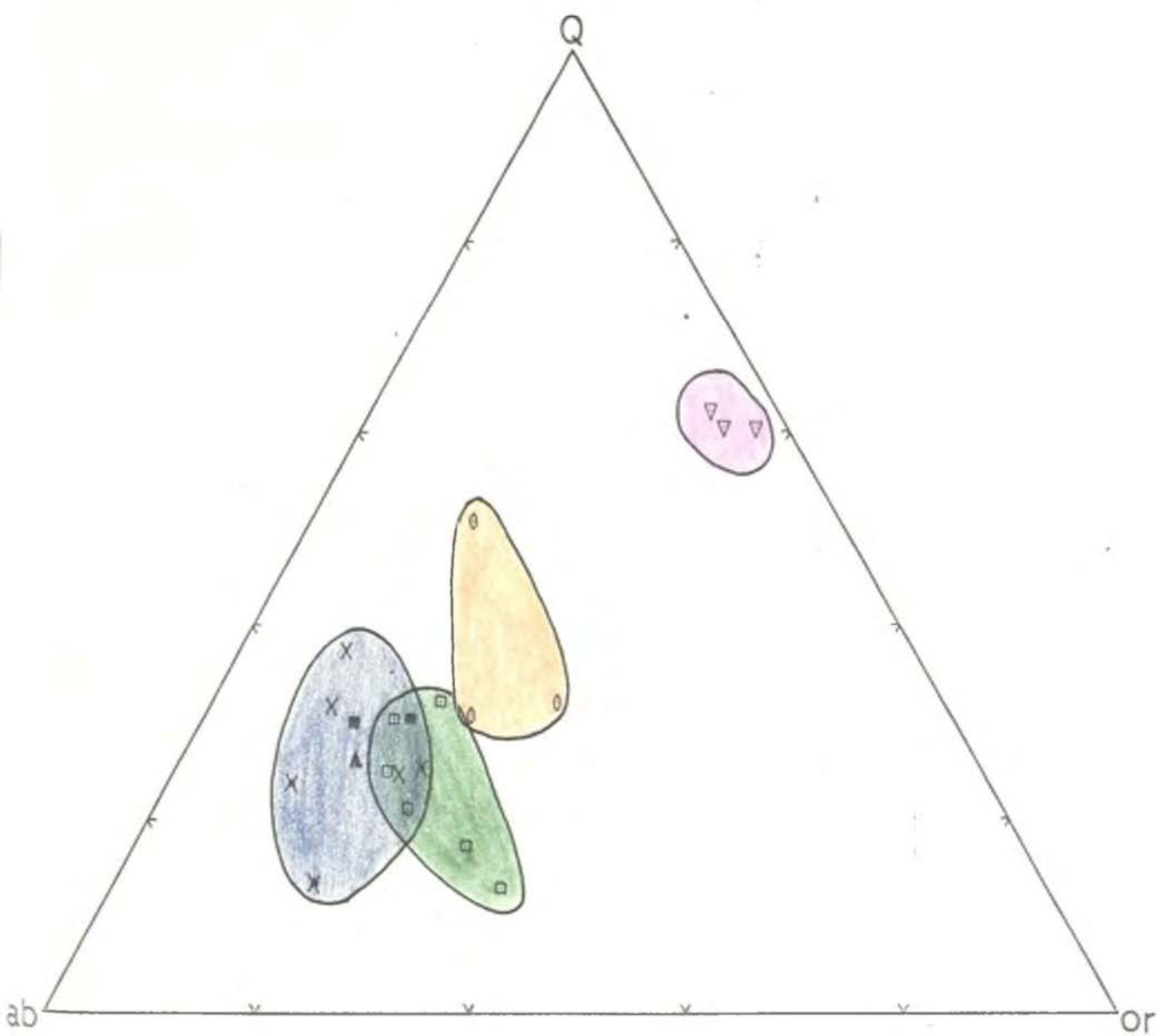
Figure 23.   Normative Q-ab-or triangle for alteration
              assemblages.

Biotite zone assemblages - ⊡

Quartz-sericite - pyrite assemblages - ▽

Sericite-clay assemblages - ◊

Chlorite zone - after porphyritic tonalites, etc. - ✕

Chlorite zone - after andesitic - dacitic dykes - ✕

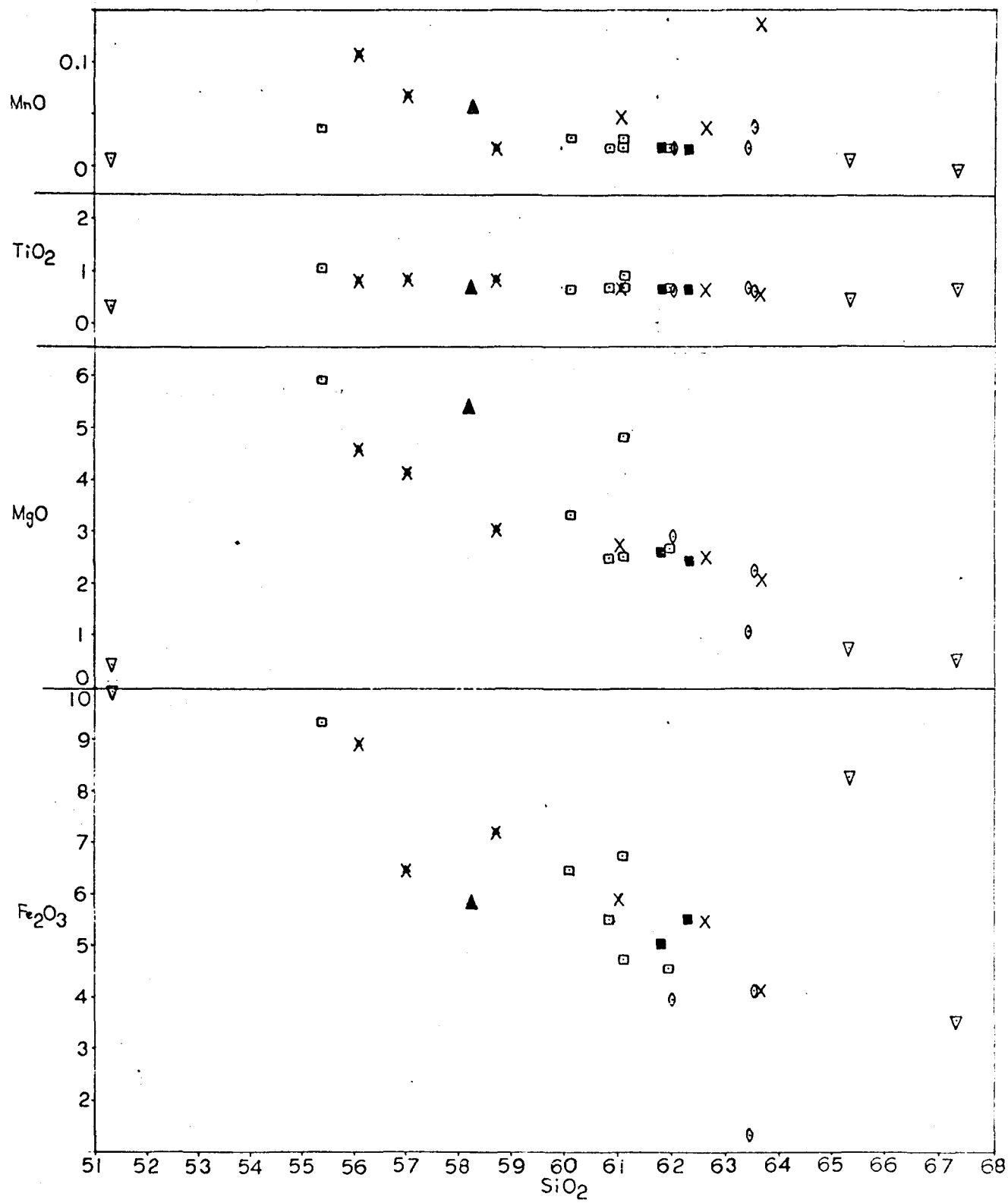Porphyritic microtonalite - unaltered - ▨

Porphyritic andesite - unaltered - ▲
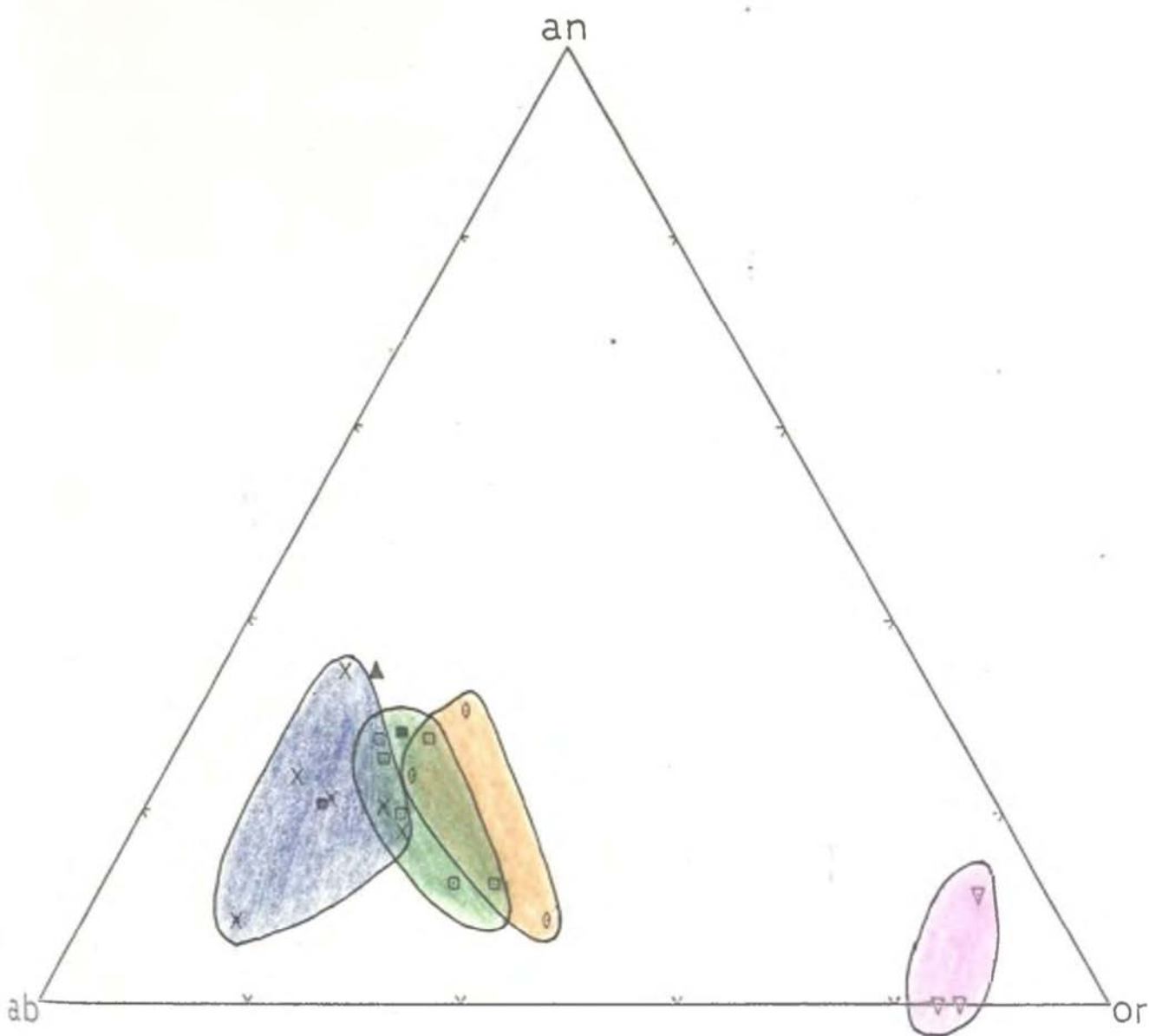
Figure 24.   Normative feldspar (ab-an-or) triangle for
alteration assemblages.

and the presence of sulphides.   Additional iron appears to have been introduced   to   form the sulphide minerals while biotitization accounts **for the** addition of potassium.   The apparent addition of magnesium may possibly indicate that hydrothermal biotite is more Mg-rich than magmatic biotite; this will be discussed further in chapter 6.

The major element variations from Coalstoun are very similar to those reported by Fountain (1972), Hemley and Jones (1964), Meyer and Hemley (1967) and Rose (1970).

Plots of the analyses onto Q-ab-an and ab-an-or (ie. normative quartz - feldspar triangles), (figures 23 and 24) show that it is possible to break the rocks into the four types of alterations, although there is overlap between three of these alteration type fields.

TRACE ELEMENTS:-

The results of quantitative analysis for trace elements are shown on table 4;   many of the elements do not show significant variations between alteration types.

Copper differs the most between alteration types, and assemblages within the biotite zone contain > 400 ppm Cu. Two samples of intense biotitization average > 0.2% Cu, CL 179 and CL 180 contain 3156 ppm and 1465 ppm Cu respectively.   The copper content within all other alteration types is low, except where supergene chalcocite occurs, exemplified by samples CL 151 and CL 152 with copper values of 1881 ppm and 3644 ppm respectively.

The rubidium content within samples of the biotite
zone has an average of 126 ppm with an average Rb/Sr ratio
of 0.34.   The content of rubidium is similar in the quartz-
sericite-pyrite assemblage but the Rb/Sr ratio is much
higher (averaging 111 ppm Rb and a Rb/Sr ratio of 5.5) due
to the very low content of Sr (averaging 23 ppm).   Within
the chlorite-epidote-carbonate zone the Rb/Sr ratio decreases
markedly to .26. The distribution of Rb and Sr is controlled
by the abundance of K and Ca respectively.   Because of
similar ionic properties, Rb substitutes for K, whereas
Sr replaces Ca (Heier and Adams, 1964; Turekian and
Kulp, 1956).   This distribution of Rb and Sr has been
investigated by Olade and Fletcher (1975) who showed
similar distributions to Coalstoun in some British Columbian
porphyry copper deposits.

CHAPTER 6.   FERROMAGNESIAN MINERAL
              STUDIES.

Introduction.

Biotites

- Composition of primary magmatic
  biotites.

- Composition of hydrothermal
  biotites.

- Compositional contrasts.

Theoretical implications.

Interpretation.

Amphiboles.

Chlorites.

6. FERROMAGNESIAN MINERAL STUDIES

Hydrothermal alteration and sulphide mineralization within the Coalstoun prospect has been previously discussed with regard to alteration assemblage characteristics and their zonal distribution. Hydrothermal biotite is the most important phase associated with copper mineralization so it was beneficial to study compositional variations between primary magmatic biotites and hydrothermal biotites, as well as other ferromagnesian minerals, to indicate chemical and physical changes of the system.

BIOTITES:-

Primary magmatic biotites are present within all of the intrusive rocks, with the exception of some dykes, frequently occuring up to 20 % volume. It is associated with plagioclase, quartz, magnetite, apatite and occasionally amphibole and traces of K-feldspar. It characteristically occurs with red-brown to fawn pleochroism in euhedral books or flakes up to 5mm in size. Frequently the biotite contains inclusions of magnetite, rutile, zircon and apatite.

On the other hand, hydrothermal biotite, which is the dominant mafic silicate alteration mineral, coexists with sulphides, anhydrite, rutile, weakly sericiterized plagioclase, quartz and minor K-feldspar. Hydrothermal biotite lacks the red-brown tint in pleochroism but characteristically possesses a greeny-brown tint.

Anhedral crystals of hydrothermal biotite occur both as
pseudomorphous aggregates after preexisting ferromagnesian
minerals and as single flakes flooding the altered rock.
Total biotite within these altered rocks ranges from
15-50% by volume.

Composition of Primary Magmatic Biotites;

Primary magmatic biotite analyses are shown in
table 5 where deficiencies within the X and Y sites are
noted and may represent vacant structural sites or the
result of incomplete analyses.   Biotites may contain small
amounts of various other elements including Ba, Co, Cr, Cu,
Nb, Ni, Sc, Sr, V, Y and Zr and is exemplified by trace
element analysis of CL180 biotite concentrate (table 7).
Other factors which may contribute to several low totals,
excluding the amounts of water, chlorine or fluorine within
the structure, are the presence of iron in the ferric state,
or inadequate polish.

The major octahedral atoms are Fe, Mg and Ti, with
Fe + Mg filling 80 - 90% of the six available sites.   Total
Fe expressed as FeO wt% has a mean of 14.29 ± 0.55, with
the exception of samples from CL 611 which have a lower
total FeO; average 11.30%.   The titanium content within
these magmatic biotites is generally high with a mean
3.22 ± 0.28 wt%.   Following Hall (1941) these factors would
account for the red-brown colour of these biotites; ie high
TiO_2 + high FeO + low MgO.   Flood (1971, p 340) reports
that the "colour of the biotites can be closely correlated

Sample No.	CL269		CL614		CL257	CL601				CL685			CL587		x̄	±	s	CL611	
SiO_2	39.18	39.74	39.19	39.02	38.69	37.73	37.98	38.00	38.63	37.71	37.69	38.23	37.09	36.69	38.27	±	.08	39.78	38
TiO_2	3.04	3.28	3.96	3.65	2.96	3.29	3.37	2.97	3.02	3.36	3.09	3.10	3.23	3.11	3.25	±	.78	3.38	2
Al_2O_3	16.02	15.44	14.11	13.66	14.83	15.80	15.40	14.92	15.39	15.18	16.12	15.94	14.95	15.44	15.23	±	.70	14.45	1
FeO*	15.44	14.67	14.65	13.56	14.24	14.12	14.26	14.49	13.17	14.18	14.38	14.44	14.71	13.75	14.29	±	.55	11.24	11
MnO	.08	.05	.16	.00	.09	.08	.03	.04	.06	.09	.07	.08	.16	.17	.08	±	.00	.08	
MgO	13.73	14.63	14.92	15.55	14.98	14.63	14.80	14.71	14.67	14.01	15.10	14.90	15.60	15.22	14.32	±	.51	16.78	16
CaO	.00	.00	.00	.00	.00	.00	.00	.00	.01	.00	.00	.02	.00	.00	.00	±	.00	.00	
Na_2O	.18	.19	.29	.21	.24	.22	.24	.21	.21	.15	.24	.18	.25	.17	.21	±	.00	.35	
K_2O	9.12	8.97	9.28	8.79	8.70	8.97	8.99	9.05	8.87	9.30	8.26	8.72	8.60	8.94	8.90	±	.26	9.13	9
Total	96.79	96.97	96.76	94.44	94.73	94.84	95.07	94.39	94.03	93.98	94.95	95.61	94.59	93.49				95.19	92
Si	5.72	5.76	5.76	5.80	5.74	5.61	5.63	5.69	5.75	5.67	5.58	5.63	5.55	5.54	5.67	±	.10	5.80	5
Al	2.28	2.24	2.24	2.20	2.26	2.39	2.37	2.31	2.25	2.33	2.42	2.37	2.45	2.46	2.33	±	.10	2.20	2
Al	.48	.40	.19	.19	.34	.38	.33	.32	.45	.36	.39	.40	.19	.29	.34	±	.10	.28	
Ti	.33	.36	.43	.41	.33	.37	.38	.33	.34	.38	.34	.34	.36	.35	.36	±	.00	.37	
Fe	1.89	1.78	1.79	1.69	1.77	1.76	1.77	1.82	1.64	1.78	1.78	1.78	1.84	1.74	1.77	±	.00	1.37	1
Mn	.01	.01	.02	.01	.01	.01	.00	.01	.01	.01	.01	.01	.02	.02	.01	±	.00	.01	
Mg	2.99	3.16	3.25	3.45	3.32	3.24	3.28	3.28	3.26	3.14	3.33	3.27	3.48	3.43	3.28	±	.14	3.65	3
Ca	.00	.00	.00	.00	.00	.00	.00	.00	.00	.00	.00	.00	.00	.00	.00	±	.00	.00	
Na	.05	.05	.08	.06	.07	.06	.07	.06	.06	.04	.07	.05	.07	.05	.06	±	.00	.10	
K	1.70	1.66	1.73	1.67	1.65	1.70	1.70	1.73	1.68	1.79	1.56	1.64	1.64	1.72	1.68	±	.00	1.70	1

Table 5. Composition and structural formula of magmatic biotites.

Number of cations on the basis of 22 (O). *Total Fe as FeO.

Mean and standard deviation given for grouped data.

with the ratio Fe^{3+} / Fe^{2+} + Fe^{3+} ", with a low ratio existing
in red brown biotites, and a higher ratio within the green
biotites.   This factor may also account for the red-brown
tint within the magmatic biotites.   Octahedral aluminium,
$[Al]^6$, ranges from 0.19 to 0.48 atoms per structural
formula; mean = 0.34 ± 0.10.

Composition of Hydrothermal Biotites;

Hydrothermal biotite analyses in table 6 show
similar deficiencies in both the X and Y sites for the
reasons stated above.   Totals within these biotites are
slightly lower than should be expected but may be accounted
for by the presence of iron in the ferric state as in sample
CL180 (table 7), or because they are hydrothermal biotites
and may have up to 6% bound water, chlorine or fluorine.

The major octahedral atoms within these biotites are
Mg, Fe, Al with Fe + Mg filling 80 - 90% of the octahedral
sites as with the magmatic biotites.   In one sample the
Fe + Mg comprises only 71.5% of the six sites, but is rich
in alumina.   Iron allocated as FeO ranges from 12.41 wt %
to 14.45 wt% with a mean of 13.23 ± 0.57, while samples from
CL611, like the corresponding magmatic biotites, have lower
total FeO wt% with a mean of 10.36 ± 0.22.   Octahedral
aluminium is variable but reasonably high with an average of
o.55 ± 0.20;   atoms per structural formula range from 0.23
to as high as 1.08.   Titanium within these biotites is low
averaging 1.93 ± 0.47 wt%.   These relationships would

Sample No.	CL601		CL537		CL269	CL614				CL657			$\bar{x}$ ± s		CL611			
SiO$_2$	36.87	38.44	37.95	35.87	37.56	40.76	36.33	39.77	40.03	38.96	38.45	40.41	38.47 ±	1.64	38.92	39.22	38.69	3
TiO$_2$	.85	2.21	1.73	2.48	1.52	2.16	1.64	1.93	2.46	1.90	1.66	1.79	1.93 ±	.47	2.40	2.07	2.70	
Al$_2$O$_3$	20.79	17.34	14.59	14.73	17.51	15.05	18.82	14.74	13.97	18.53	17.23	15.51	16.57 ±	2.12	16.54	15.52	16.01	1
FeO*	13.36	12.82	13.49	13.95	13.12	13.57	12.41	12.91	13.00	12.55	14.45	13.18	13.23 ±	.57	11.10	10.91	10.84	1
MnO	.06	.14	.12	.09	.07	.11	.11	.11	.11	.07	.10	.09	.10 ±	.00	.07	.05	.12	
MgO	12.89	15.36	15.88	15.38	15.56	16.08	15.40	16.91	17.36	15.62	15.37	15.19	15.58 ±	1.08	16.76	17.20	16.65	1
CaO	.98	.13	.00	.00	.00	.05	.23	.00	.00	.00	.01	.00	.12 ±	.28	.00	.00	.00	
Na$_2$O	.13	.09	.05	.25	.17	.09	.06	.10	.14	.12	.15	.16	.13 ±	.00	.14	.14	.12	
K$_2$O	8.37	8.15	8.53	8.51	9.35	8.43	8.55	8.90	8.75	9.70	8.63	8.98	8.74 ±	.44	9.69	8.90	8.92	8
Total	94.25	94.68	92.34	91.26	94.86	96.30	93.55	95.37	95.82	96.52	96.05	95.31			95.62	94.01	94.05	9
Si	5.45	5.64	5.76	5.56	5.56	5.89	5.46	5.82	5.83	5.58	5.62	5.90	5.67 ±	.14	5.66	5.77	5.72	5
Al	2.55	2.36	2.24	2.44	2.44	2.11	2.54	2.18	2.17	2.42	2.38	2.10	2.33 ±	.14	2.34	2.23	2.28	2
Al	1.08	.64	.37	.25	.61	.45	.79	.36	.23	.71	.59	.57	.55 ±	.24	.49	.46	.51	
Ti	.09	.24	.20	.29	.17	.23	.09	.21	.27	.21	.18	.20	.20 ±	.00	.26	.23	.30	
Fe	1.65	1.57	1.71	1.81	1.62	1.64	1.56	1.58	1.58	1.50	1.77	1.61	1.63 ±	.10	1.35	1.34	1.25	1
Mn	.01	.02	.02	.01	.01	.01	.01	.01	.01	.01	.01	.01	.01 ±	.00	.01	.01	.02	
Mg	2.84	3.36	3.60	3.56	3.43	3.46	3.45	3.69	3.77	3.33	3.35	3.31	3.43 ±	.24	3.63	3.77	3.67	3
Ca	.16	.02	.00	.00	.00	.01	.04	.00	.00	.00	.00	.00	.0 ±	.00	.00	.00	.00	
Na	.04	.03	.01	.08	.05	.03	.02	.03	.04	.04	.04	.05	.04 ±	.00	.04	.04	.04	
K	1.58	1.52	1.65	1.68	1.76	1.55	1.64	1.66	1.63	1.77	1.61	1.67	1.64 ±	.10	1.80	1.67	1.68	1

Table 6. Composition and structural formula of hydrothermal biotites.
Number of cations on the basis of 22(O). *Total Fe as FeO.
Mean and standard deviation given for grouped data.

Sample	CL 180	CL 179
SiO_2	38.04	37.67
TiO_2	2.16	2.09
Al_2O_3	17.52	17.32
FeO^*	13.20	13.15
MnO	.12	.10
MgO	13.89	13.26
CaO	.54	1.15
Na_2O	.50	2.78
K_2O	7.29	7.23
P_2O_5	.10	.45
LOI.	5.06	4.78
Total	98.42	99.98
Fe_2O_3	5.78	nd
FeO	8.00	nd
Zn	.021	nd
Cu	.018	nd
Ni	.019	nd
Cr	.044	nd
V	.029	nd
Ba	.054	nd

Table 7. Analyses of biotite concentrates.

* Total Fe as FeO. All as wt.%.

therefore agree with the "brownish green" biotites of Hall
(1941); ie low TiO_2 + low FeO + high MgO.   The greenish
brown hydrothermal biotites of CL180 plot within the
"yellowish to greenish brown" colour field of Hayama (1959)
in figure 25.   Following the previous statement quoted
from Flood (1971, p. 340) this greenish tint may indicate
higher ferric/ferrous iron ratios within all the hydro-
thermal biotites.

Compositional Contrasts;

Magmatic and hydrothermal biotites can be separated
compositionally by there variations in

1. TiO_2 content;

2.   Total Fe as FeO content;

3. $Fe^{3+}/Fe^{2+} + Fe^{3+}$ ratio;

4.   Fe/Fe + Mg ratio;   and

5.   Si/Si + Al ratio.

The most striking chemical change between magmatic
and hydrothermal biotites is in their TiO_2 contents (figure 26).
Magmatic biotites have > 2.7 wt% TiO_2 (with an average of
3.22 wt% and only three samples analysed < 3.0 wt%),
compared with < 2.7 wt% TiO_2 for hydrothermal biotites
(only one sample analysed was > 2.5 wt%, the rest average
1.93 wt%.)   This decrease in titanium results in the
crystallization of rutile in close proximity to the hydro-
thermal biotites.   Also displayed on figure 26 is the
decline in the total Fe content (expressed as FeO wt%) which
may be explained by an increase in the ferric iron content
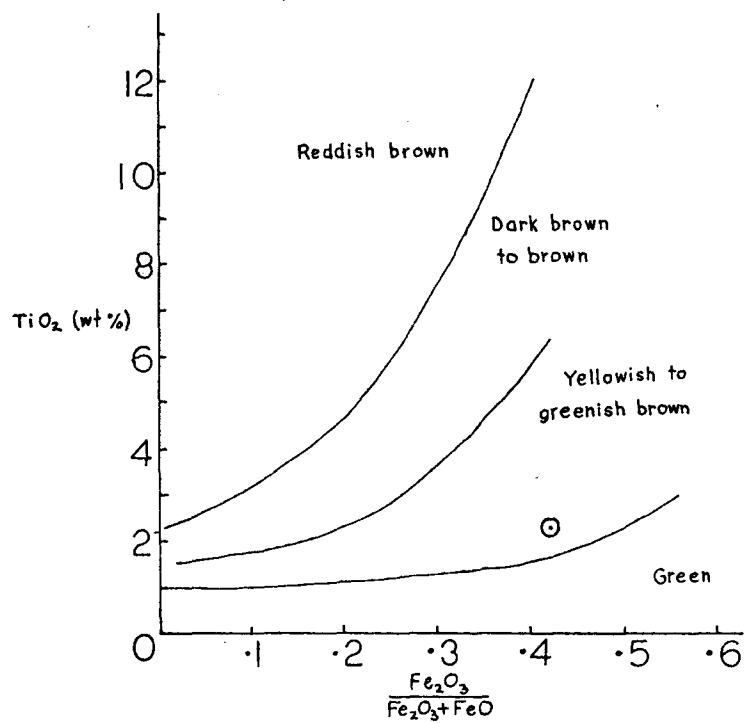
Figure 25.   TiO$_2$ (wt%)   vs.   Fe$_2$O$_3$ / FeO+Fe$_2$O$_3$ (wt%)

and colours of biotites after Hayama (1959).

CL180 biotite concentrate - ⊙ .
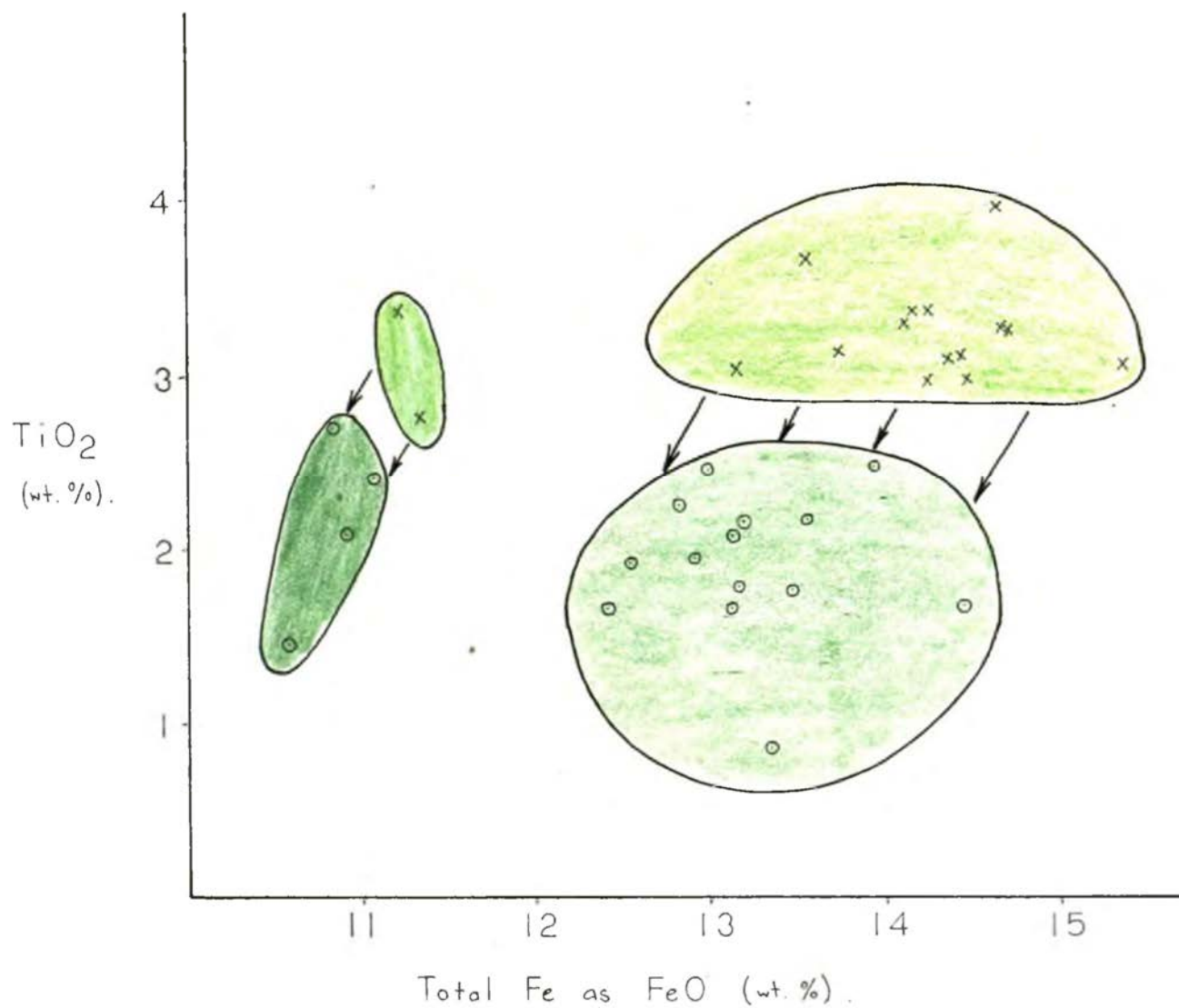
Figure 26.   TiO$_2$ (wt%) vs.   FeO (wt%) of biotites.

Magmatic biotites   –   x .

Hydrothermal biotites   – ⊙ .

within the hydrothermal biotites, or by a decrease in the
actual total Fe content within these biotites.   A combination
of both processes seems likely as evidence for martitization
of magnetite has previously been cited (plate 13) and the
codeposition of hydrothermal biotites and iron sulphides
has also been clearly noted (plate 11 and 20).   The hydro-
thermal biotites are inferred to contain higher ferric iron
content on the basis of colour and data reported by Hayama
(1959) and Flood (1971).

The other marked differences between these two modes
of biotites are shown in figure 27.   There is a definite
decrease in both the Fe / Fe + Mg and Si / Si + Al ratios,
which is possibly explained by a relative decrease in Fe,
accompanied by an increase in Al, as demonstrated by the
higher $\begin{bmatrix} Al \end{bmatrix}^6$ within hydrothermal biotites.

These variations are also shown on portions of
FeO – MgO – TiO_2 and FeO – MgO – Al_2O_3 triangular diagrams
(figure 28) adopted from Hall (1941) and Nockolds (1947)
respectively.   From Nockold's diagram the magmatic
biotites plot within fields II and III;   ie those
unaccompanied by other mafic minerals, and those associated
with either hornblende, pyroxene, or olivine respectively.
Magmatic biotites showing least alumina (CL 614) stably
coexisted with hornblende and plot well within field III.
Magmatic biotites unaccompanied by other mafic silicates
plot either within field II or close to the boundary line.

The magnesium content within hydrothermal biotites
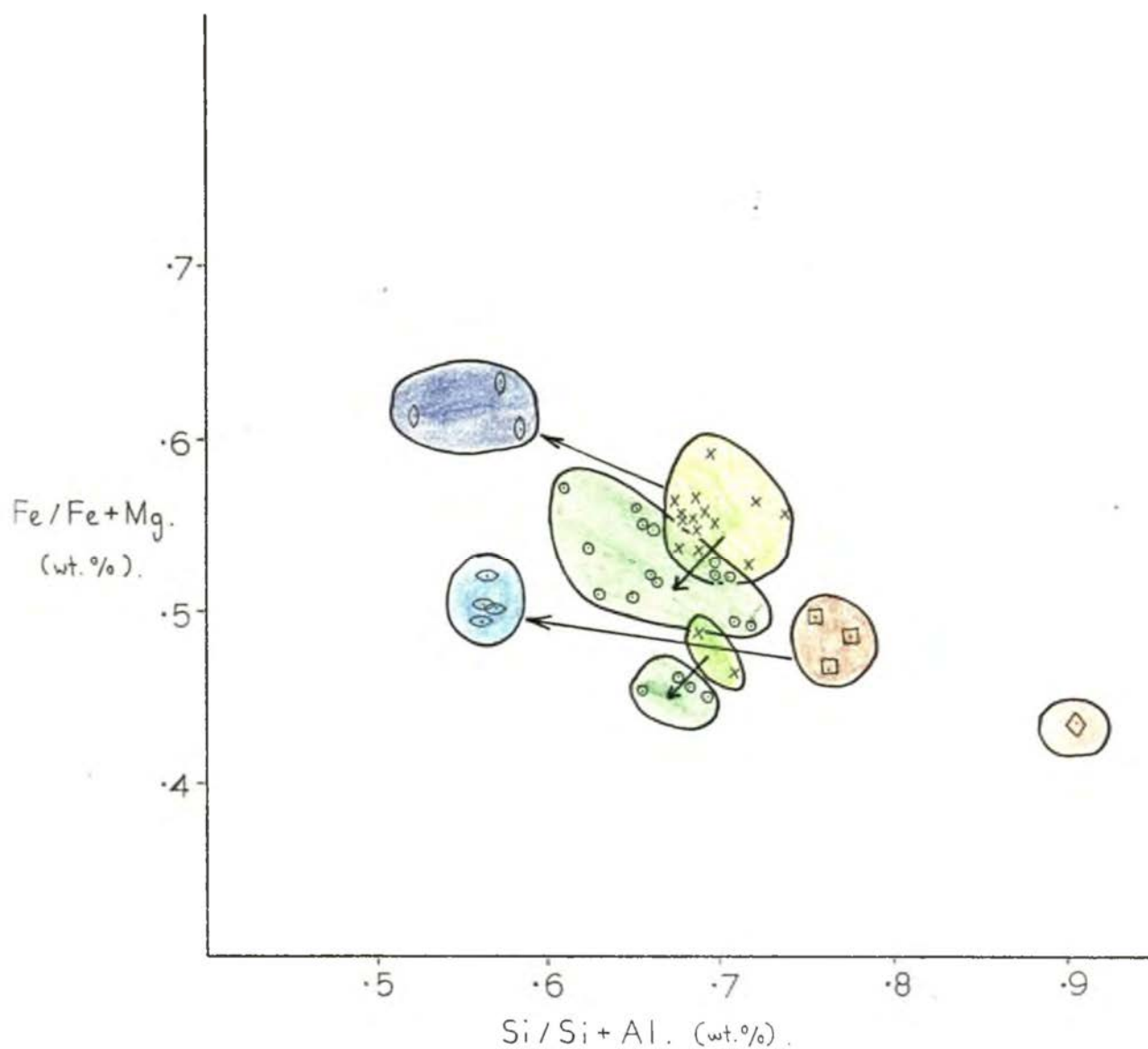
Figure 27.   Fe/Fe + Mg vs Si/Si + Al (all as wt%)

for analysed ferromagnesian minerals.

Magmatic biotites – X .   Hydrothermal biotites – ⊙ .

Dioritic amphibole – ◇ .   Andesitic amphiboles – ▫ .

Chlorite after amphibole – ⊙ .   Chlorite after biotite – .
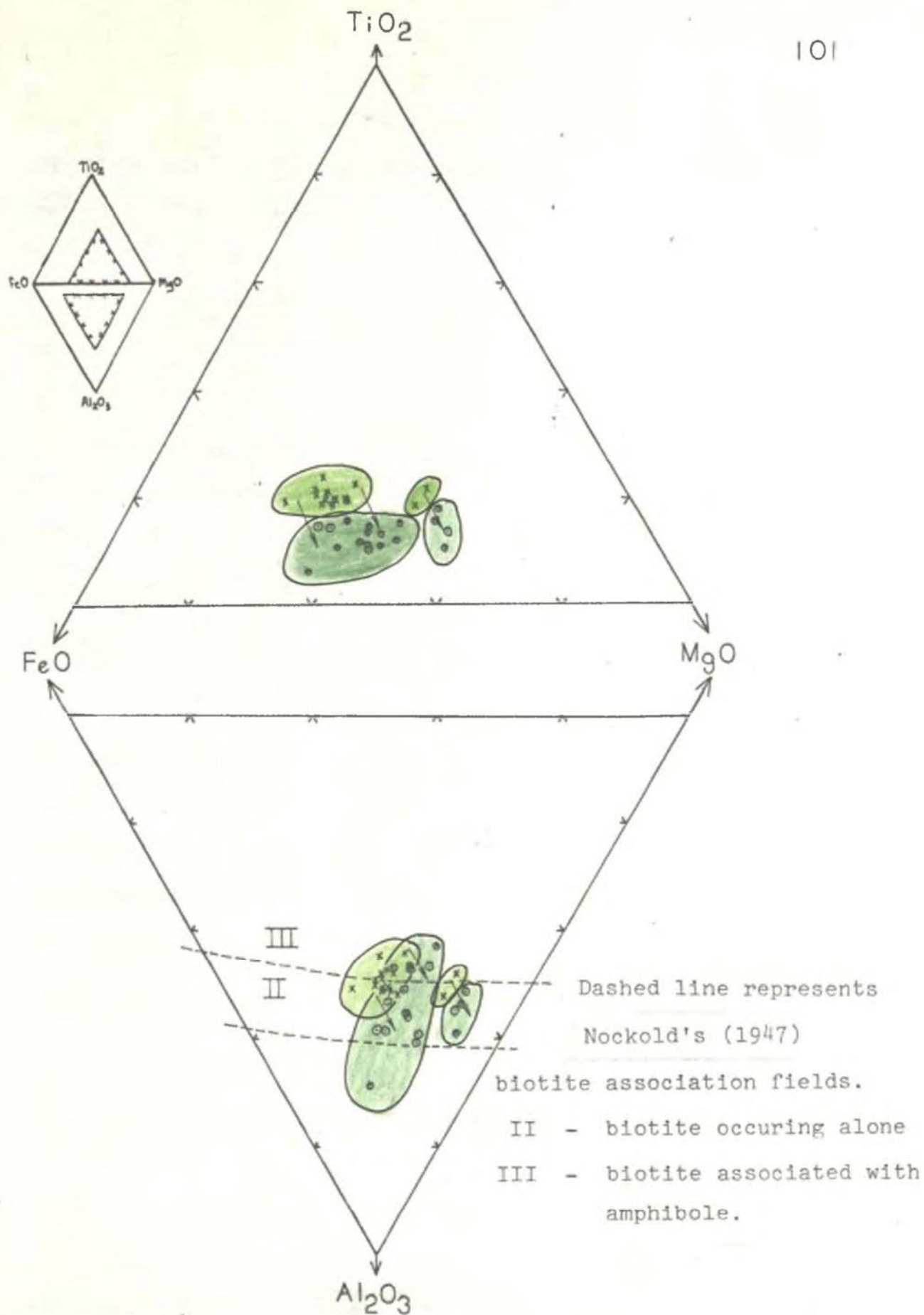
Figure 28.   Portions of FeO - MgO - TiO$_2$ and FeO-MgO-Al$_2$O$_3$

triangles.   Magmatic biotites   - X.

Hydrothermal biotites   - ⊙.

Dashed line represents

Nockold's (1947)

biotite association fields.

II - biotite occuring alone

III - biotite associated with amphibole.

appears to vary slightly, with the most magnesian rich hydrothermal biotites coexisting in areas of high copper content.   Sample CL614 has an average increase in the octahedral magnesium between magmatic and hydrothermal biotites of 0.24 atoms, and coincides with > 0.34% copper content.   The trends for Coalstoun are similar to those found by Anderson et. al. (1955), Carson and Jambor (1974), Fullager et. al. (1967), Moore and Czamanske (1973) and Nielson (1968).

THEORETICAL IMPLICATIONS:-

The variations in chemical compositions of the biotites needs explanation, and is probably related to the proportion of elements available and the geological environment prevailing under which they crystallized.   It has been observed (Heinrich, 1946) that biotites from less siliceous igneous rocks are in general more magnesian than more siliceous igneous rocks, with the titanium and iron contents showing a reverse pattern to magnesium.   Nockold's (1947), however showed that these chemical variations were dependent upon the nature of the other mafic minerals present.

Within the "Coalstoun Microtonalite" the close association between copper mineralization and biotitization is probably best explained by the work of Helgeson (1970). Theoretically, through computer evaluation and thermodynamic calculations, he reacted an idealized granodiorite with a sulphide-deficient hydrothermal solution at 200° C and one

atmosphere pressure,and found that the appearance of biotite
as a reaction product (B', figure 29) strongly influenced
the chemical potentials of Fe^{2+} and Cu^{2+}. Precipitation
of biotite at point B' (figure 30) caused a decrease in the
activity of Fe^{2+} in solution, and the resulting change in
the direction of the reaction path (figure 29) was
responsible for later saturation in chalcopyrite, as
opposed to later appearance of magnetite if biotite had not
reached saturation and crystallization. It is therefore
possible through Helgeson's hypothetical reaction to explain
the observed association between copper sulphides and
secondary biotite.

Hammarback and Lindqvist (1972) studied the hydro-
thermal stability of annite in the presence of sulphur,and
revealed variations in the prevailing fugacity of sulphur
(fS_2) in equilibrium with a particular biotite composition,
when coexisting with pyrrhotite, magnetite and sanidine
(figure 31). From this figure it is clear that slight
increases in fS_2 at constant temperature, cause an increase
in the magnesium content of the biotite, or that for a
constant fS_2, the magnesium content in the biotite will
increase with increase in temperature.

Annite under hydrothermal conditions was also invest-
igated by Eugster and Wones (1962), and Wones and Eugster
(1965). These authors concluded that its stability range
was dependent upon temperature (T), fugacity of oxygen
(fO_2) and water (fH_2O), as well as pressure (P) as shown
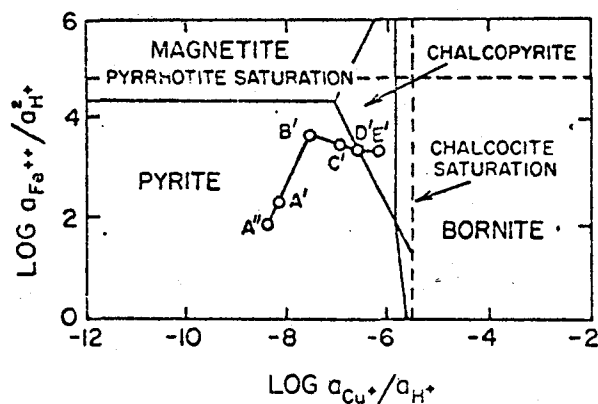
Fig. 22. Theoretical activity diagram for the system FeCl₂-CuCl-HCl-H₂S-H₂SO₄-H₂O in the presence of an aqueous phase in which $a_{H_2O} = 1.0$ and $a_{H_2S} = 10^{-4}$ at 200°C and one atmosphere. The letter annotations and lines connecting the circles refer to the reaction depicted in Figs. 18 and 21 (reaction 3, Table 4).

Figure 29.   Theoretical activity diagram after Helgeson (1970).
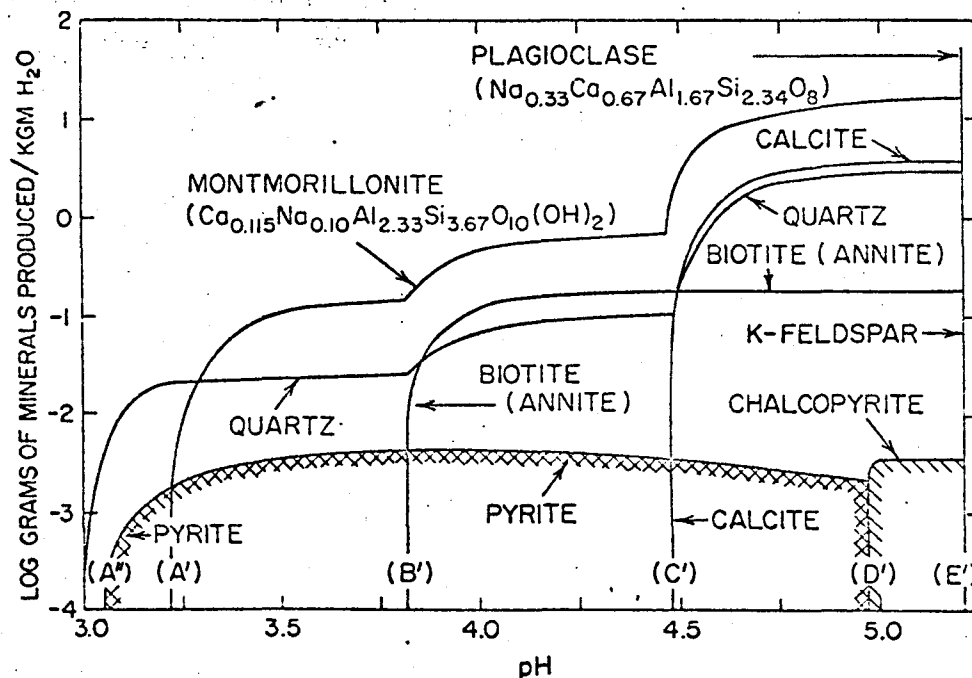
Fig. 21. Mass of minerals produced (kgm H₂O)⁻¹ as a function of progress in the reaction of an acid chloride-rich, sulfide (and sulfate)-deficient hydrothermal solution with an hypothetical granodiorite at 200°C and one atmosphere (reaction 3, Table 4). The letter annotations refer to sequential events in reaction progress (see Figs. 18 and 22).

Figure 30.   Reaction progress vs. reaction product mass formed, after Helgeson (1970).
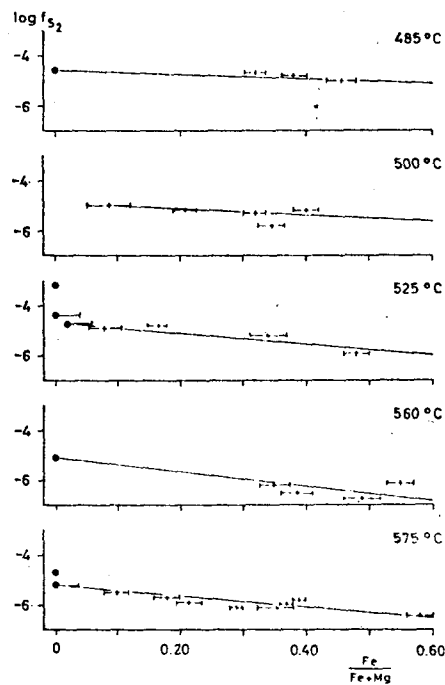
Fig. 3. Plots of biotite compositions against sulfur fugacity at different temperatures. Total pressure = 1600 atm. The standard deviation of each biotite composition is marked.

Figure 31.   Biotite composition vs. sulphur fugacity, after Hammarback and Lindqvist (1972).
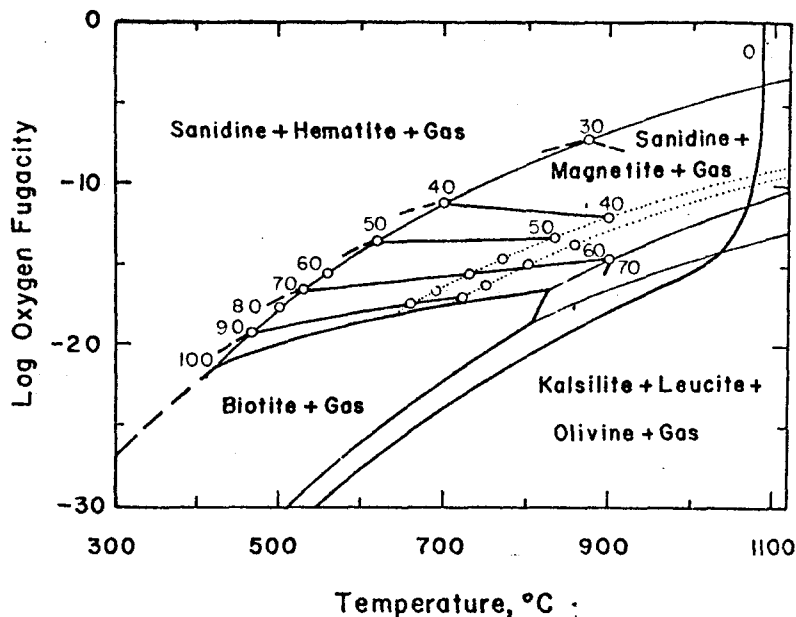
FIG. 4. A projection from the Fe/Fe+Mg axis of the biotite equilibria onto the f_{O_2}-T plane at 2070 bars total pressure. The positions of biotite-sanidine-magnetite equilibria as determined in this study are shown by heavy contours of constant Fe/Fe+Mg×100 values for the biotites and are taken from Fig. 3. Heavy curve labeled O represents maximum phlogopite stability, area bounded by curve labeled 100 is the annite stability field. Light weight lines and dotted lines represent "buffer" curves (see Table 1). See also Figs. 13 and 14.

Figure 32. Stability of biotite in relation to oxygen
fugacity and temperature, after Wones and
Eugster (1965).
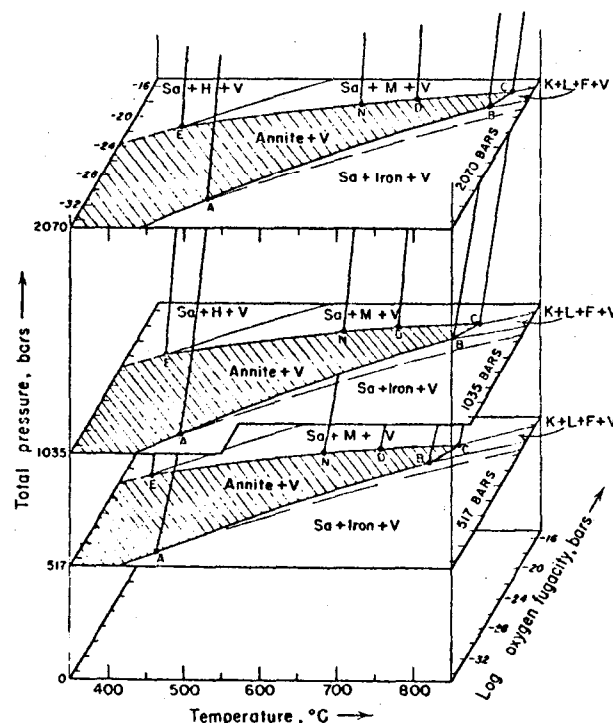
FIG. 8. Block diagram of the phase relations of annite (+vapor) bulk composition as a function of temperature, total pressure, and oxygen fugacity, constructed from sections at constant pressure. A, B, C, D, N, E are points of Fig. 4. Light lines through A, B, C, E are oxygen buffer curves (see Fig. 4). Sa = sanidine; H = hematite; M = magnetite; K = kalsilite; L = leucite; F = fayalite; V = vapor.

Figure 33. 'Stability of annite in relation to temperature,
total pressure and oxygen fugacity, after
Eugster and Wones (1962).

in figures 32 and 33. A decrease in P or T, or an increase
in fO_2, or any combination thereof, will cause the original
biotite to react with O_2. The products would be magnetite,
sanidine, water and a more magnesian biotite, the
composition of which would depend upon the prevailing P, T
and fO_2 conditions.

INTERPRETATION:-

Although the composition of biotites alone are being
considered, rather than equilibrium mineral assemblages, some
general statements may be made regarding the observed
compositional variations. The relative magnesium differences
between primary magmatic and hydrothermal biotites may
indicate an overall drop in total pressure of the system
after crystallization of the phenocryst phases, but may
incorporate also a drop in temperature as well as increases
in fO_2 and fS_2. The occurrence of magnesium-rich hydro-
thermal biotites within areas of intense copper mineraliza-
tion may indicate a thermal gradient, with temperatures
decreasing away from these zones, and the presence of Fe^{3+} in
the hydrothermal biotites suggests higher oxygen activity,
although the content of ferric iron in magmatic biotites
was not determined, it is inferred that the Fe^{3+} content is
low due to its reddish tint.

AMPHIBOLES:-

Amphiboles are uncommon in the intrusives of the
Coalstoun prospect. They occur in porphyritic hornblende

microdioite phases of the southern and northern valley areas

and within andesitic-dacitic dykes.   Most of the amphibole

within the central valley has been hydrothermally altered

to biotite or chlorite depending upon the original rock

type and its position within the alteration pattern.

Analyses for these amphiboles are shown in table 8.

Three fresh amphiboles from an andesitic dyke

(CL619) are ferroan pargasitic hornblende (figure 34) from

Leake's (1968) classification.

The pleochroic scheme for these amphiboles is -

$\propto$ -   colourless

β -   pale brown

γ -   pale brown

2V   -   + ive;   60-70$^{\text{o}}$

maximum extinction angle observed was approximately 25$^{\text{o}}$.

One fresh amphibole from a porphyritic hornblende

microdiorite (CL614) from within the central valley was

identified as common hornblende based on pleochroic scheme;

$\propto$ -   colourless

β -   pale brown-green or

yellow-green

γ -.   pale green

extinction on longitudinal sections ranged from 12$^{\text{o}}$ - 24$^{\text{o}}$,

with a -ive 2V.   Chemically this hornblende plots within the

actinolitic   hornblende field after Leake (1968), figure 34.

This hornblende coexists with magmatic biotites whose

composition showed the least alumina of those analysed and

Sample No.	CL 619			CL 614
SiO_2	43.61	42.80	43.27	52.00
TiO_2	2.31	2.14	2.42	.49
Al_2O_3	12.01	12.29	11.18	4.76
FeO*	10.25	11.31	10.88	10.51
MnO	.13	.13	.14	.38
MgO	15.05	14.77	14.91	17.74
CaO	12.09	12.05	11.72	11.57
Na_2O	2.48	2.39	2.47	.63
K_2O	.45	.44	.40	.20
Total	98.38	98.32	97.39	98.28
Si	6.32	6.24	6.35	7.39
Al	1.68	1.76	1.65	.61
Al	.37	.35	.29	.19
Ti	.25	.24	.27	.05
Fe	1.24	1.38	1.34	1.25
Mn	.02	.02	.02	.05
Mg	3.25	3.21	3.26	3.76
Ca	1.88	1.88	1.85	1.76
Na	.70	.68	.70	.18
K	.08	.08	.08	.04

Table 8. Composition and structural formula of
analysed amphiboles. Number of ions based on
23 Oxy's.

Ca + Na + K less than 2.50 ; Ti less than 0.50

		Si in the unit cell							
mg 1.00 8.00	7.75	7.50	7.25	7.00	6.75	6.50	6.25	6.00	5.75 mg 1.00
Tremolite		Tremolitic hornblende							
Actinolite		Actinolitic hornblende		Magnesio-hornblende		Tschermakitic hornblende		Tschermakite	0.75
Ferro-actinolite		Ferro-actinolitic hornblende		Ferro-hornblende		Ferro-tschermakitic hornblende		Ferro-tschermakite	0.25

Ca + Na + K greater than 2.50 ; Ti less than 0.50

Richterite		Richteritic edenite	Edenite	Edenitic hornblende	Pargasitic hornblende	Pargasite	
					Ferroan pargasitic hornblende	Ferroan pargasite	
Ferro-richterite		Ferro-richteritic edenite	Ferro-edenite	Ferro-edenitic hornblende	Magnesian hastingsitic hornblende	Magnesian hastingsite	
					Hastingsitic hornblende	Hastingsite	

Ti greater than 0.50

Kaersutite
Ferro-kaersutite

Figure 2. Basic names for the calciferous and subcalciferous amphiboles with respect to their Si, Ca+Na+K, mg, and Ti values in the half-unit cell.

Figure 34.   Composition and names of amphiboles after Leake (1968).

Dioritic amphibole – ◇ ;   Andesitic amphibole – ▢ .

therefore plotted well within the hornblende association
field III after Nockolds (1947) of figure 28.

CHLORITES:

Chlorites do not occur as a primary magmatic mineral,
but are ubiquitous to the outer zone of the central
intrusive stock and surrounding altered metasediments,
ie. the chlorite-epidote-carbonate zone of hydrothermal
alteration.

Chlorites occur replacing other ferromagnesian
minerals, such as biotites and amphiboles, and their chemical
analyses are shown in table 9. Although the seven analysed
chlorites are probably pycnochlorite, after the classific-
ation of Hey (1954) (figure 35), there is a marked difference
in their iron, manganese and magnesium contents depending
upon the replaced magmatic mineral. Chlorites after
biotites are richer in iron and poorer in manganese and
magnesium compared with chlorites replacing amphiboles.
These apparent chemical differences probably reflect the
composition of the replaced ferromagnesian mineral rather
than the chemical conditions at the time of hydrothermal
alteration.

For constant volume replacement of biotite by
chlorite, Dodge (1973, p. 63) suggests a decrease in "Si, Na,
K, Ti, F, Ba, and V and increase of Al, total Fe, Mg, Mn,
Co, Cu, Vi, perhaps Ga, and, of course, H_2O." Several of
these changes are evident within the chlorites examined,

Sample No.	CL625			CL619	CL609		
Type.	after	biotite.		after	amphibole.		
SiO$_2$	30.98	27.00	28.24	28.60	27.54	28.48	28.34
TiO$_2$	.20	.23	1.59	.03	.00	.02	.01
Al$_2$O$_3$	19.44	21.73	18.47	19.49	18.37	19.66	19.44
FeO*	19.73	19.74	21.79	17.53	16.93	16.55	16.87
MnO	.04	.04	.02	.21	.24	.27	.29
MgO	16.63	16.15	16.37	20.86	21.74	21.83	21.45
CaO	.07	.04	.04	.03	.05	.04	.06
Na$_2$O	.00	.02	.01	.07	.02	.07	.02
K$_2$O	.63	.14	.12	.00	.28	.05	.00
Total	87.72	85.09	86.65	86.82	85.17	86.97	86.48
Si	6.26	5.66	5.88	5.81	5.73	5.76	5.77
Al	1.74	2.34	2.12	2.19	2.27	2.24	2.23
Al	2.90	3.03	2.42	2.48	2.24	2.45	2.44
Ti	.03	.04	.25	.01	.00	.00	.01
Fe	3.34	3.46	3.80	2.98	2.95	2.80	2.87
Mg	5.01	5.05	5.09	6.32	6.74	6.58	6.51
Ca	.02	.01	.01	.01	.01	.01	.01
Na	.00	.01	.01	.03	.01	.03	.01
K	.16	.04	.03	.00	.07	.01	.00

Table 9. Composition and structural formula of chlorites.

* Total Fe as FeO.

No. of ions calculated on the basis of 28 oxygens.
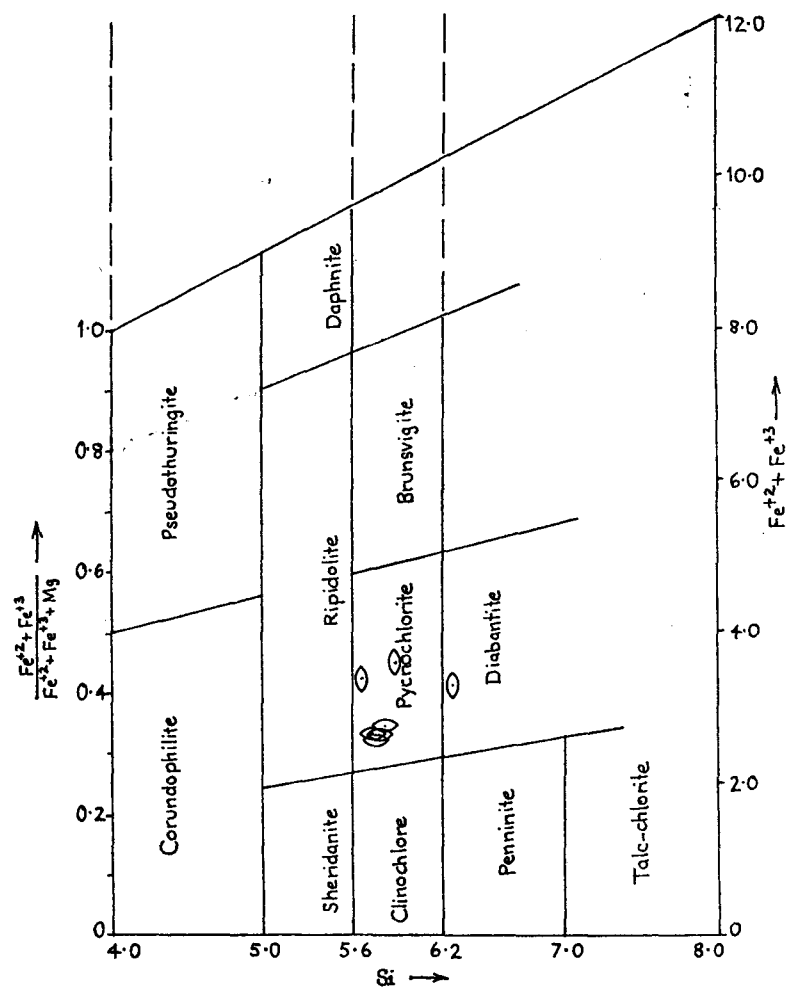
Figure 35.   Nomenclature of chlorites (after Hey, 1954)
taken from Deer, Howie and Zussman (1962).

Chlorite after biotite - ⊘ .

Chlorite after amphibole - ⬭ .

especially the Si/Al ratio (figure 27) which has a marked
decrease, as well as a slight increase in the Fe/Mg ratio.
Reluctance of Ti to be accepted within the chlorite
structure is reflected in the close association of rutile
(plate 22).

CHAPTER 7.   SUMMARY AND INTERPRETATION.

Introduction.

Copper mineralization and biotitization.

Sulphide zoning.

Interpretation.

Conclusion.

7.   SUMMARY AND INTERPRETATION

SUMMARY:-

Within the Coalstoun prospect there appears to exist
a regular zonal distribution of hydrothermal alteration
minerals and sulphide mineralization.   This zonal pattern
consists of an inner biotite zone passing outwardly into
chloritized intrusive and sedimentary rocks, thence into
recrystallized sediments.   Copper sulphide mineralization
occurs within the zone of biotitization with the copper
content decreasing toward the outer chlorite-epidote-carbonate
alteration zone.   Complementary to this, the pyrite content
increases outwardly into the chloritized zone, and decreases
out into the recrystallized sediments.

COPPER MINERALIZATION AND BIOTITIZATION:-

A prominent result of this study is the close relation-
ship between copper mineralization and the content of hydro-
thermal biotite.   The hydrothermal biotites show marked
physical and chemical differences compared to primary magmatic
biotites and are appreciably much finer grained, possess a
greenish tint to their pleochroism in contrast to the coarse
euhedral books of reddish magmatic biotites.   Chemically the
hydrothermal biotites are poorer in TiO_2 and FeO and convers-
ely relatively richer in MgO and Al_2O_3.   Hydrothermal
biotites associated with intense copper mineralization show
the highest magnesium content and possibly higher Fe^{3+}/Fe^{2+}
ratios.   These variations have been shown in figures 25 - 28.

SULPHIDE ZONING:-

Hypogene sulphides comprise pyrite and chalcopyrite with lesser amounts of molybdenite and bornite, and traces of tetrahedrite, galena and sphalerite. The zonal configuration of these sulphides consists of an inner deep core zone low in both sulphides and copper content. This core is surrounded by an envelope of higher copper grades with low pyrite/chalcopyrite ratios. This zone of higher Cu also contains traces of bornite and significant molybdenite. Outward progression is marked by an increase in the pyrite content with chalcopyrite decreasing markedly. Pyrite predominates within the chloritized zone, and gradually decreases in the surrounding metasediments.

INTERPRETATION:-

The prospect of Coalstoun shows geological, mineralogical and chemical features similar to other porphyry copper deposits distributed throughout southwestern North America, South America, Canada and the Southwest Pacific. A model for the origin of the Coalstoun prophyry copper prospect is suggested which centres on hypogene alteration and mineralization resulting from hydrothermal fluids. These fluids are proposed to have been released from the stock during the last stages of magmatic crystallization and is diagrammatically shown in figures 36: 1-10.

The Perry Fault and its associated steeply dipping fault planes, and their steeply plunging intersections,

probably penetrated to lower crustal depths and were possible
channelways for tapping magma from within the crust (figure
36: 1).   This tapped magma, initially probably undersaturated
with water at the prevailing load pressure, could have risen
rapidly; due to its high buoyancy, the ascent rate of which
was determined by the density difference between the magma
and the adjacent wall rocks as well as the viscosity of the
magma. · This rapid rise under slow cooling rates would
continue, with only gradual crystallization of plagioclase,
and probably biotite, until water saturation was reached, at
approximately 10-15km depth, depending upon the initial
concentration of water in the melt (Burnham, 1967).

Continued upward movement of the magma above this
point of saturation would induce future boiling off of the
aqueous phase, whenever P_{H_2O} in the melt exceeded P_T, as by
upward movement.   Continued rise of the magma therefore
promoted expulsion of some of the agueous phase (Burnham,
1967) which possibly combined with meteoric fluids causing
crackling and veining of the overlying sediments (figure 36: 2),
as evidenced by the random fine quartz veins, as well as
block faulting and formation of "shatter pipes" (Graham,
1973, p 8).

The porphyritic magma probably continued to rise engulf-
ing sedimentary blocks, caused by previous crackling, which is
especially evident in the northern part of the central valley.
The magma ceased upward movement at a shallow depth of approx-
imately 1-2 km (0.5- 5 kms is recorded for most porphyry

36-1

36-2

fault

magma
+ +
? ?

shatter
pipes

crackling

rising
magma
+
+
+ +
? ?

36-4

36-5

crystallized
shell

+
+ ◇ +
◇
+ ◇
+

quartz-
sericite-
pyrite

pocket

+
+ ◻
+ ◻
+
+
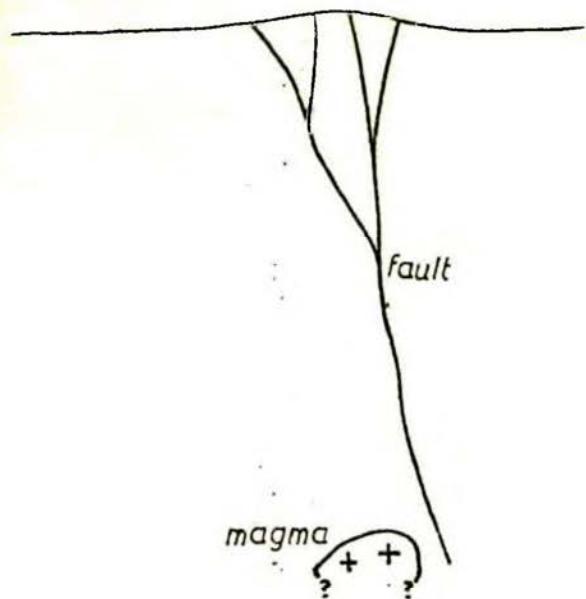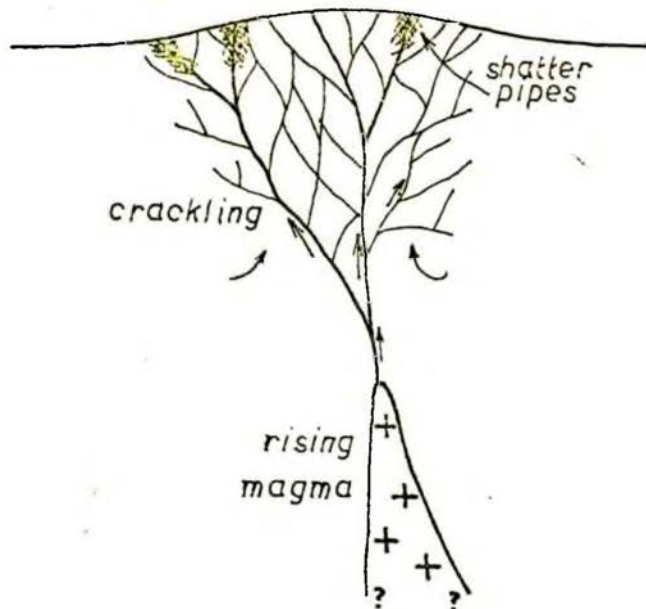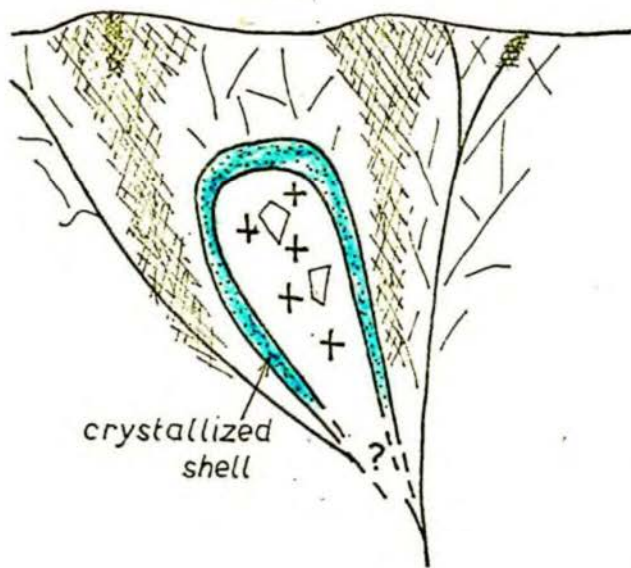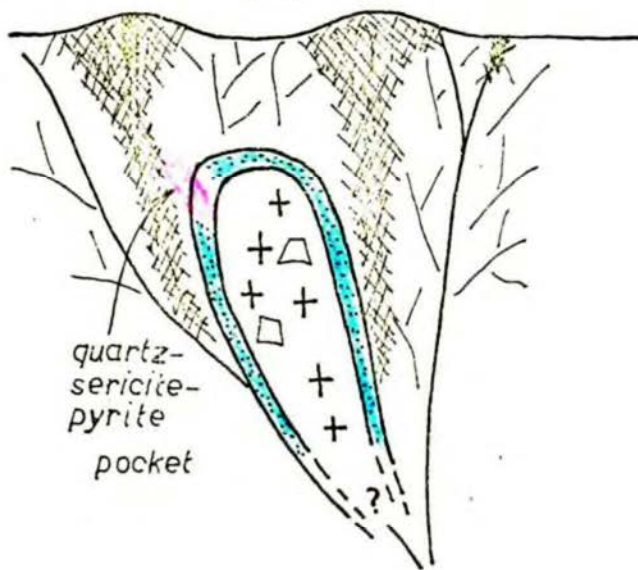
copper deposits) (figure 36: 3).   Rise of· the magma to this position resulted in brecciation in columnar zones which were localized at certain favoured fault interstions.

Initial crystallization of the stock began at the shell with formation of porphyritic quartz diorite around a partially crystallized mush (figure 36: 4).   A thermal gradient was thus set up with the highest temperatures at centres within the partially crystallized core.   Continuous episodic bleeding of volatites through this shell along fault zones resulted in complete hydrolysis of feldspars and leaching of calcium, magnesium and sodium with restriction of potassium to sericite in the formation of quartz-sericite-pyrite assemblages.   These episodes are indicated by growth rings within pyrite balls (plate 21).   These assemblages were located in pockets around the intrusive stock (figure 36: 5) and probably incorporated some contamination by meteoric waters (eg. Sheppard et. al., 1971; Meyer and Hemley, 1967).

Tectonic adjustments reactivating the Perry Fault and its branches fractured the solid shell causing rapid crystallization of the magma to porphyritic microtonalites· and quartz microdiorites along with the emplacement of dykes (figure 36: 6), which invaded the surrounding shell and metasediments along fault zones.   Volatiles and hydrothermal solutions released at this stage permeated through the intrusive stock with replacement by, and crystallization of, magnesium - enriched biotites followed by copper sulphides.

This alteration was concentrated in areas .of relatively high temperatures; $500 - 700^\circ$ C (eg. Gilluly, 1946; Creasey, 1966; Fourier, 1967; Putman and Alfars, 1969; Rose, 1970; Roedder, 1971) and at locations where aK^+ / aH^+ and aMg^+ / aH^+ were high enough to both stabilize biotite and avoid removal of magnesium. Due to relatively high activities of iron and/or magnesium compared with the bulk of southwestern North American porphyry copper deposits, the stability field of biotite extended to the outer margins of the intrusive stock[*] passing outwardly into chloritized - pyritized rocks (figure 36 -7). This outward change resulted from some degree of mixing of magma derived fluids and meteoric waters thereby decreasing the activity of K^+ and increasing the activities of Ca^{2+} and $CO_3{}^{2-}$ ions.

A dominant period of stockwork veining was associated with the last stages of this episode of fluid activity. Veinlets within the biotite zone contain combinations of quartz, biotite, K-feldspar,anhydrite, chalcopyrite, pyrite, molybdenite and magnetite. Outward into the chlorite zone the constituents change to quartz, pyrite, sericite and chlorite (figure 36: 8).

---

[*]   Biotite and sericite are structurally virtually
       identical with biotite differing from sericite
       only in the composition of the octahedral layer;
       biotite having $3(Mg + Fe)^{2+}$ as opposed to
       sericite having $2(Al^{3+})$. Biotite in effect
       has replaced sericite in the high iron-magnesian
       environment which has resulted in the wide
       biotite zone and absence of a "phyllic" zone.

36-7

chloritization

biotitization

?

36-8

veining

?

36-10

erosion

surface leaching
supergene en
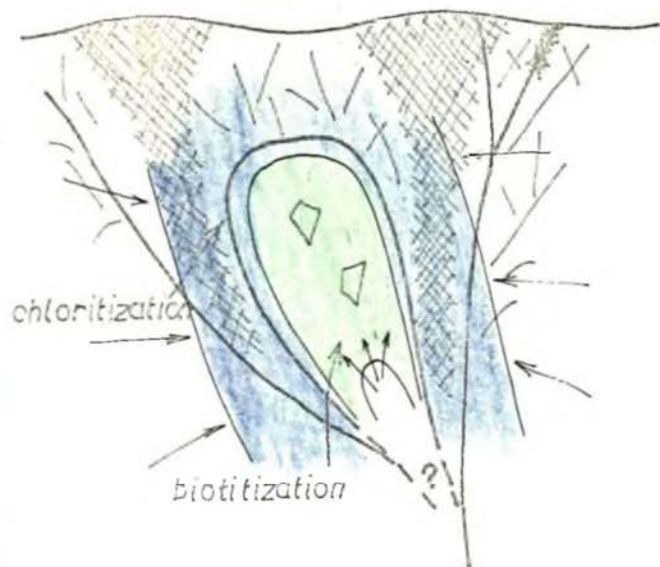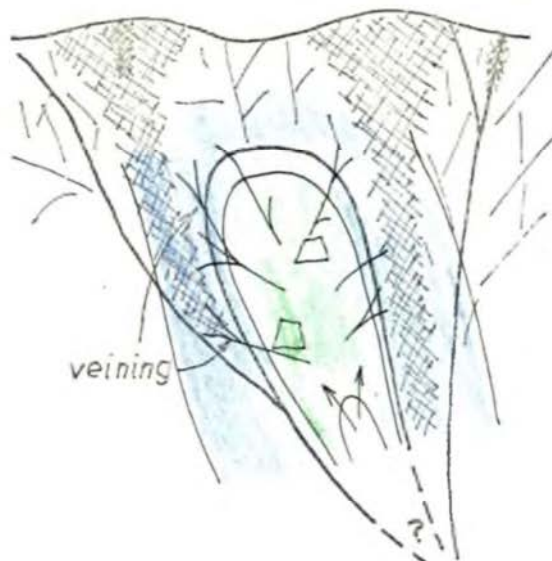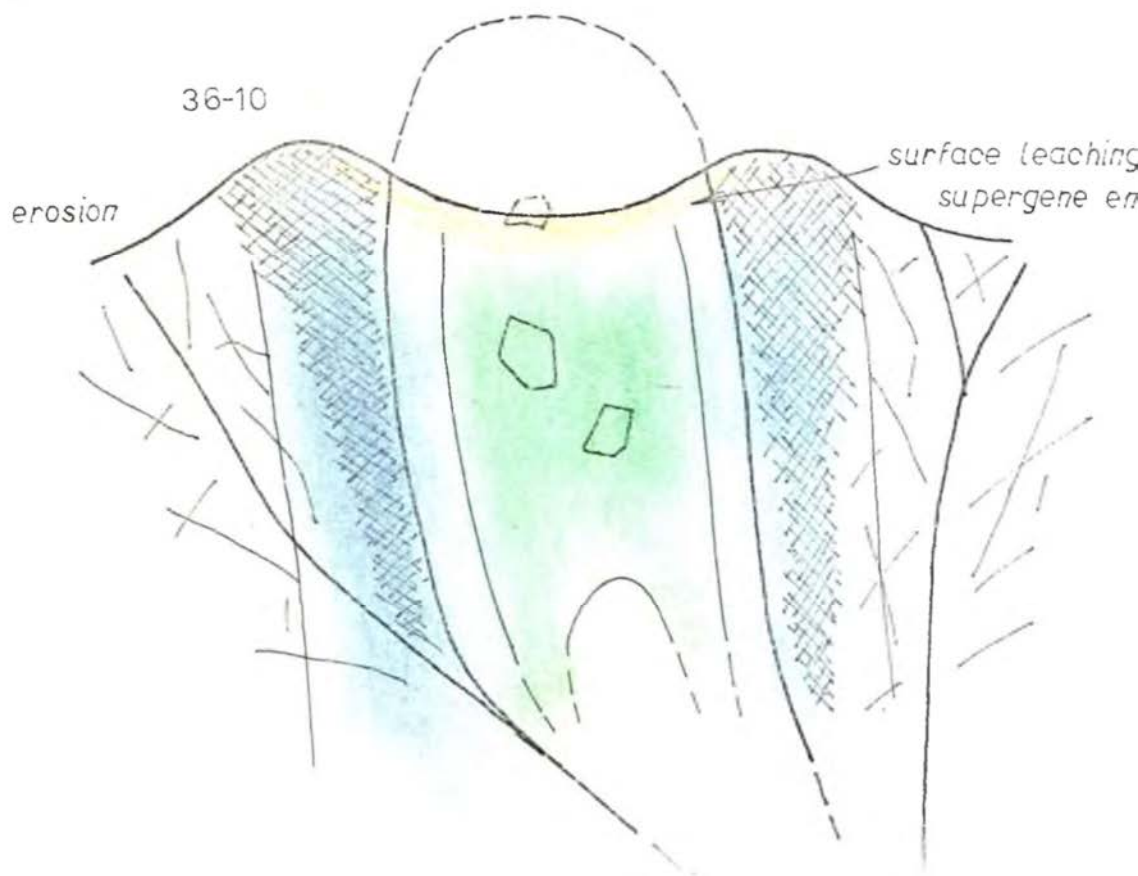
Towards the close of this hydrothermal alteration stage, a withdrawl of some remaining magma may have occured with concomittant veining which generally carried only quartz. Several of the gypsum veins are also likely to have followed at this time, while some may have resulted from latter hydration of anhydrite. After a period of quiesence, several andesitic and dacitic dykes are considered to have been intruded, perhaps related to further fault movement (figure 36: 9).

With continued dormancy, the effects of surface erosion set in with the prospect encouraging supergene enrichment and hydrolytic decomposition of silicates to clays and chlorite in the surface zones (figure 36: 10).

CONCLUSION:

Guilbert and Lowell (1974) demonstrated how a large variety of possible alteration assemblages and their zonal pattern may be obtained within porphyry ore deposits depending upon "depth of exposure, composition of pre-mineral wall rocks, pre-ore structural controls on intrusion, variations in composition of both igneous host rock and mineralizing fluids, size of the mineralizing system, variations in development of contemporaneous controls on mineralization (veinlets, veins and brecciation), and the breadth of stability fields of important silicate alteration minerals."

Undoubtedly the Coalstoun prospect fits into a

combination of one or more of these diversions from the norm

and a generalized pattern is schematically shown in figure 37.
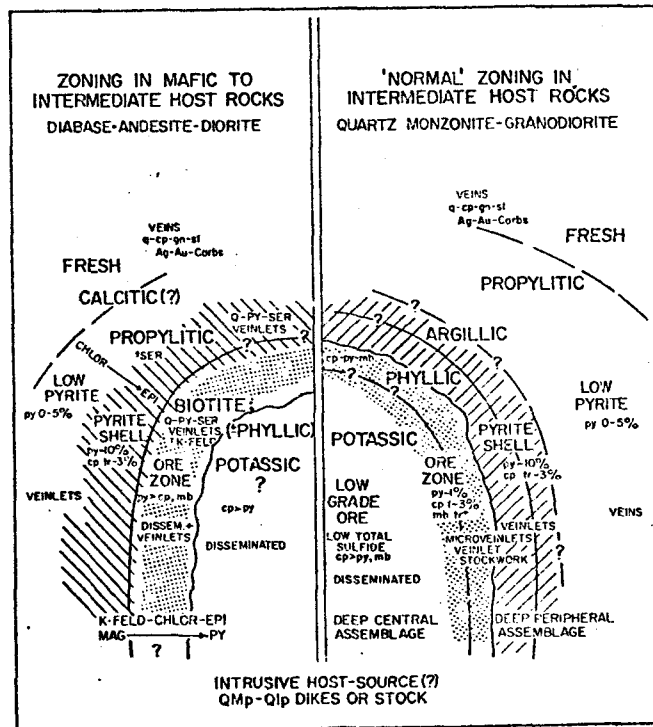
Figure 37.   Schematic comparison of alteration and
mineralization in mafic and intermediate
rocks after Guilbert and Lowell (1974).

8. REFERENCES.

8. REFERENCES

ANDERSON, C.A., SCHOLZ, E.A., and STROBELL, J.D., Jr.,
1955: Geology and ore deposits of the Bagdad area,
Yavapai County, Arizona; U.S. Geol. Survey Prof.
Paper 278, 103p.

ASHLEY, P.M., 1974: Ban Ban Authority to Prospect 1254M;
Qld. Dep. Mines Company Report 5145.

BRAY, R.E., 1969: Igneous rocks and hydrothermal alteration
at Bingham, Utah; Econ. Geol., 64, pp. 34-49.

BRYAN, W.H., and WHITEHOUSE, F.W., 1937: The Gayndah
earthquake of 1935; Proc. Roy. Soc. Qld.,
49, pp. 116-119.

BURNHAM, C.W., 1962: Facies and types of hydrothermal
alteration; Econ. Geol., 57, pp. 768-784.

CARSON, D.J.T., and JAMBOR, J.L., 1974: Mineralogy, zonal
relationships and economic significance of
hydrothermal alteration at porphyry copper
deposits, Babine Lake Area, British Columbia;
Bull. Can. Inst. Min. Metall., 67, pp. 110-133.

CREASEY, S.C., 1959: Some phase relations in the hydro-
thermally altered rocks of porphyry copper
deposits; Econ. Geol., 54, pp. 351-373.

CREASEY, S.C., 1966: Hydrothermal alteration; in
Geology of the Porphyry Copper Deposits,
Southwestern North America; S.R. Titley and
C.H.Hicks (eds.); Tucson, Arizona, The
University of Arizona Press, pp. 233-244.

DAY, R.W., CRANFIELD, LC., and SCHWARZBOCK, H., 1974:
Stratigraphy and structural setting of Mesozoic
basins in southeastern Queensland and north-
eastern New South Wales; in The Tasmanian
Geosyncline: A Symposium; Denmead, A.K.,
Tweedale, G.W., Wilson, A.F., (eds.); Geol.
Soc. Aust., Qld. Div., pp. 319-363.

DE GEOFFROY, J., and WIGNALL, T.K., 1972: . A statistical
        study of geological characteristics of porphyry
        copper-molybdenum deposits in the Cordilleran
        belt - application to the rating of porphyry
        prospects; Econ. Geol., 67, pp. 656-668

DEER, W.A., HOWIE, R.A, and ZUSSMAN, J., 1962: Rock
        forming mineral, Vol. 3. Sheet silicates;
        Longmans, Great Britain, 270 pp.

ELLIS, P.L., 1968: Geology of the Maryborough 1:250000
        sheet area; Geol. Surv. Qld. Rep., 26, 101 pp.

EUGSTER, H.P., and WONES, D.R., 1962: Stability
        relations of the ferruginous biotite, annite;
        Jour. Pet., 3, pp. 82-125.

FOUNTAIN, R.J., 1972: Geological relationships in the
        Panguna porphyry copper deposit, Bougainville
        Island, New Guinea; Econ. Geol., 67,
        pp. 1040-1064.

FOURNIER, R.O., 1967: The porphyry copper deposit
        exposed in the Liberty open-pit mine near Ely,
        Nevada. Part I. Syngenetic formation; Part II.
        The formation of hydrothermal alteration zones;
        Econ. Geol., 62, pp. 57-81 and 207-227.

FULLAGAR, P.D., BROWN, H.S., and HAGNER, A.F., 1967:
        Geochemistry of wall rock alteration and the
        role of sulfurization in the formation of the
        Ore Knob Sulphide deposit; Econ. Geol., 62,
        pp. 798-825.

GILLULY, J., 1946: The Ajo mining district, Arizona;
        U.S. Geol. Survey Prof. Paper 209, 112 pp.

GRAHAM, R.L., 1973: Coalstoun Authority to prospect
        1050M, Annual Report to Queensland Mines
        Department for year ending December 31, 1972.

GRAHAM, R.L., 1975:   Breccia Pipe Formation in relation
          to the Coalstoun Porphyry Copper System;
          M. Sc. Thesis, James Cook University of North
          Queensland (unpubl.), 121 pp.

GUILBERT, J.M., and LOWELL, J.D., 1974:   Variations in
          zoning patterns in porphyry ore deposits,
          Bull. Can. Inst. Min. Metall., 67,
          pp. 99-109.

GUPTA, S.P. DAS, GUPTA, P.R. SEN, and MURPHY, M.V.N., 1965:
          Nature and significance of wall rock alteration
          in some hydrothermal ore deposits in India;
          Econ. Geol., 60, pp. 1702-1708.

HALL, A.J., 1941:   The relation between colour and
          chemical composition in the biotites;
          Am. Min., 26, pp. 29-33.

HAMMARBÄCK, S., and LINDQVIST, B., 1972:   The hydrothermal
          stability of annite in the presence of sulphur;
          Geol. Fören, Förh., 94, pp. 549-564.

HAYAMA, Y., 1959:   Some considerations on the colour of
          biotite and its relation to metamorphism;
          Jour. Geol. Soc. Japan, 65, pp. 21-30.

HEIER, K.S., and ADAMS, J.A.S., 1964:   The geochemistry
          of the alkali metals; in Physics and Chemistry
          of the Earth; New York, Macmillan Company;
          v. 5, pp. 253-381.

HEINRICH, E.W.M., 1946:   Studies in the mica group; the
          biotite-phlogopite series; Am. Jour. Sci.,
          244, pp. 836-853.

HELGESON, H.C., 1970:   A chemical and thermodynamic
          model of ore deposition in hydrothermal systems;
          Mineral. Soc. Amer., Special Paper 3,
          pp. 155-186.

HEMLEY, J.J., and JONES, W.R., 1964:   Chemical aspects of
          hydrothermal alteration with emphasis on
          hydrogen metasomatism; Econ. Geol., 65,
          pp. 920-936.

HEY, M.H., 1954:   A review of the chlorites;   Min.
        Mag., 30, pp. 270.

HILL, D., 1955:   Contributions to the correlation and
        fauna of the Permian in Australia and New
        Zealand; J. Geol. Soc. Aust., 2,
        pp. 83-107.

JAMES, A.L., 1971:   Hypothetical diagrams of several
        porphyry copper deposits; Econ. Geol., 66,
        pp. 43-47.

KENTS, P., 1963:   Hydrothermal developments in the
        Andes; Econ. Geol., 58, pp. 1110-1118.

LACY, W.C., 1974:   Porphyry copper deposits; Aust. Min.
        Foun., Workshop Course May 1974, Adelaide
        (unpublished).

LEAKE, B.E., 1968:   A catalogue of analysed calciferous
        and subcalciferous amphiboles together with
        their nomenclature and associated minerals;
        Geol. Soc. Amer. Spec. Paper 98, 210 pp.

LOWELL, J.D., 1968:   Geology of the Kalamazoo orebody,
        San Manuel District, Arizona; Econ. Geol., 63,
        pp. 645-654.

LOWELL, J.D., 1973:   Regional characteristics of south-
        western North American porphyry copper deposits;
        Soc. Min. Engrs., Preprint 73-5-12 (cited in
        Lacy, 1974).

LOWELL, J.D., and GUILBERT, J.M., 1970:   Lateral and
        vertical alteration - mineralization zoning in
        porphyry ore deposits; Econ. Geol., 65,
        pp. 373-408.

MEYER, C., and HEMLEY, J.J., 1967:   Wall rock alteration;
        in Geochemistry of Hydrothermal Ore Deposits;
        H.L. Barnes(ed.):   New York, Holt, Rinehart
        and Winston, Inc., pp. 166-235.

MOORE, W.J., and CZAMANSKE, G.K., 1973:   Compositions of
        biotites from unaltered and altered monzonitic
        rocks in the Bingham Mining district, Utah;
        Econ. Geol., 68, pp. 269-280.

NEALE, R.C., 1974:   Coalstoun Authority to Prospect
        1050M for 1973;   Qld. Dept. Mines Company
        Report.

NIELSEN, R.L., 1968:   Hypogene texture and mineral
        zoning in a copper-bearing granodiorite
        porphyry stock, Santa Rita, New Mexico;
        Econ. Geol., 63, pp. 37-50.

NOCKOLDS, S.R., 1947:   The relation between chemical
        composition and paragenesis in the biotite
        micas of igneous rocks;   Am. Jour. Sci., 245,
        pp. 401-420.

OLADE, M.A., and FLETCHER, W.K., 1975:   Primary dispersion
        of Rubidium and Strontium around porphyry copper
        deposits, Highland Valley, British Columbia;
        Econ. Geol., 70, pp. 15-21.

PUTMAN, G.W., and ALFORS, J.T., 1969:   Geochemistry and
        petrology of the Rocky Hill stock, Tulare County,
        California;   Geol. Soc. Amer. Spec. Paper 120,
        109 pp.

ROEDDER, E., 1971:   Fluid inclusion studies on the
        porphyry-type ore deposits at Bingham, Utah,
        Butte, Montana, and Climax, Colorado;
        Econ. Geol., 66, pp. 98-120.

ROSE, A.W., 1970:   Zonal relationships of wallrock
        alteration and sulphide distribution at
        porphyry copper deposits;   Econ. Geol., 65,
        pp. 920-936.

SHEPPARD, S.M.F., NIELSEN, R.L., and TAYLOR, H.P. Jr., 1971:
        Hydrogen and oxygen isotope ratios in minerals
        from porphyry copper deposits;   Econ. Geol., 66,
        pp. 515-542.

STEVENS, N.C., 1961:   Cainozoic vulcanism near Gayndah,
        Queensland;   Proc. Roy. Soc. Qld., 72,
        pp. 75-82.

STRECKEISEN, A., 1974:   Classification and nomenclature
        of plutonic rocks; Geol. Rund., 63,
        pp. 773-786.

STOKES, H.N., 1906:   On the solution, transportation
        and deposition of copper, silver and gold;
        Econ. Geol., 1, pp. 644-650.

TITLEY, S.R., and HICKS, C.L., (Eds.), 1966:   Geology of
        the porphyry copper deposits.   Univ. Arizona
        Press, Tucson, 287 pp.

TUREKIAN, K.L., and KULP. J.L., 1956:   The geochemistry
        of Strontium; Geochim. et Cosmochim. Acta, 10.
        pp. 245-296.

WEBB, A.W., and McDOUGALL, I., 1967:   Isotope dating
        evidence on the age of the Upper Permian and
        Middle Triassic; Earth Planet. Sci. Lett.,
        2, pp. 483-488.

WEBB, A.W., STEVENS, N.G., and McDOUGALL, I., 1968:
        Isotopic age determinations on Tertiary
        volcanic rocks and intrusives of southeastern
        Queensland; Proc. Roy. Soc. Qld., 79,
        pp. 79-92.

WELLMAN, P., 1971:   Age and palaeomagnetism of Australian
        Cainozoic volcanic rocks; Ph.D. Thesis,
        A.N.U. Canberra, (unpublished).

WINKLER, H.G.F., 1967:   Petrogensis of Metamorphic Rocks;
        Springer-Verlag, New York, 237 pp.

WONES, D.R., and EUGSTER, H.P., 1965:   Stability of
        biotite: experiment, theory and application;
        Amer. Mineral., 50, pp. 1228-1272.

ADDENDA.

References;

Bence,   , and Albee,   , 1968: Empirical correction factors for the
      electron microprobe analysis of silicates and oxides; J. Geol.,
      76, pp. 382-403.

Burnham, C.W., 1967: Hydrothermal fluids at the magmatic stage; in
      Geochemistry of Hydrothermal Ore Deposits; Barnes, H.L. (Ed.);
      Holt, Rinehart and Winston; New York; pp. 34-76.

Dodge, F.C.W., 1973: Chlorites from granitic rocks of the central
      Sierra Nevada batholith, California; Min. Mag., 39, pp. 58-64.

Flood, R.H., 1971: A study on part of the New England Bathylith;
      Ph. D. Thesis, University of New England (unpubl.).

Norrish, K., and Chappell, B.W., 1967: X-ray fluoresence spectrography;
      in Physical Methods in Determinative Mineralogy; pp. 161-214.

Wilson, A.D., 1955: A new method for the determination of ferrous ion
      in rocks and minerals; Bull. Geol. Surv., Gt. Britain, 9, pp. 56-58.

APPENDIX

1. ANALYTICAL METHODS:-

    A. X-ray Fluoresence;

The major oxides; SiO_2, TiO_2, Al_2O_3, total Fe as FeO, MnO, MgO, CaO, K_2O and P_2O_5, were determined by x-ray fluorescent spectrometry following the fused lithium tetraborate glass disc method of Norrish and Chappell (1967).

The trave elements; Y, Sr, Zr, U, Rb, Th, Pb, Ga, Zn, Cu, Ni, Mn, Cr, V, Ti, and Ba, were also determined by x-ray fluorescent spectrometry using pressed pellets of ground material with a boric acid backing.

The equipment used for the above analyses was the school's Siemens SRS XRF spectrometer, with a 4kW generator and a standard counting rack.

Standards for the major and trace element analyses were the U.S. Geol. Survey rock standards; W-1, PCC-1, DTS-1, GSP-1, G-2, BCR-1, and AGV-1.

    B. Flame photometry;

The major oxide, Na_2O, was determined using flame photometric techniques (Hitachi 205 Flame Photometry) with closely spaced artificial standards and the use of Li_2SO_4 to suppress inter-element interference.

    C. Wet chemistry;

FeO was determined by a minor modification to the method of Wilson (1955).

2. LOSS ON IGNITION:-

Total loss on ignition (LOI.) was determined by oven drying
at 1000°C for 1 hour.

3. MINERAL ANALYSES:-

The composition of ferromagnesian minerals and plagioclase
feldspars (Table 10), were determined by electron microprobe analysis.
Analyses were conducted with the School of Earth Sciences',Macquarie
University, ETEC Autoprobe microprobe at an accelerating potential
of 15kv, a specimen current of 30nA on brass, and a beam diameter
of approximately 10 m. Analyses were performed using three spectrometers
in the series Ti, Mn, Fe; Na, Mg, Al; and Si, K, Ca. Corrections
were made according to the method of Bence and Albee (1968).

Standards were continually checked for accuracy and analyses are
given in table 11.

Sample No.	CL 601		CL 625		CL 609		CL 537		CL 537	
	R	C	R	C	R	C	R	C	R	C
SiO_2	58,27	56.80	65.79	66.13	62.96	62.22	59.00	57.65	59.51	58.9:
TiO_2	.01	.01	.01	.01	.00	.00	.00	.00	.00	.0(
Al_2O_3	24.32	26.01	21.36	20.01	21.66	22.58	24.48	25.20	23.49	24.0:
FeO	.16	.14	.10	.12	.35	.27	.18	.16	.16	.1:
MnO	.01	.00	.03	.03	.01	.00	.02	.01	.01	.0(
MgO	.04	.04	.04	.02	.27	.20	.01	.00	.02	.0
CaO	7.69	9.37	2.23	.79	.65	.64	6.67	7.31	6.63	6.6!
Na_2O	7.20	6.43	9.93	11.08	9.00	9.04	7.60	7.12	7.68	7.7(
K_2O	.34	.26	.22	.21	1.95	1.61	.36	.33	.37	.3!
Total	98.04	99.06	99.71	98.40	96.85	96.56	98.32	97.78	97.87	97.9!

Table 10. Plagioclase compositions. *Total Fe as FeO.

C= core of phenocryst. R= rim of phenocryst.

	Kaersutite standard.	Probe run results.			
SiO_2	40.37	40.43	41.35*	39.79	40.33
TiO_2	4.38	4.11	4.38	4.51	4.43
Al_2O_3	14.9	14,28	14.28	14.81	13.91*
FeO	10.92	10.83	10.99	11.21	10.90
MnO	.09	.07	.09	.09	.09
MgO	12.8	12.67	12.50	12.80	12.69
CaO	10.3	10.82	10.76	10.97	10.52
Na_2O	2.6	2.70	2.67	2.70	2.72
K_2O	2.05	2.17	2.16	2.19	2.14

*These were restandardized.

Table 11. Kaersutite standard analysis compared with analyses during probe runs.

4. ROCK CATALOGUE:-

Below is a list of catalogue numbers (Macquarie University

collection), field numbers (prefixed by CL), and drill hole

number with depth in feet.

Catalogue No.	Field No.	DDH/ depth.	Catalogue No.	Field No.	DDH/ depth.
MU 10815	151	E6/117	MU 10840	260	E15/881
6	152	143.5	1	261	909
7	153	166	2	262	943
8	154	305	3	263	988
9	155	341	4	264	1038
MU 10820	156	426	5	265	1053
1	157	468.5	6	266	1105
2	158	501	7	267	1112
3	159	511	8	268	1139.5
4	160	536.5	MU 10849	269	E15/1147
4	161	536.5			
MU 10825	162	E6/573.5	MU 10850	426	E27/91
			1	427	179
MU 10826	176	E12/188	2	428	205.5
7	177	246	3	429	457.5
8	178	319	4	430	486.5
9	179	409.25	5	431	629.5
MU 10830	180	E12/422.25	6	432	646
			7	433	709
MU 10831	251	E15/124	8	434	780.5
2	252	285	9	435	827
3	253	379	MU 10860	436	854
4	254	416	MU 10861	437	E27/934
5	255	471			
6	256	501.5	MU 10862	451	E28/1174
7	257	616.5	3	452	1184
8	258	651	MU 10864	453	E28/1298
MU 10839	259	E15/759.25			

Catalogue No.	Field No,	DDH/ depth.	Catalogue No,.	Field No.	DDH/ depth.
MU 10865	526	E32/273.5	MU 10898	588	E34/716
6	527	323	MU 10899	589	E34/861.5
7	528	335			
8	529	467	MU 10900	601	E36/72
9	530	520	1	602	113.5
MU 10870	531	812	2	603	127
1	532	820.5	3	604	166.5
2	533	882.5	4	605	174.5
3	534	987	5	606	180.5
4	535	1050.75	6	607	243
5	536	1221	7	608	255
6	537	1250.5	8	609	262
7	538	1300.5	9	610	301
8	539	1350	MU 10910	611	322
9	540	1370	1	612	345.5
MU 10880	541	1403.5	2	613	359.5
MU 10881	542	E32/1457.5	3	614	379
			4	615	401.5
MU 10882	551	E33/171.5	5	616	461
3	552	253.5	6	617	603
4	553	455	7	618	635.75
MU 10885	554	E33/498.75	8	619	706
			9	620	1069
MU 10886	576	E34/75.5	MU 10920	621	1074
7	577	86	1	622	1076
8	578	165.5	2	623	1098.5
9	579	225.5	3	624	1133.75
MU 10890	580	340	4	625	1208
1	581	418	5	626	1375.5
2	582	497.5	6	627	1561.75
3	583	506.5	MU 10927	628	E36/1735.5
4	584	507			
5	585	520.25			
6	586	585			
MU 10897	587	E34/525.75			

Catalogue No.	Field No.	DDH/ depth.	Catalogue No.	Field No.	DDH/ depth.
MU 10928	701	E41/347	Samples from Gebangle, to the		
9	702	390	north of Coalstoun.		
MU 10930	703	406.5	MU 10940	G1	E1/89
1	704	449.5	MU 10941	G2	E1/663
2	705	583			
3	706	745			
4	707	913.5			
5	708	1034			
6	709	1103.5			
7	710	1160			
MU 10938	711	E41/1253			

ESSO Thin Sections:-

Kennecott DDH/ depth.	ESSO DDH/ depth.	ESSO DDH/ depth.	ESSO DDH/ depth.
K1/168	E1/23.5	E6/537	E28/294.5
212	88	657.5	311.5
401.5	99	E8/177.25	323
464	196.5	E10/100.5	353.5
799.5 (9)	236.5	E12/255,5	361
1074	295.5	371	371
K5/335.5	305.5	387	613.25
458	546	401.5	674.5
K7/323	555	409	1297,5
K8/50	561 (26)	422.5	E29/129.5
258	588	435	148
342.5 (17)	847.5	477	165
K9/79.5	E2/84.5	E13/376	E30/188.5
196.5	217	E23/435.5	E32/1431
K10/89	E3/301 (4)	888	1457.5
312 (21)	E4/166	902	E36/442
K11/327	174	902	E37/623
K11/337	E5A/282.5 (23)	920.5	Surface sample.
	E6/122	935	
	E6/143.5	E23/1316.5	E of A.
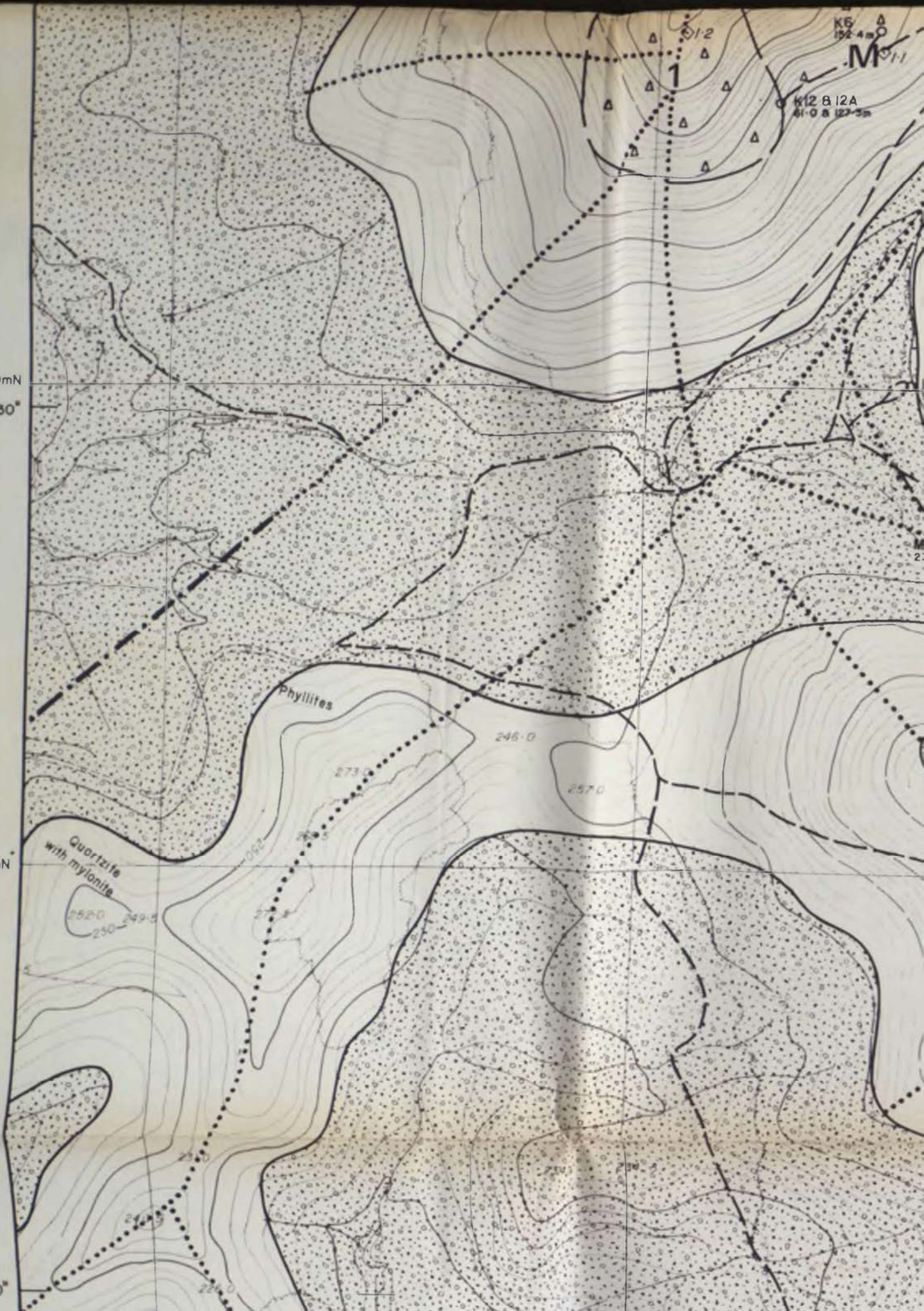
161500mN

161000mN

25° 40' 00"

160500mN

204.5

212.0

216.3

200.5

175

174.0

188.0

186.0

169.5

168.5

168.0

169.5

168.0

167.5

169.5

168.0

167.5

165.5

176.0

187.0

OVERLAYS 1-7

OVERLAY 1.

LEGEND.
see figure 14
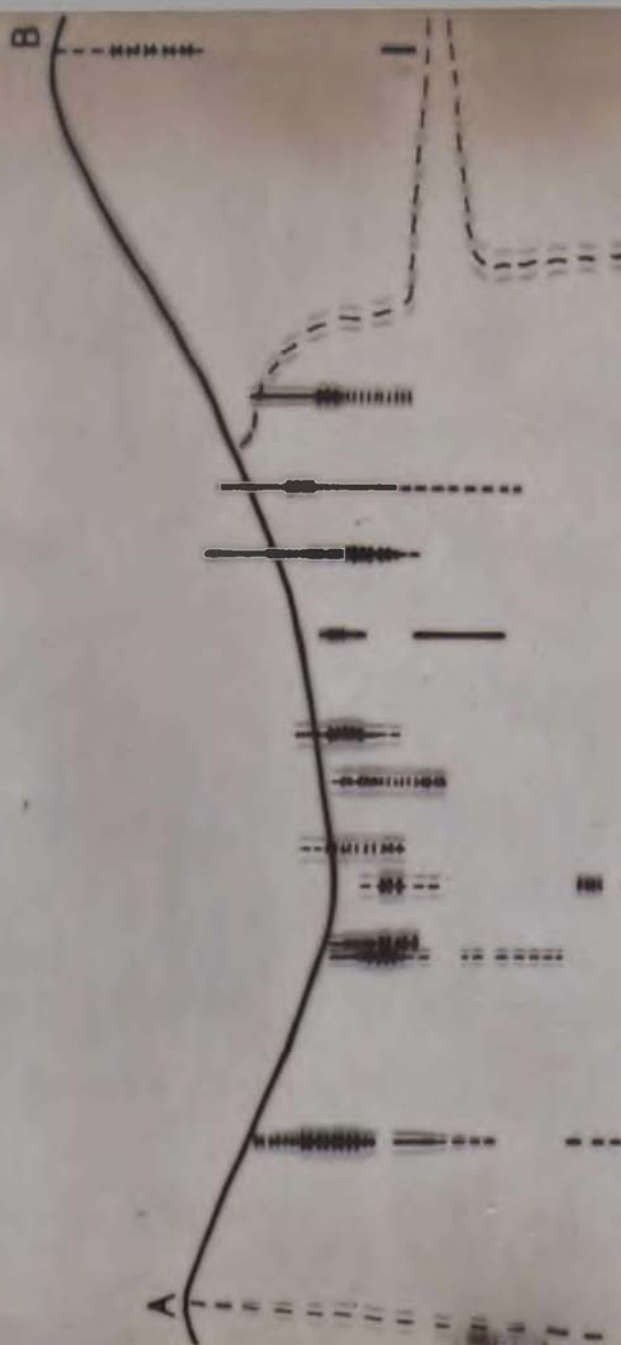
OVERLAY 2.

OVERLAY 3.

LEGEND.
Chloritization.
strong.   weak.
F   Fault or shear zone.

OVERLAY 4.

A

B

LEGEND.
Hydrothermal biotitization.

‖ strong.

⫶ weak.
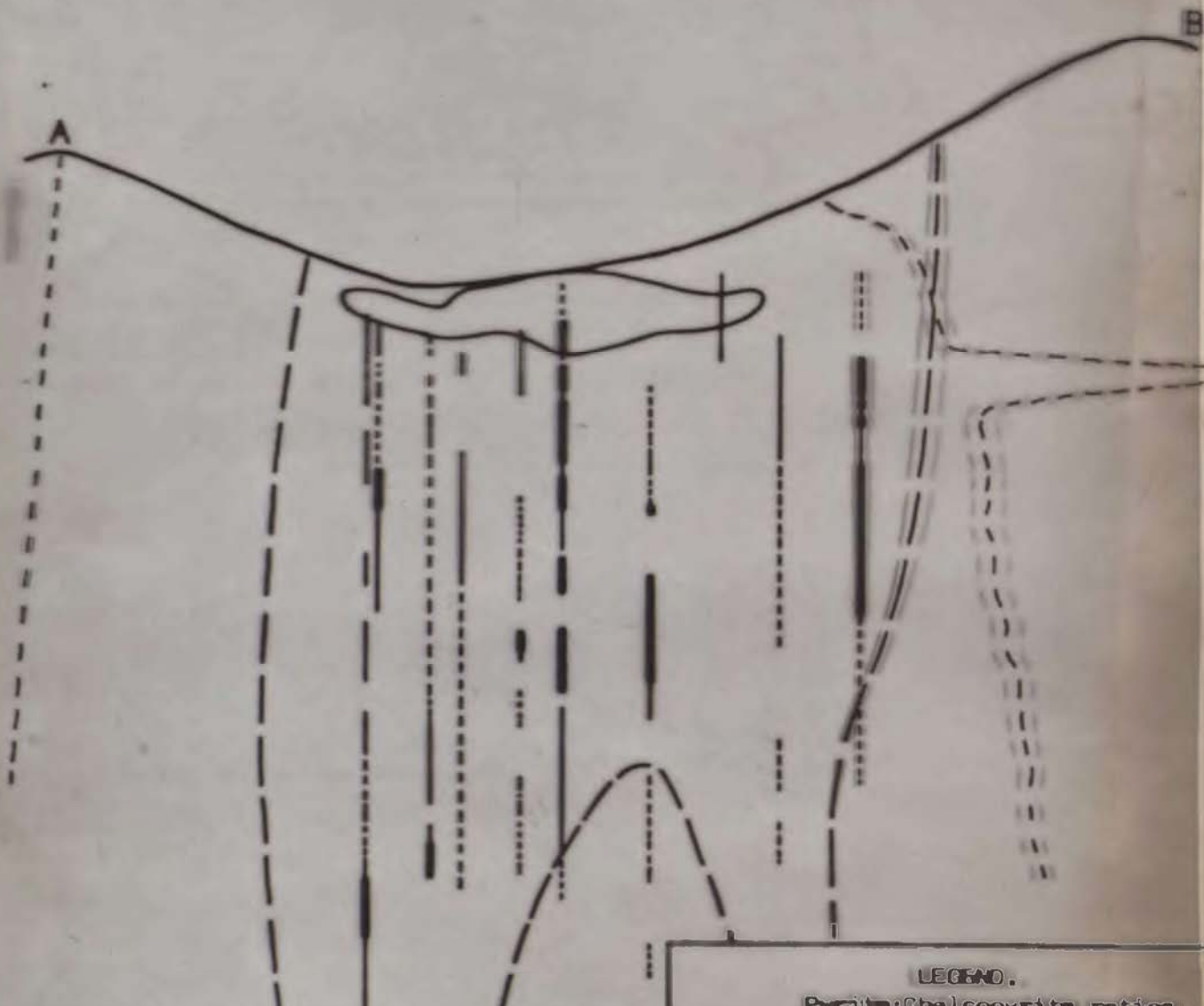
OVERLAY 5.

LEGEND.

Pyrite:Chalcopyrite ratios.

<1:1.   2:1 - 1:1

5:1 - 2:1.   > 5:1.

Supergene sulphides.
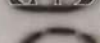
< 3 % total sulphides by vol.
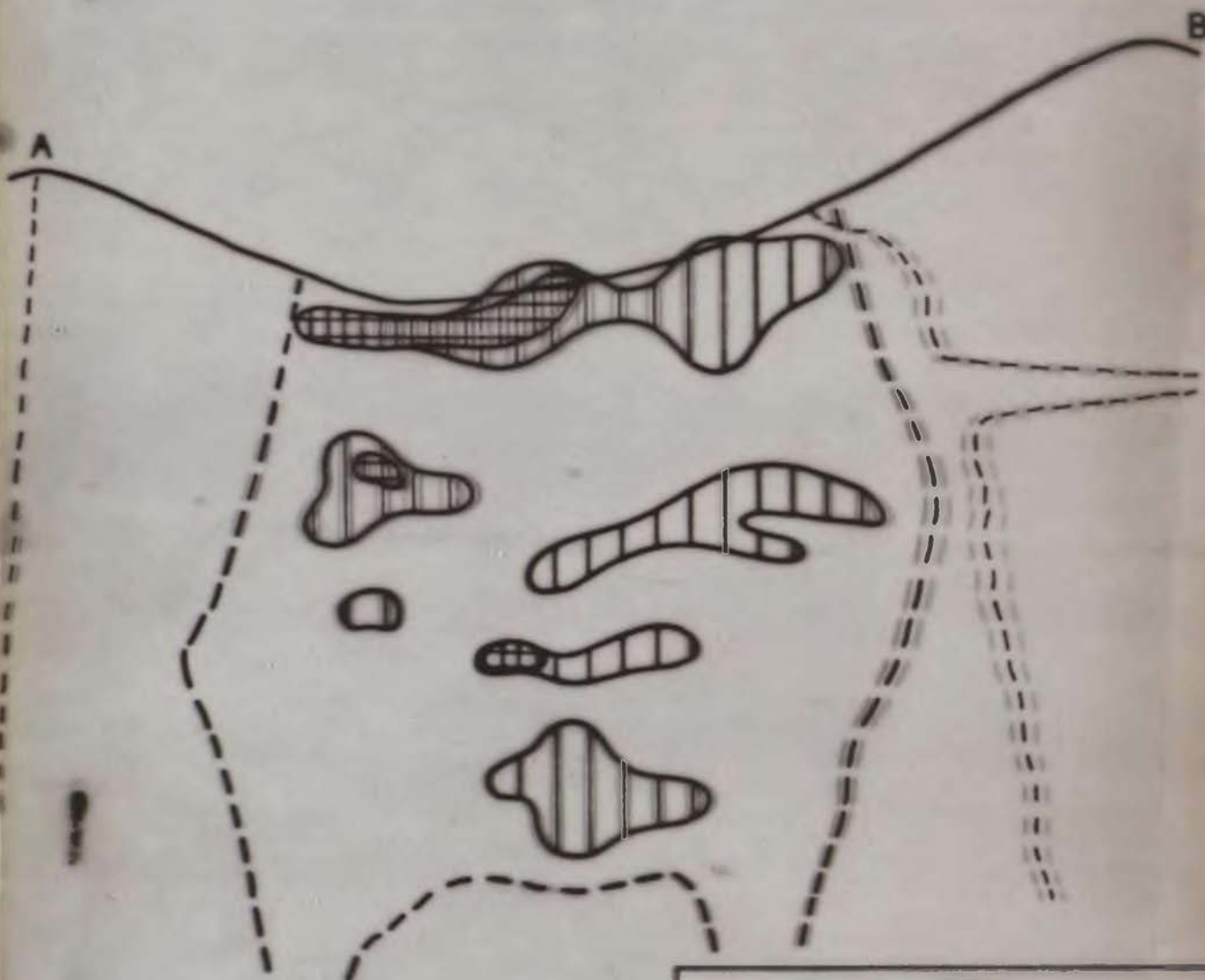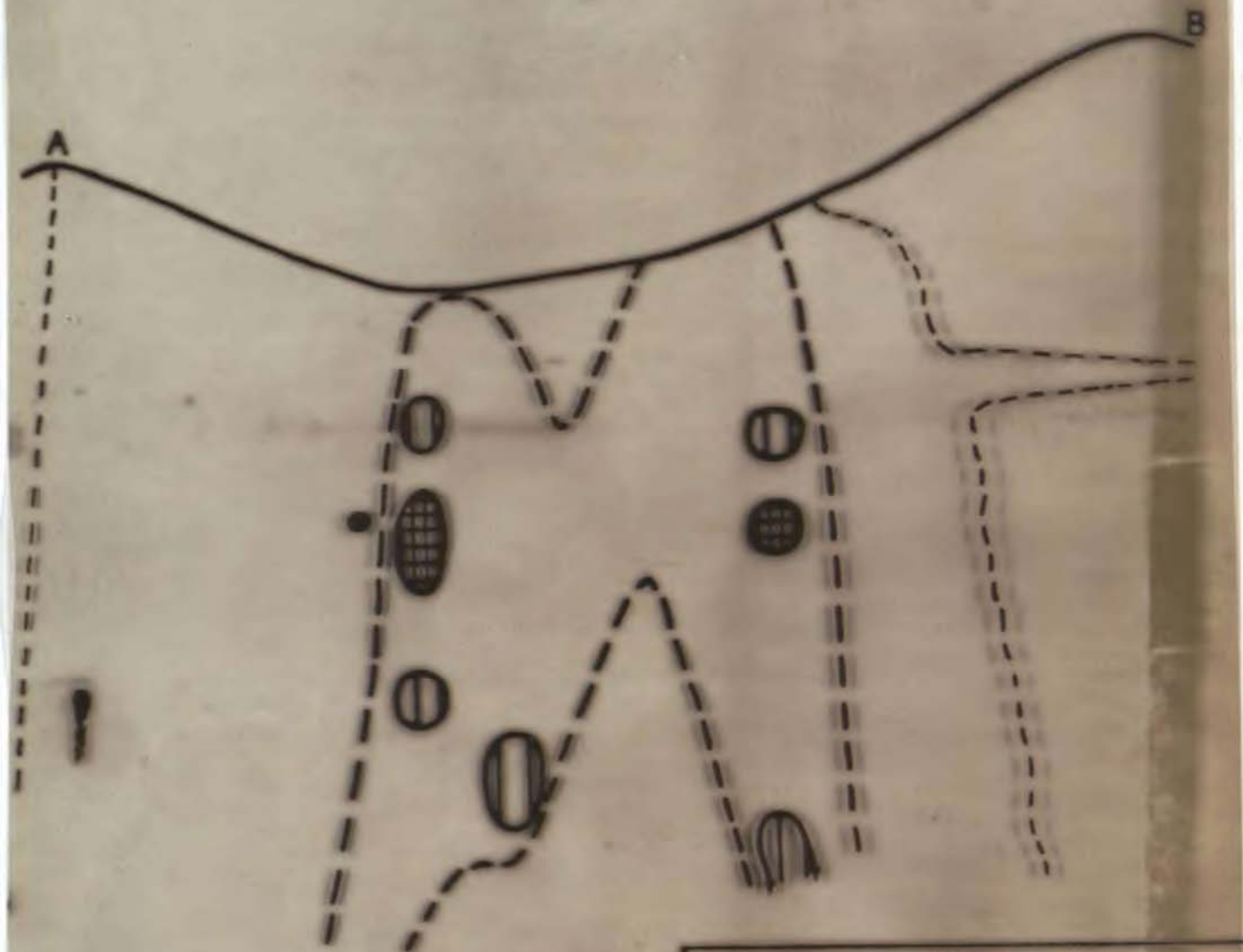
OVERLAY 6.

LEGEND.
Cu mineralization.

> 5100 ppm (≈1.5 wt% cp
> 3400 ppm (≈1.0 wt% cp
> 1700 ppm (≈0.5 wt% cp
(average for 50° intervals

OVERLAY 7.

LEGEND.

No mineralization.

> 150 ppm.

> 100 ppm.

> 40 ppm.
(average over 100' interval)

Au mineralization.

20' interval averaging   200 ppb